NOTE TO USERS

Modelling, Simulation and Control of Nonlinear Flexural-Flexural-Inextensional Rotating Beam

by

Yun Zhao

A thesis

presented to Lakehead University

in fulfilment of the

thesis requirement for the degree of

Master of Science in Engineering

in

Control Engineering

Thunder Bay, Ontario, Canada, 2004

Your file Votre référence
ISBN: 0-612-92264-2
Our file Notre référence
ISBN: 0-612-92264-2

I hereby declare that I am the sole author of this thesis.

I authorize Lakehead University to lend this thesis to other institutions or individuals for the purpose of scholarly research.

I further authorize Lakehead University to reproduce this thesis by photocopying or by other means, in total or in part, at the request of other institutions or individuals for the purpose of scholarly research.

Lakehead University requires the signatures of all persons using or photocopying this thesis. Please sign below, and give address and date.

Abstract

A continuous rotating beam that undergoes flexure about two principal axes is modelled. The beam is characterized by gyroscopic type nonlinearities. The beam is of significant importance for applications such as large space structures, helicopter rotor blades, robot manipulators and long-span structures. Hamilton's principle is used in deriving the Partial Differential Equations of motion (PDEs). An Ordinary Differential Equation (ODEs) solver based on the conventional Runge-Kutta method and a Differential Algebraic Equation (DAEs) solver based on Average Acceleration Formulation (AAF) have both been applied to simulate the system and the results are compared. Spectral analysis is carried out using FFT.

In the second part of this work, vibration suppression strategy based on Internal Resonance (IR) state is developed. By setting up different IR ratios, the modal coupling is greatly strengthened. Establishing IR state involves tuning the stiffness of the nonlinear beam by applying piezo-electric actuators to the system. A conceptual controller design is also presented. After the IR state is established, damping (velocity feedback) is introduced into the system and the vibration is thus successfully suppressed through two IR based PD controllers.

Acknowledgements

I would like to thank my supervisor, Professor Sultan Siddiqui for offering continuous support, guidance and encouragement through my master's program. His assistance will be cherished and appreciated for the rest of my life.

I would also like to thank Professor Kefu Liu and Professor Donatus Oguamanam for their time and efforts for serving as my internal and external examiners, respectively.

During the research program, I obtained many valuable suggestions from the faculty members in our MACE group. Special thanks to Professor Xiaoping Liu for checking my controller design and introducing me to nonlinear control theory.

Finally, I would like to thank my wife for her sincere love and my parents for taking care of our son.

To my beloved wife

Sophie

Contents

1 Introduction **1**

1.1 Overview 1

1.2 Background Material 4

1.2.1 Flexural-Flexural-Inextensional Euler-Bernoulli Beam 5

1.2.2 Gyroscopic System 5

1.3 Literature Survey 5

1.4 Thesis Outline 8

2 Modelling **10**

2.1 System Model 10

2.2 System Parameters 15

2.3 Development of the Equations of Motion 15

2.3.1 Displacement Field 16

2.3.2 Velocity Field 16

2.3.3 Strains 18

2.3.4 Strain Energy of the Beam 19

2.3.5 Kinetic Energy of the Beam 21

2.3.6 Lagrangian 21
2.3.7 Equations of Motion 22
2.3.8 Natural and Essential Boundary Conditions 25
2.3.9 Initial Conditions 27

3 Spatial Discretization **33**
3.1 Symmetric Formulation 34
3.2 Spatial Discretization 37
3.3 Eigenfunction of a Cantilever Beam 40

4 Vibration Suppression **43**
4.1 Control Efforts 44
4.2 Linearized Equations of Motion 45
4.2.1 Equilibrium Position 45
4.2.2 Characteristic Equation 47
4.2.3 Variation of Natural Frequencies 50
4.3 Vibration Suppression 55
4.4 Implementation of IR Control Strategy 55

5 Numerical Simulation **62**
5.1 Solution Techniques 62
5.1.1 Runge-Kutta Method 63
5.1.2 Average Acceleration Formulation 64
5.1.3 Average Acceleration Method 64
5.1.4 Discretized Equations-Acceleration Formulation 66

5.2 Solution of Nonlinear Algebraic Equations 70
5.3 Numerical Algorithms 73
5.4 Excitation in Different Directions 74
5.5 Non-Resonant Response Using AAF Method 78
5.6 Comparison of Runge-Kutta Method and AAF Method 80
5.7 Comparison of Single Mode Shape Model and Four Mode Shape Model 90
5.8 Comparison of 1:1 IR and 1:2 IR 96
5.9 Vibration Suppression Results 98

6 Conclusion and Future Work **105**

6.1 Conclusion 105
6.2 Future Work 107

A Nondimensional Model **108**

A.1 Nondimensional Parameters 108
A.2 Nondimensional Equations of Motion 109
A.3 Spatial Discretization 111
A.3.1 Symmetric Form 111
A.3.2 Discretized Equations of Motion 114
A.4 Basis Functions and the Matrices 115
A.5 Linearized Equations of Motion 118
A.6 Coefficients in Nondimensional Linear Algebraic Equations 119
A.7 Discretized Equations of Motion 120
A.8 Variation of Natural Frequencies 122

Bibliography 125

List of Figures

1.1 Flexural-Flexural Beam. 4

2.1 Flexural-Flexural Beam. 11

2.2 Deformation angle sequence 12

2.3 Deflection of differential element. 14

2.4 Initial values (a) (-)u, (- -)u', (...)u'', (b) (-)v, (- -)v', (...)v'', (c) (-)w, (- -)w', (...)w'', (d) (-)u''', (- -)v''', (...)w'''. (dimensional case) . . . 30

2.5 Initial values (a) (-)u, (- -)u', (...)u'', (b) (-)v, (- -)v', (...)v'', (c) (-)w, (- -)w', (...)w'', (d) (-)u''', (- -)v''', (...)w'''. (nondimensional case) . 31

3.1 Dimensional mode shapes, (-) ϕ_1, (-.) ϕ_2, (...) ϕ_3, (- -) ϕ_4 42

4.1 Variation in ω_1 and ω_2 with respect to Ω, (-) ω_1, (- -) ω_2 51

4.2 Variation in ω_1 and ω_2 with respect to K_{pu}, (a) 1:1 IR and (b) 1:2 IR, (-) ω_1, (- -) ω_2 52

4.3 Variation in ω_1 and ω_2 with respect to K_{pv}, k is IR ratio, (-) ω_1, (- -) ω_2 53

4.4 Conceptual view of actuators applied to the beam for setting up IR and suppress vibrations in u, v and w directions 59

4.5 Control logic, k is the ratio of ω_1 to ω_2 for setting up 1:1 IR and 1:2 IR, **a** is acceleration vector, **v** is velocity vector and **d** is displacement vector. Ω stands for angular velocity. 60

5.1 Four mode shape dimensional system response obtained by exciting in w direction only, AAF Method is applied. $\Omega = 50$, $w_{t0} = 0.2$. 1:2 IR, (a), (b) and (c) are time responses in u, v, and w directions respectively. 76

5.2 Four mode shape dimensional system response obtained by exciting in v direction only, AAF Method is applied. $\Omega = 50$, $v_{t0} = 0.2$, (a), (b) and (c) are time responses in u, v, and w directions respectively. 77

5.3 Four mode shape dimensional system response away from internal resonance, AAF Method is applied. $\Omega = 50$, $w_{t0} = 0.2$, $K_{pu} = 0$, $K_{pv} = 1e{+}5$, $K_{pw} = -1.6124e4$. (a), (b) and (c) are time responses in u, v, and w directions respectively. 79

5.4 Single mode shape dimensional system response, 1:2 IR by tuning K_{pu} and K_{pw}, Runge-Kutta Method is applied. (a), (b) and (c) are time responses in u, v, and w directions respectively, (d), (e) and (f) are power spectrums in u, v, and w directions respectively 81

5.5 Single mode shape dimensional system response, 1:2 IR by tuning K_{pu} and K_{pw}, AAF Method is applied. (a), (b) and (c) are time responses in u, v, and w directions respectively, (d), (e) and (f) are power spectrums in u, v, and w directions respectively 82

5.6 Four mode shape dimensional system response, 1:2 IR by tuning K_{pu} and K_{pw}, Runge-Kutta Method is applied. (a), (b) and (c) are time responses in u, v, and w directions respectively, (d), (e) and (f) are power spectrums in u, v, and w directions respectively 83

5.7 Four mode shape dimensional system response, 1:2 IR by tuning K_{pu} and K_{pw}, AAF Method is applied. (a), (b) and (c) are time responses in u, v, and w directions respectively, (d), (e) and (f) are power spectrums in u, v, and w directions respectively. 84

5.8 Single mode shape nondimensional system response, 1:2 IR by tuning K_{pu} and K_{pw}, Runge-Kutta Method is applied. (a), (b) and (c) are time responses in u, v, and w directions respectively. 86

5.9 Single mode shape nondimensional system response, 1:2 IR by tuning K_{pu} and K_{pw}, AAF Method is applied. (a), (b) and (c) are time responses in u, v, and w directions respectively, (d), (e) and (f) are power spectrums in u, v, and w directions respectively 87

5.10 Four mode shape nondimensional system response, 1:2 IR by tuning K_{pu} and K_{pw}, Runge-Kutta Method is applied. (a), (b) and (c) are time responses in u, v, and w directions respectively. 88

5.11 Four mode shape nondimensional system response, 1:2 IR by tuning K_{pu} and K_{pw}, AAF Method is applied. (a), (b) and (c) are time responses in u, v, and w directions respectively, (d), (e) and (f) are power spectrums in u, v, and w directions respectively. 89

5.12 Single mode shape dimensional system response, 1:1 IR by tuning K_{pu} and K_{pw}, AAF Method is applied. (a), (b) and (c) are time responses in u, v, and w directions respectively, (d), (e) and (f) are power spectrums in u, v, and w directions respectively. 92

5.13 Four mode shape dimensional system response, 1:1 IR by tuning K_{pu} and K_{pw}, AAF Method is applied. (a), (b) and (c) are time responses in u, v, and w directions respectively, (d), (e) and (f) are power spectrums in u, v, and w directions respectively. 93

5.14 Single mode shape nondimensional system response, 1:1 IR by tuning K_{pu} and K_{pw}, AAF Method is applied. (a), (b) and (c) are time responses in u, v, and w directions respectively, (d), (e) and (f) are power spectrums in u, v, and w directions respectively. 94

5.15 Four mode shape nondimensional system response, 1:1 IR by tuning K_{pu} and K_{pw}, AAF Method is applied. (a), (b) and (c) are time responses in u, v, and w directions respectively, (d), (e) and (f) are power spectrums in u, v, and w directions respectively. 95

5.16 Four mode shape dimensional system response, 1:1 IR and 1:2 IR by tuning K_{pu} and K_{pw}, AAF Method is applied. (a), (b) and (c) are time responses in u, v, and w directions respectively for 1:1 IR, (d), (e) and (f) are time responses in u, v, and w directions respectively for 1:2 IR. 97

5.17 Single mode shape dimensional system with damping K_{dv} only, (a), (b) and (c) are time responses for 1:1 IR in u, v, and w directions respectively by tuning K_{pu} and k_{pw}. (d), (e) and (f) are time responses for 1:2 IR in u, v, and w directions respectively by tuning K_{pu} and k_{pw}. AAF Method is applied. 100

5.18 Four mode shape dimensional system with damping K_{dv} only, (a), (b) and (c) are time responses for 1:1 IR in u, v, and w directions respectively by tuning K_{pu} and k_{pw}. (d), (e) and (f) are time responses for 1:2 IR in u, v, and w directions respectively by tuning K_{pu} and k_{pw}. AAF Method is applied. 101

5.19 Single mode shape dimensional system with damping, (a), (b) and (c) are time responses for 1:1 IR in u, v, and w directions respectively by tuning K_{pu} and k_{pw}. (d), (e) and (f) are time responses for 1:2 IR in u, v, and w directions respectively by tuning K_{pu} and k_{pw}. AAF Method is applied. 102

5.20 Four mode shape dimensional system with damping, (a), (b) and (c) are time responses for 1:1 IR in u, v, and w directions respectively by tuning K_{pu} and k_{pw}. (d), (e) and (f) are time responses for 1:2 IR in u, v, and w directions respectively by tuning K_{pu} and k_{pw}. AAF Method is applied. 103

A.1 Nondimensional mode shapes, (-) ϕ_1, (-.) ϕ_2, (...) ϕ_3, (- -) ϕ_4 117

A.2 Variation in ω_1 and ω_2 with respect to K_{pu}, (a) 1:1 IR and (b) 1:2 IR. (-) ω_1, (- -) ω_2 123

A.3 Variation in ω_1 and ω_2 with respect to K_{pv}, k is IR ratio, (-) ω_1, (- -) ω_2 124

List of Tables

4.1 Tuning parameters for dimensional model 54

4.2 Tuning parameters for nondimensional model 54

4.3 Beam frequencies obtained using the dimensional single mode equations 54

4.4 Beam frequencies obtained using the nondimensional single mode equations 55

5.1 Comparison between Runge-Kutta and AAF method for dimensional model 80

5.2 Difference between Runge-Kutta and AAF for nondimensional model 85

5.3 Comparison between single mode shape and four mode shape models 90

5.4 Comparison between single mode shape and four mode shape models 91

5.5 Comparison between 1:1 IR and 1:2 IR cases 96

5.6 Vibration suppression results with only K_{dv} applied 98

5.7 Vibration suppression results 98

Chapter 1

Introduction

1.1 Overview

In this thesis we study the dynamic behaviour of a nonlinear flexural-flexural-inextensional rotating beam in both time and spectral domains. The beam is a continuously distributed gyroscopic type system of significant importance for applications such as large space rotating structures and helicopter rotor blades. The emphasis of this work is on modelling, simulation and vibration suppression. Equations of motion and boundary conditions for the system are derived in a unified and mathematically consistent manner. It is assumed here that the material is Hookean. Nonlinearities in the system are of geometric and kinematic type. Geometric nonlinearities are due to large deformation of the beam and kinematic nonlinearities are due to the rotation. One of the distinguishing characteristics of this thesis is that both dimensional and nondimensional cases are taken into account in deriving the equations of motion, simulating the system and suppressing the vibrations.

Vibration suppression strategy used in this work is based on strengthening the modal coupling in the system. Several recent studies [1-7] have shown that modal coupling in dynamic systems can be effectively used as an energy-based control strategy for vibration suppression. The coupling in the system is the basic reason for the energy transfer between the modal amplitudes (*i.e.* amplitudes that correspond to the natural frequencies of the system). The coupling becomes much stronger when a state of Internal Resonance (IR) is established. The vibration suppression strategy used in this work is to maximize the effect of linear and nonlinear coupling through IR and then by introducing damping into the system, vibration suppression is accomplished. Internal resonance occurs when the natural frequencies of the system become commensurable (linearly dependant, *i.e.* $a_1\omega_1+a_2\omega_2+a_3\omega_3+...a_i\omega_i = 0$, where $i = 1...n$, a_i are positive or negative integers and ω_i are system natural frequencies). One of the important attributes of IR is that when IR exists in the system, energy laid up initially in some particular modes will be continuously and rapidly exchanged among other resonant modes involved in that specific Internal Resonance. Consequently, when all the modes in the system are coupled strongly enough, damping applied via an actuator in one particular mode can directly suppress vibrations in that mode and indirectly suppress vibrations in other coupled modes. The distinct advantage and feature of this vibration suppression technique is that by applying damping in one mode, we can successfully suppress vibration in all other resonant modes. In order to establish Internal Resonance, the eigenvalues of the system are computed and analyzed to determine the tuning parameter for the controller.

Hamilton's principle [8, 9] is used in deriving the equations of motion. It involves extremizing the time integral of the difference between kinetic and potential energy of the system.

The equations of motion obtained using Hamilton's principle are nonlinear partial differential equations which are discretized first and thus reduced to ordinary differential equations for the development of their solutions. By applying Galerkin [8, 9] approach, the resulting partial differential equations are reduced to a set of ordinary differential equations. Here the selection of proper basis function is important in developing a solution to the equations of motion. Finite Element shape functions are initially chosen for our formulation. However, the numerical simulations of the beam could not be successfully carried out because of the difficulty and complexity of the formulations. Hence the eigenfunctions for cantilever beam are used as basis functions.

The equations of motion obtained after applying Galerkin method are solved using two methods, a conventional Ordinary Differential Equation (ODEs) solver based on Runge-Kutta Method and a Differential Algebraic Equation (DAE) solver based on the Average Acceleration Formulation (AAF) method originally proposed by Siddiqui *et al.* [10]. Another DAE solver SUNDIAL-IDA was tried but was not successful due to convergence problems.

The simulation results are analyzed in time domain as well as in spectral domain using the Fast Fourier Transform (FFT) approach.

The symbolic computational software package Maple is used to perform most of the derivations presented in this thesis. Numerical simulations were performed using

software developed in C. Obtaining numerical solution is computationally intensive and requires significant computing power. A supercomputer Silicon Graphics Origin 2000 was used for this purpose. Matlab was also used in some matrix related computation, programming and plotting.

This thesis is motivated by the work presented by Siddiqui and Golnaraghi in [1, 2], where a gyroscopic two-degree of freedom discrete system was modelled and simulated.

1.2 Background Material

The system shown in Figure 1.1 is a two-dimensional rotating Euler-Bernoulli beam which undergoes flexure about two principal axes and meanwhile rotating with a constant angular velocity Ω. The system is a nonlinear continuously distributed gyroscopic system. Gyroscopic forces arise due to the coupling of the vibratory modes with the angular velocity Ω. The system model is quite complex and deriving the equations and subsequent simplification is an intensive task.

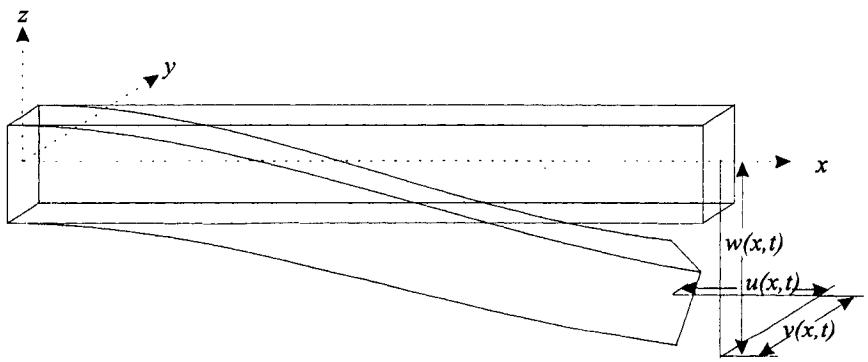

Figure 1.1: Flexural-Flexural Beam.

1.2.1 Flexural-Flexural-Inextensional Euler-Bernoulli Beam

Euler-Bernoulli beam is characterized by its plane cross sections before deformation remaining plane after deformation and normal to its neutral reference line. Also, generally shear force effects are neglected. To make the Euler-Bernoulli beam account for geometrically nonlinear behavior due to large displacements, the commonly used infinitesimal strains assumption is dropped and replaced by Green's strain tensor [8].

1.2.2 Gyroscopic System

Linearized gyroscopic systems are characterized by skew-symmetric coupling matrix arising due to gyroscopic forces. Such systems are described by the following type of differential equations:

$$M\ddot{X} + G\dot{X} + KX = 0 \tag{1.1}$$

where M is the mass matrix and K is the stiffness matrix. Both matrices are generally symmetric. The skew-symmetric matrix G represents the gyroscopic terms in the model, X is the displacement vector, $\dot{X}$ is the velocity vector and $\ddot{X}$ is the acceleration vector.

1.3 Literature Survey

During the last several decades, the study of nonlinear beam behaviour that represents the fundamental characteristics of many important engineering structures

has been extensively conducted and thus yielding many theories and strategies on modelling, simulation and vibration control. The previous work laid down theoretical foundations for a variety of applications such as space structures, helicopter rotor blades (see [11]), and robot manipulators (see [12]).

Since the Euler-Bernoulli beam theory was established in the eighteenth century, it has mostly been used for modelling small oscillation motion. However, in recent years a number of papers have been published which extended the application of Euler-Bernoulli beam model to large deformation analysis. Bishopp and Drucker [13] studied large deflection motion of cantilever beams in 1945. Srinivasan [14] investigated large amplitude free oscillations of beams and plates in 1965. Bathe and Bolourchi [15] showed large displacement analysis of three dimensional beam structures in 1979. Other recent publications include Crespo da Silva [16, 17, 18] and Crespo da Silva and Glynn [19, 20]. Crespo da Silva and Glynn [19] formulated a set of mathematically consistent governing equations of motion describing the nonplanar, nonlinear dymamics of an inextensional beam. Later Crespo da Silva [18] further expanded this model and derived the nonlinear differential equations of motion and boundary conditions for an extensional Euler-Bernoulli beam able to experience flexure along two principal directions and torsion. In 1991 Crespo da Silva [16] formulated a set of governing differential equations for a gyroscopic Euler-Bernoulli beam that undergoes flexural-flexural-torsional-extensional (3D) motions while rotating with an angular velocity.

It is always a very difficult and challenging task to develop solutions to the Partial Differential Equations (PDEs) that govern continuous nonlinear systems

undergoing large deformation. Many different approaches have been undertaken in this respect, among which the Finite Element Method is particularly worth of mention. Over the years, it has been extensively used for the accurate solution of complex engineering problems. Pestel [21] illustrated Hermitian polynomial application as finite element basis functions. Mei [22, 23] proposed a displacement based finite element method to determine the nonlinear frequency of beams [22] and plates [23] for large amplitude free vibrations. Bathe, Ramm and Wilson [24] presented finite element formulations for large deformation dynamic analysis. Both the total Lagrangian formulation and the updated lagrangian formulation were considered for problems with large displacements, large strains, and material nonlinearities. The nonlinear terms in [24] were carried out with linearization and the dynamic problems have been solved with only limited success. Some of the solution techniques using finite element method applicable to nonlinear problems are presented in [25]. Rao and Raju [26] applied finite element formulation to the large amplitude free vibrations of beams and orthotropic circular plates. In [10], Siddiqui *et al.* proposed a numerical technique for solving differential equations arising in finite element problems. The technique is based on a different formulation of the conventionally used average acceleration method. Some other publications in this area are by Becker *et al.* [27], Beltzer [28], Cardona and Geradin [29], Dawe [30], Dupuis [31], Dhatt and Touzot [32], and Rao [33].

The conventional way of controlling nonlinear systems is by the application of any linear controllers, such as PID, to the linearized model and by the examination of the stability of the nonlinear model using Lyapunov stability theory. One can also

design nonlinear controllers directly for the nonlinear systems. The latter choice is rather complicated and the issue of designing nonlinear controllers is still of interest to researchers. To apply linear controllers to the nonlinear systems directly and effectively with satisfactory stability, Internal Resonance (IR) control technique is an ideal option. This technique involves harmonizing the linear natural frequencies of the nonlinear system. One of the first authors to investigate in this realm is Sethna [34]. Thereafter several other authors, Stupnicka [35], Van Dooren [36], Haddow *et al.* [37], and Mook *et al.* [38] investigated resonant response of a system under harmonic excitation forces. More recently, Golnaraghi [39, 40] discussed vibration control techniques for flexible structures using nonlinear coupling and IR. Siddiqui and Golnaraghi [2, 3] investigated modal coupling and stability problems for flexible gyroscopic systems. In [1] Siddiqui also applied the IR control strategy to a two-degree of freedom discrete gyroscopic system.

1.4 Thesis Outline

In this thesis, Chapter 1 is the general synopsis and provides a brief introduction to the following chapters. Chapter 2 presents detailed process of modelling for both dimensional and nondimensional systems. As mentioned in the previous sections, the equations of motion are derived by applying Hamilton's principle. The resulting equations of motion have polynomial nonlinearities. Unlike the approach used in [17, 20], this technique does not require using Taylor series expansion to reduce trigonometric nonlinearities to polynomial nonlinearities.

In Chapter 3, by applying Galerkin method, the obtained partial differential

equations are first reduced to symmetric form by multiplying them with a weighting function $p(x)$ and integrating by parts twice. Then by substituting the boundary conditions, the symmetric equations are further reduced to nonlinear ordinary differential equations, which completes the process of spatial discretization.

In Chapter 4 the vibration suppression strategies using Internal Resonance (IR) method are presented. IR control strategy requires tuning the stiffness of the control mode, which is accomplished through position (tip deflection) feedback. Once IR is established, the vibration in the system can be significantly suppressed by introducing damping (velocity feedback) into system. This is demonstrated in Chapter 5 via numerical simulations.

The systems are simulated, in Chapter 5, through two numerical approaches: Adaptive Step-Size Runge-Kutta method and Average Acceleration Formulation method. The distinct effectiveness of the proposed vibration suppression strategies is strongly supported by numerical simulation results. Finally, the dynamics of the systems are analyzed in detail in both time and spectral domains.

In Chapter 6 we draw some conclusions and outline some future works.

Chapter 2

Modelling

In this chapter, the equations of motion of a flexural-flexural-inextensional rotating beam are developed for both dimensional and nondimensional cases using an energy approach. The equations of motion for the beam obtained in this chapter are valid for arbitrarily large motions. The approach taken in deriving the equations of motion is similar to that proposed by Crespo da Silva and Glynn [19] for 3D motions of inextensional beams. However the technique used for reducing the PDE to ODE is different in that it does not require using Taylor series expansion as used in [19]. The use of Taylor series expansion limits the analysis to motion about equilibrium position.

2.1 System Model

The system model is a simplified helicopter rotor blade from the NASA Army Aeroelastic Rotor Experimental System (ARES) [41]. The rotor consists of four

blades. The blades have rectangular cross section and free of built-in twist. The blades undergo flapwise and chordwise elastic deformations when rotating about the rotor hub. Therefore each blade can be modelled as a rotating Euler-Bernoulli beam undergoing the same flexural motions. The beam model was shown earlier in Figure 1.1 and is repeated in Figure 2.1 for convenience.

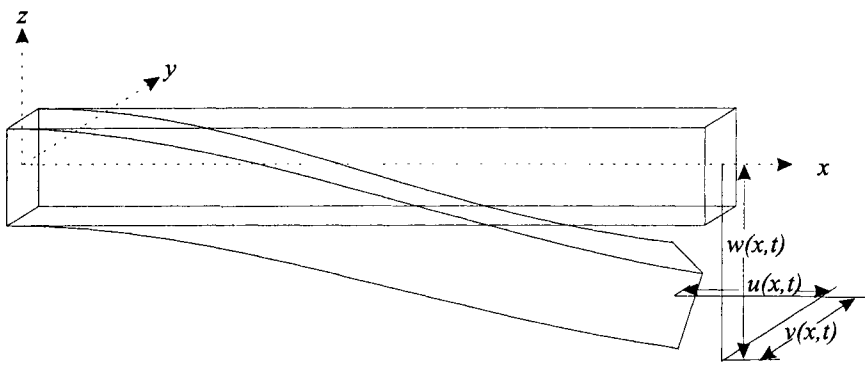

Figure 2.1: Flexural-Flexural Beam.

The rotating beam model is an Euler-Bernoulli beam undergoing flexure about two principal axes and rotating with a constant angular velocity (Ω). The beam parameters are length (l), area of cross section (A), mass density (ρ), flapwise area moment of inertia (I_z), chordwise area moment of inertia (I_y), and modulus of elasticity (E). The beam is assumed to be straight when in its undeformed configuration. The beam material is assumed to be isotropic. The beam is modelled using the deformation angle sequence shown in Figure 2.2.

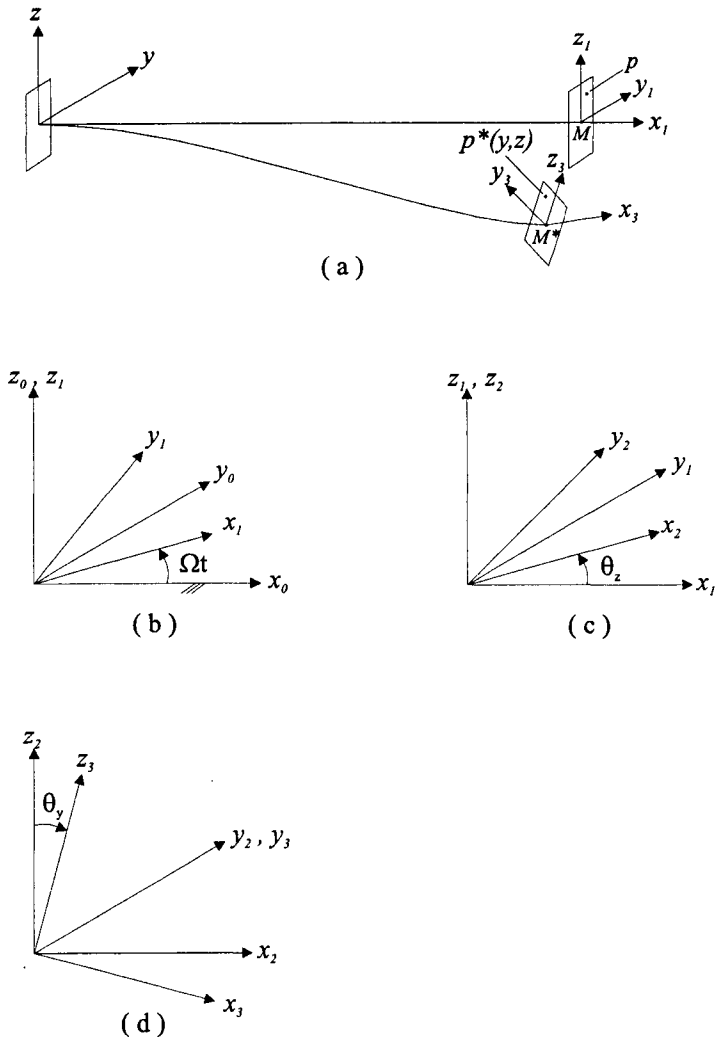

Figure 2.2: Deformation angle sequence

In Figure 2.2, $\{x_0, y_0, z_0\}$ is a fixed frame, $\{x_1, y_1, z_1\}$ is a rotating frame with angular velocity Ω, $\{x_2, y_2, z_2\}$ is rotated by an angle θ_z about z_1 relative to the frame $\{x_1, y_1, z_1\}$ and $\{x_3, y_3, z_3\}$ is rotated by an angle θ_y about y_2 relative to the frame $\{x_2, y_2, z_2\}$.

Figure 2.2 shows the longitudinal axis of the beam before and after deformation. In the figure, the reference coordinate frame $\{x_1, y_1, z_1\}$ is rotating with a constant angular velocity Ω relative to a fixed inertial frame $\{x_0, y_0, z_0\}$. The components along x, y, z axes of the elastic deformation at point M^* are denoted by $(u(x,t), v(x,t), w(x,t))$, where t denotes time. The cantilever beam is assumed not to subject the external axial force and therefore to be inextensional. Consequently, the axial stiffness is not taken into account when deriving the governing differential equations later, which prevents the introduction of an extra one degree of freedom motion to the system axially. The inextensionality constraint is derived using the differential deformations shown in Figure 2.3.

By letting primes denote partial differentiation with respect to x, the relationships between the elastic deformation $(u(x,t), v(x,t), w(x,t))$ and the orientation angles θ_y and θ_z can be derived as follows using Figure 2.3:

$$\begin{aligned} \tan\theta_z &= \frac{v'}{1+u'} \\ \tan\theta_y &= -\frac{w'}{\sqrt{(1+u')^2+v'^2}} \\ (1+u')^2 &+ v'^2 + w'^2 = 1 \end{aligned} \tag{2.1}$$

the last equation in (2.1) is the constraint equation that would be used in the

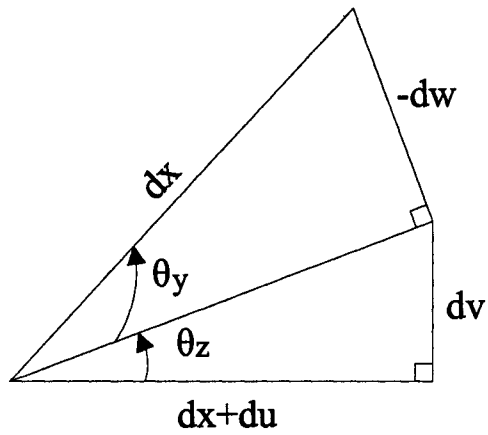

Figure 2.3: Deflection of differential element.

derivation of the equations of motion.

The transformation matrices between the various frames are obtained as:

$$T_{12} = \begin{bmatrix} \cos(\theta_z) & -\sin(\theta_z) & 0 \\ \sin(\theta_z) & \cos(\theta_z) & 0 \\ 0 & 0 & 1 \end{bmatrix} \tag{2.2}$$

$$T_{23} = \begin{bmatrix} \cos(\theta_y) & 0 & \sin(\theta_y) \\ 0 & 1 & 0 \\ -\sin(\theta_y) & 0 & \cos(\theta_y) \end{bmatrix} \tag{2.3}$$

$$T_{13} = \begin{bmatrix} \cos(\theta_z)\cos(\theta_y) & -\sin(\theta_z) & \cos(\theta_z)\sin(\theta_y) \\ \sin(\theta_z)\cos(\theta_y) & \cos(\theta_z) & \sin(\theta_z)\sin(\theta_y) \\ -\sin(\theta_y) & 0 & \cos(\theta_y) \end{bmatrix} \tag{2.4}$$

where T_{12} is the transformation matrix of frame $\{x_2, y_2, z_2\}$ relative to $\{x_1, y_1, z_1\}$, T_{23} is the transformation matrix of $\{x_3, y_3, z_3\}$ relative to $\{x_2, y_2, z_2\}$, T_{13} is the transformation matrix of frame $\{x_3, y_3, z_3\}$ relative to $\{x_1, y_1, z_1\}$. The transformation matrices are used in deriving the displacement field in Section 2.3.1.

2.2 System Parameters

The following physical parameters are chosen for the Euler-Bernoulli beam. They are selected to give approximately the same first natural frequency at zero angular velocity as the NASA Army Aeroelastic Rotor Experimental System (ARES) [41]:

Mass density: $\rho = 7810 \ kg/m^3$

Modulus of elasticity: $E = 207 \ GPa$

Cross section area (Rectangle): $A = 0.0022 \ m^2$

Flapwise area moment of inertia: $I_z = 2.2 \times 10^{-6} \ m^4$

Chordwise area moment of inertia: $I_y = 7.5 \times 10^{-8} \ m^4$

Angular velocity: $\Omega = 0 \sim 50 \ rad/s$

Length of the blade: $l = 1.397 \ m$

2.3 Development of the Equations of Motion

Since Hamilton's principle involves extremizing the time integral of the difference between kinetic energy and potential energy (*i.e.* the Lagrangian $\mathcal{L}$) of the system, all the energy terms that contribute to the Lagrangian need to be developed first

in order to derive the equations of motion.

2.3.1 Displacement Field

The displacement field is modelled using three dependant variables $u(x,t)$, $v(x,t)$ and $w(x,t)$ as shown in Figure 2.1, where $u(x,t)$ measures the foreshortening of the beam in the horizontal direction, $v(x,t)$ measures the horizontal deflection of the reference axis, and $w(x,t)$ measures the deflection of the reference axis in the xz plane. Considering displacements due to rotation θ_y and θ_z, of a point located at a distance y along the y axis and a distance z along the z axis gives the following displacement field:

$$\begin{aligned} u_x &= u(x,t) - y\sin(\theta_z) + z\sin(\theta_y)\cos(\theta_z) \\ u_y &= v(x,t) - y(1-\cos(\theta_z)) + z\sin(\theta_y)\sin(\theta_z) \\ u_z &= w(x,t) - z(1-\cos(\theta_y)) \end{aligned} \tag{2.5}$$

where u_x, u_y and u_z represent the displacement of the centroid M shown in Figure 2.2 in the undeformed x, y and z directions respectively.

2.3.2 Velocity Field

The velocity field $\mathbf{V}$ with components V_x, V_y and V_z is given by:

$$\mathbf{V} = \boldsymbol{\Omega} \times \mathbf{u} + (\mathbf{V})_{\mathbf{rel}} \tag{2.6}$$

where $\mathbf{\Omega}$ is angular velocity vector with Ω as z component, $\mathbf{u}$ is the displacement field of the centroid M in the undeformed x, y and z directions respectively and $(\mathbf{V})_{\mathbf{rel}}$ is the velocity field measured relative to the rotating frame (x_1, y_1, z_1).

By differentiating the displacement field with respect to time, the following relative velocity field is obtained:

$$\begin{aligned}
(V_x)_{rel} &= u_{,t} - y\cos(\theta_z)\,\theta_{z,t} + z\cos(\theta_y)\cos(\theta_z)\,\theta_{y,t} - z\sin(\theta_y)\sin(\theta_z)\,\theta_{z,t} \\
(V_y)_{rel} &= v_{,t} - y\sin(\theta_z)\,\theta_{z,t} + z\cos(\theta_y)\sin(\theta_z)\,\theta_{y,t} + z\sin(\theta_y)\cos(\theta_z)\,\theta_{z,t} \\
(V_z)_{rel} &= w_{,t} - z\sin(\theta_y)\,\theta_{y,t}
\end{aligned} \tag{2.7}$$

In (2.7), the $(.)$ implies differentiation with the notation $u_{,t} = \frac{\partial u}{\partial t}$, $v_{,t} = \frac{\partial v}{\partial t}$, $w_{,t} = \frac{\partial w}{\partial t}$, $\theta_{y,t} = \frac{\partial \theta_y}{\partial t}$ and $\theta_{z,t} = \frac{\partial \theta_z}{\partial t}$. Besides, $(V_x)_{rel}$, $(V_y)_{rel}$ and $(V_z)_{rel}$ are components of $(\mathbf{V})_{\mathbf{rel}}$ along x_1, y_1, z_1 directions respectively. Consequently, the absolute velocity field is given by:

$$\begin{aligned}
V_x &= -\Omega\,(v - y\,(1 - \cos(\theta_z)) + z\sin(\theta_y)\sin(\theta_z)) + u_{,t} \\
&\quad -y\cos(\theta_z)\,\theta_{z,t} + z\cos(\theta_y)\,(\theta_{y,t})\cos(\theta_z) \\
&\quad -z\sin(\theta_y)\sin(\theta_z)\,\theta_{z,t} \\
V_y &= \Omega\,(u - y\sin(\theta_z) + z\sin(\theta_y)\cos(\theta_z)) \\
&\quad +v_{,t} - y\sin(\theta_z)\,\theta_{z,t} + z\cos(\theta_y)\,(\theta_{y,t})\sin(\theta_z) \\
&\quad +z\sin(\theta_y)\cos(\theta_z)\,\theta_{z,t} \\
V_z &= w_{,t} - z\sin(\theta_y)\,\theta_{y,t}
\end{aligned} \tag{2.8}$$

where V_x, V_y and V_z represent the absolute velocity components along the undeformed x, y and z directions respectively.

2.3.3 Strains

Since the rotating Euler-Bernoulli beam undergoes large deformation, the nonlinear terms in the strain displacement relationships cannot be discarded. Therefore the Green's finite strain tensor formula [8] below is used to derive nonlinear displacement relationships:

$$\epsilon_{ij} = \frac{1}{2}\left(u_{i,x_j} + u_{j,x_i} + u_{k,x_i}u_{k,x_j}\right) \tag{2.9}$$

where the index notation is used with $i, j, k = 1, 2, 3$ corresponding to x, y, z coordinates, respectively. The first index i in ϵ_{ij} represents the plane on which the strains act and the second index j is the specific strain acting directions. The repeated index k implies summation over $1, 2$ and 3. The $(,)$ implies differentiation (i.e. $u_{i,x_j} = \frac{\partial u_i}{\partial x_j}$). From (2.9) it follows that the strains on the x plane in the x, y and z directions are given by:

$$\begin{aligned}
\epsilon_{xx} &= u_{x,x} + \frac{1}{2}\left(u_{x,x}\right)^2 + \frac{1}{2}\left(u_{y,x}\right)^2 + \frac{1}{2}\left(u_{z,x}\right)^2 \\
\epsilon_{xy} &= \frac{1}{2}\left(u_{x,y} + u_{y,x} + u_{x,x}u_{x,y} + u_{y,x}u_{y,y} + u_{z,x}u_{z,y}\right) \\
\epsilon_{xz} &= \frac{1}{2}\left(u_{x,z} + u_{z,x} + u_{x,x}u_{x,z} + u_{y,x}u_{y,z} + u_{z,x}u_{z,z}\right)
\end{aligned} \tag{2.10}$$

For the displacement field (2.5) it follows that all the other strains in (2.9) are zero. By using the displacement field (2.5) and the strain-displacement relationship

(2.10), the following strains are obtained:

$$\begin{aligned}
\epsilon_{xx} &= \frac{1}{2} y^2 \left(\theta_{z,x}\right)^2 + \left(-\left(\theta_{z,x}\right) z \cos\left(\theta_y\right) \theta_{y,x} - \cos\left(\theta_y\right) \theta_{z,x}\right) y + \\
&\quad \left(\frac{1}{2} \left(\theta_{z,x}\right)^2 - \frac{1}{2} \left(\theta_{z,x}\right)^2 \left(\cos\left(\theta_y\right)\right)^2 + \frac{1}{2} \left(\theta_{y,x}\right)^2\right) z^2 + z\theta_{y,x} \\
\epsilon_{xy} &= \frac{1}{2} z \sin\left(\theta_y\right) \theta_{z,x} \\
\epsilon_{xz} &= -\frac{1}{2} \sin\left(\theta_y\right) y \theta_{z,x}
\end{aligned} \tag{2.11}$$

The inextensionality constraint equation (2.1) is incorporated into the Lagrangian through the Lagrange multipliers $\lambda(x,t)$. The corresponding term that would appear in the Lagrangian is given by:

$$C = \frac{1}{2} \int_0^l \lambda(x,t) \left(\left(1 + u_{,x}\right)^2 + \left(v_{,x}\right)^2 + \left(w_{,x}\right)^2 - 1\right) dx \tag{2.12}$$

2.3.4 Strain Energy of the Beam

The strain energy function is given by [8]:

$$U = \frac{1}{2} \int_0^l \left(\left(M + 2G\right) \epsilon_{xx}^2 + 4G \left(\epsilon_{xy}^2 + \epsilon_{xz}^2\right)\right) dx \tag{2.13}$$

where M and G are the Lamé constants and given by the following equations:

$$\begin{aligned}
G &= \frac{E}{2\left(1 + v\right)} \\
M &= \frac{E\,v}{\left(1 + v\right)\left(1 - 2\,v\right)}
\end{aligned} \tag{2.14}$$

In (2.14), E denotes Young's modulus and υ represents Poisson ratio. Using the strain equations (2.11) and (2.13), the strain energy is obtained as:

$$\begin{aligned} U = \frac{1}{2}\int_0^l \Big[& \frac{1}{2} I_y M \left(\theta_{y,x}\right)^2 - \frac{3}{2} I_y M y \left(\theta_{y,x}\right)^2 \left(\theta_{z,x}\right) \cos\left(\theta_y\right) \\ & + \frac{1}{2} I_y M y \left(\cos\left(\theta_y\right)\right)^3 \left(\theta_{z,x}\right)^3 - \frac{1}{2} I_y M y \cos\left(\theta_y\right) \left(\theta_{z,x}\right)^3 + \frac{1}{4} I_z I_y M \left(\theta_{z,x}\right)^4 \\ & + \frac{1}{4} I_z I_y M \left(\theta_{z,x}\right)^2 \left(\theta_{y,x}\right)^2 + 2 I_z I_y G \left(\theta_{z,x}\right)^2 \left(\cos\left(\theta_y\right)\right)^2 \left(\theta_{y,x}\right)^2 \\ & + \frac{1}{2} I_z I_y M \left(\theta_{z,x}\right)^2 \left(\cos\left(\theta_y\right)\right)^2 \left(\theta_{y,x}\right)^2 - \frac{1}{4} I_z I_y M \left(\theta_{z,x}\right)^4 \left(\cos\left(\theta_y\right)\right)^2 \\ & + \frac{1}{2} I_z M \left(\theta_{z,x}\right)^2 \left(\cos\left(\theta_y\right)\right)^2 + I_z M z \left(\cos\left(\theta_y\right)\right)^2 \left(\theta_{z,x}\right)^2 \theta_{y,x} \\ & + \frac{1}{2} I_z M z \left(\theta_{y,x}\right) \left(\theta_{z,x}\right)^2 \Big] \, dx \end{aligned} \tag{2.15}$$

where

$$\begin{aligned} I_y &= \iint_A z^2 \, dy \, dz \\ I_z &= \iint_A y^2 \, dy \, dz \end{aligned} \tag{2.16}$$

The y^2 and z^2 terms in (2.11) lead to the fourth moment of area which is very small (compare the second moment $\frac{bh^3}{12}$ with the fourth moment $\frac{bh^5}{80}$ for rectangular beams) and thus dropped from (2.15).

2.3.5 Kinetic Energy of the Beam

For evaluating kinetic energy of the beam, the following formula is applied:

$$T = \frac{1}{2}\rho A \iiint_{\mathcal{V}} (V_x^2 + V_y^2 + V_z^2)\, d\mathcal{V} \tag{2.17}$$

where V_x, V_y and V_z are absolute velocity components given in (2.8) and $\mathcal{V}$ represents volume. Substituting (2.8) in (2.17) and simplifying gives the following expression for kinetic energy of the beam:

$$\begin{aligned} T = \frac{1}{2}\int_0^l \Big[& \frac{1}{2}\rho I_y\, (\theta_{z,t})^2 - \frac{1}{2}\rho I_y\, (\theta_{z,t})^2 (\cos(\theta_y))^2 \\ & -\rho I_y \Omega\, (\theta_{z,t}) (\cos(\theta_y))^2 + \rho I_y \Omega \theta_{z,t} + \frac{1}{2}\rho I_y \Omega^2 + \frac{1}{2}\rho I_y\, (\theta_{y,t})^2 \\ & -\frac{1}{2}\rho I_y \Omega^2 (\cos(\theta_y))^2 + \frac{1}{2}\rho I_z\, (\theta_{z,t})^2 - \rho I_z \Omega^2 \cos(\theta_z) \\ & +\rho I_z \Omega \theta_{z,t} + \rho I_z \Omega^2 - \rho I_z \Omega \cos(\theta_z)\, \theta_{z,t} + \rho A \Omega u v_{,t} + \frac{1}{2}\rho A \Omega^2 u^2 \\ & +\frac{1}{2}\rho A (w_{,t})^2 + \frac{1}{2}\rho A (v_{,t})^2 + \frac{1}{2}\rho A \Omega^2 v^2 + \frac{1}{2}\rho A (u_{,t})^2 \\ & -\rho A \Omega v u_{,t}\Big]\, dx \end{aligned} \tag{2.18}$$

2.3.6 Lagrangian

The Lagrangian from various energy terms ((2.15)-(2.18)) can be expressed as:

$$\begin{aligned} \mathcal{L} &= T - V \\ &= T(u, v, u_{,t}, v_{,t}, w_{,t}, \theta_z, \theta_y, \theta_{z,t}, \theta_{y,t}) - U(\theta_y, \theta_{y,x}, \theta_{z,x}) \\ &\quad -C(\lambda, u_{,x}, v_{,x}, w_{,x}) \end{aligned} \tag{2.19}$$

where T is the kinetic energy of the beam, V is the potential energy of the beam, U is the strain energy of the beam and C represents the inextensibility constraint multiplied by the Lagrange multiplier λ.

2.3.7 Equations of Motion

In this section, the equations of motion are obtained using Hamilton's principle as discussed earlier, which is accomplished by taking the first variation of the time integral of the Lagrangian [8]:

$$\delta^{(1)} \int_{t_1}^{t_2} \mathcal{L} dt = 0 \tag{2.20}$$

Taking variations with respect to u, v, w and λ according to (2.19) and (2.20), the following equations of motion are obtained:

u variation:

$$\begin{aligned}\int_0^l \Bigg\{ & \frac{\partial T}{\partial u} - \frac{d}{dt}\left(\frac{\partial T}{\partial \dot{u}}\right) - \frac{d}{dx}\left(\frac{d}{dt}\left(\frac{\partial T}{\partial \dot{\theta}_z}\right)\frac{\sin\theta_z}{\cos\theta_y}\right) + \frac{d}{dx}\left(\frac{\partial T}{\partial \theta_z}\frac{\sin\theta_z}{\cos\theta_y}\right) \\ & + \frac{d}{dx}\left(\frac{\partial T}{\partial \theta_y}\cos\theta_z \sin\theta_y\right) - \frac{d}{dx}\left(\frac{d}{dt}\left(\frac{\partial T}{\partial \dot{\theta}_y}\right)\cos\theta_z \sin\theta_y\right) \\ & - \frac{d}{dx}\left(\frac{\partial U}{\partial \theta_y}\cos\theta_z \sin\theta_y\right) + \frac{d}{dx}\left(\frac{d}{dx}\left(\frac{\partial U}{\partial \theta_y'}\right)\cos\theta_z \sin\theta_y\right) \\ & + \frac{d}{dx}\left(\frac{d}{dx}\left(\frac{\partial U}{\partial \theta_z'}\right)\frac{\sin\theta_z}{\cos\theta_y}\right) + \frac{d}{dx}\left(\frac{\partial C}{\partial u'}\right)\Bigg\} dx = 0\end{aligned} \tag{2.21}$$

v variation:

$$\int_0^l \left\{ \frac{\partial T}{\partial v} - \frac{d}{dt}\left(\frac{\partial T}{\partial \dot{v}}\right) + \frac{d}{dx}\left(\frac{d}{dt}\left(\frac{\partial T}{\partial \dot{\theta}_z}\right)\frac{\cos\theta_z}{\cos\theta_y}\right) - \frac{d}{dx}\left(\frac{\partial T}{\partial \theta_z}\frac{\cos\theta_z}{\cos\theta_y}\right) - \frac{d}{dx}\left(\frac{\partial T}{\partial \theta_y}\sin\theta_z\sin\theta_y\right) + \frac{d}{dx}\left(\frac{d}{dt}\left(\frac{\partial T}{\partial \dot{\theta}_y}\right)\sin\theta_z\sin\theta_y\right) - \frac{d}{dx}\left(\frac{\partial U}{\partial \theta_y}\sin\theta_z\sin\theta_y\right) + \frac{d}{dx}\left(\frac{d}{dx}\left(\frac{\partial U}{\partial \theta_y'}\right)\sin\theta_z\sin\theta_y\right) - \frac{d}{dx}\left(\frac{d}{dx}\left(\frac{\partial U}{\partial \theta_z'}\right)\frac{\cos\theta_z}{\cos\theta_y}\right) - \frac{d}{dx}\left(\frac{\partial C}{\partial v'}\right)\right\} dx = 0 \tag{2.22}$$

w variation

$$\int_0^l \left\{ -\frac{d}{dt}\left(\frac{\partial T}{\partial \dot{w}}\right) - \frac{d}{dx}\left(\frac{\partial T}{\partial \theta_y}\right)\cos\theta_y + \frac{d}{dx}\left(\frac{d}{dt}\left(\frac{\partial T}{\partial \dot{\theta}_y}\right)\cos\theta_y\right) - \frac{d}{dx}\left(\frac{\partial U}{\partial \theta_y}\cos\theta_y\right) + \frac{d}{dx}\left(\frac{d}{dx}\left(\frac{\partial U}{\partial \theta_y'}\right)\cos\theta_y\right) - \frac{d}{dx}\left(\frac{\partial C}{\partial w'}\right)\right\} dx = 0 \tag{2.23}$$

λ variation

$$\int_0^l \left\{ \frac{\partial C}{\partial \lambda} \right\} dx = 0 \tag{2.24}$$

In (2.21)-(2.24) the upper limit l of the integral represents the length of the beam. The nondimensional equations of motion have exactly the same form as (2.21)-(2.24) except that the integral limits are from 0 to 1 instead of from 0 to l. Substituting the energy terms (2.15), (2.18) into (2.21)-(2.24), the following dimensional equations of motion are obtained:

u variation:

$$\int_0^l \Big\{ A\rho\left(-2\,\Omega\, v_{,t} - \Omega^2 u + u_{,tt}\right) - E\left[\frac{\lambda}{E}\left(1+u_{,x}\right) + \sin\left(\theta_y\right)\cos\left(\theta_z\right) I_y\,\theta_{y,xx} - \frac{1}{2}\frac{\sin\left(\theta_z\right)\left(\left(\cos\left(\theta_y\right)\right)^2\left(I_y - I_z\right) - I_y - I_z\right)\theta_{z,xx}}{\cos\left(\theta_y\right)} - \frac{1}{2}\left(I_y - I_z\right)\left(\sin\left(\theta_y\right)\right)^2\cos\left(\theta_y\right)\cos\left(\theta_z\right)\left(\theta_{z,x}\right)^2 + \sin\left(\theta_y\right)\sin\left(\theta_z\right)\left(I_y - I_z\right)\theta_{y,x}\theta_{z,x}\Big]_{,x}\Big\}\, dx = 0 \tag{2.25}$$

v variation:

$$\int_0^l \Big\{ A\rho\left(2\,\Omega\, u_{,t} - \Omega^2 v + v_{,tt}\right) - E\left[\frac{\lambda}{E} v_{,x} + \sin\left(\theta_y\right)\sin\left(\theta_z\right) I_y\,\theta_{y,xx} + \frac{1}{2}\frac{\cos\left(\theta_z\right)\left(\left(\cos\left(\theta_y\right)\right)^2\left(I_y - I_z\right) - I_y - I_z\right)\theta_{z,xx}}{\cos\left(\theta_y\right)} - \frac{1}{2}\left(I_y - I_z\right)\left(\sin\left(\theta_y\right)\right)^2\cos\left(\theta_y\right)\sin\left(\theta_z\right)\left(\theta_{z,x}\right)^2 - \sin\left(\theta_y\right)\cos\left(\theta_z\right)\left(I_y - I_z\right)\theta_{y,x}\theta_{z,x}\Big]_{,x}\Big\}\, dx = 0 \tag{2.26}$$

w variation:

$$\int_0^l \left[A\rho w_{,tt} - E\left(\frac{1}{2}\left(\cos\left(\theta_y\right)\right)^2\sin\left(\theta_y\right)\left(\theta_{z,x}\right)^2\left(I_z - I_y\right) + \cos\left(\theta_y\right)\left(\theta_{y,xx}\right) I_y + \frac{\lambda}{E} w_{,x}\right)_{,x}\right] dx = 0 \tag{2.27}$$

λ variation

$$-\frac{1}{2}\int_0^l \left[\left(1+u_{,x}\right)^2 + \left(v_{,x}\right)^2 + \left(w_{,x}\right)^2 - 1\right] dx = 0 \tag{2.28}$$

The nondimensional form of these equations is presented in the Appendix A (See equations (A.2)-(A.5)).

As can be seen in (2.25)-(2.28), both trigonometric and polynomial nonlinearities appear in the resulting equations of motion. It is important to note that in the derivation of both dimensional and nondimensional equations and their corresponding boundary conditions the variations in θ_y and θ_z are replaced by:

$$\begin{aligned} \delta\theta_z &= -\frac{\sin\theta_z}{\cos\theta_y}\,\delta u' + \frac{\cos\theta_z}{\cos\theta_y}\,\delta v' \\ \delta\theta_y &= -\cos\theta_y\,\delta w' - \cos\theta_z \sin\theta_y\,\delta u' - \sin\theta_z \sin\theta_y\,\delta v' \end{aligned} \tag{2.29}$$

The trigonometric relationships between θ_y, θ_z, u, v and w are used in deriving (2.29). The detailed derivation for (2.29) is shown in A.2.

2.3.8 Natural and Essential Boundary Conditions

The equations of motion (2.25)- (2.28) must also satisfy the natural boundary conditions obtained when the variation operator δ is applied. The natural boundary conditions in dimensional form at the free end of the beam are given by:

$$\begin{aligned} &\Big[\frac{\lambda}{E}\,(1+u_{,x}) + \sin(\theta_y)\cos(\theta_z)\,I_y\,\theta_{y,xx} \\ &-\frac{1}{2}\,\frac{\sin(\theta_z)\left((\cos(\theta_y))^2(-I_z+I_y) - I_y - I_z\right)\theta_{z,xx}}{\cos(\theta_y)} \\ &-\frac{1}{2}\,(-I_z+I_y)(\sin(\theta_y))^2\cos(\theta_y)\cos(\theta_z)\,(\theta_{z,x})^2 \\ &+\sin(\theta_y)\sin(\theta_z)\,(-I_z+I_y)\,(\theta_{y,x})\,\theta_{z,x}\Big]_{x=l} = 0 \end{aligned} \tag{2.30}$$

$$\left[\frac{\lambda}{E}\, v_{,x} + \sin(\theta_y)\sin(\theta_z)\, I_y\, \theta_{y,xx} \right.$$
$$+\frac{1}{2}\,\frac{\cos(\theta_z)\left(\left(\cos(\theta_y)\right)^2(-I_z+I_y)-I_y-I_z\right)\theta_{z,xx}}{\cos(\theta_y)}$$
$$-\frac{1}{2}\,(-I_z+I_y)\left(\sin(\theta_y)\right)^2\cos(\theta_y)\sin(\theta_z)\left(\theta_{z,x}\right)^2$$
$$\left.-\sin(\theta_y)\cos(\theta_z)\,(-I_z+I_y)\,(\theta_{y,x})\,\theta_{z,x}\right]_{x=l}=0 \tag{2.31}$$

$$\left[\frac{1}{2}\left(\cos(\theta_y)\right)^2\sin(\theta_y)\left(\theta_{z,x}\right)^2(-I_y+I_z)+\cos(\theta_y)\,(\theta_{y,xx})\,I_y\right.$$
$$\left.+\frac{\lambda}{E}\,w_{,x}\right]_{x=l}=0 \tag{2.32}$$

$$\left[2\,(\theta_{y,x})\,I_y\,\sin(\theta_y)\cos(\theta_z)+\theta_{z,x}\sin(\theta_z)\cos(\theta_y)\,(I_z-I_y)\right.$$
$$\left.+\frac{\theta_{z,x}\sin(\theta_z)\,(I_y+I_z)}{\cos(\theta_y)}\right]_{x=l}=0 \tag{2.33}$$

$$\left[2\,(\theta_{y,x})\,I_y\,\sin(\theta_y)\sin(\theta_z)+\theta_{z,x}\cos(\theta_z)\cos(\theta_y)\,(I_y-I_z)\right.$$
$$\left.-\frac{\theta_{z,x}\cos(\theta_z)\,(I_y+I_z)}{\cos(\theta_y)}\right]_{x=l}=0 \tag{2.34}$$

$$\left[(\theta_{y,x})\,I_y\,\cos(\theta_y)\right]_{x=l}=0 \tag{2.35}$$

At $x = 0$, the fixed end of the beam, the following essential boundary conditions are enforced:

$$\begin{aligned} u(x,t)\,|_{x=0} &= 0 \\ u_{,x}(x,t)\,|_{x=0} &= 0 \\ v(x,t)\,|_{x=0} &= 0 \\ v_{,x}(x,t)\,|_{x=0} &= 0 \\ w(x,t)\,|_{x=0} &= 0 \\ w_{,x}(x,t)\,|_{x=0} &= 0 \\ \lambda(x,t)\,|_{x=0} &= 0 \end{aligned} \tag{2.36}$$

In nondimensional form the boundary conditions are same as in dimensional case except that now we don't have E and all the other dimensional parameters are replaced by nondimensional parameters.

2.3.9 Initial Conditions

In this thesis it is assumed that the system is not subjected to external forces and therefore only a free vibration problem is considered with the initial values being prescribed and the time evolution being investigated. The following initial values are assumed:

$$\begin{aligned} u(x,0) = u_0(x) \quad & \tfrac{\partial u(x,t)}{\partial t}\,|_{t=0} = 0 \\ v(x,0) = v_0(x) \quad & \tfrac{\partial v(x,t)}{\partial t}\,|_{t=0} = 0 \\ w(x,0) = w_0(x) \quad & \tfrac{\partial w(x,t)}{\partial t}\,|_{t=0} = 0 \end{aligned} \tag{2.37}$$

where $u_0(x)$, $v_0(x)$ and $w_0(x)$ is the initial deflection curve of the beam, and all the initial velocities are assumed to be zero.

It is essential to select the initial values such that the boundary conditions in Section 2.3.8 are satisfied. In this work the following equations are used as the initial longitudinal and transverse deflections for dimensional case:

$$\begin{aligned} v_0(x) &= \frac{v_{t0}}{2}\,(\cosh(k_1 x) - \cos(k_1 x) \\ &\quad - \frac{\cos(k_1 l) + \cosh(k_1 l)}{\sin(k_1 l) + \sinh(k_1 l)}(\sinh(k_1 x) - \sin(k_1 x))) \qquad (2.38) \\ w_0(x) &= \frac{w_{t0}}{2}\,(\cosh(k_1 x) - \cos(k_1 x) \\ &\quad - \frac{\cos(k_1 l) + \cosh(k_1 l)}{\sin(k_1 l) + \sinh(k_1 l)}(\sinh(k_1 x) - \sin(k_1 x))) \qquad (2.39) \end{aligned}$$

where v_{t0} and w_{t0} are prescribed tip deflections. Equations (2.38) and (2.39) are the scaled first mode shape of a simple cantilever beam ($k_1 = 1.34223627$). The first mode shape is chosen because all the other higher order modes are quite small and thus negligible. Taking the second and third derivatives of (2.38) and (2.39) it can be easily verified that the initial deflections described in (2.38) and (2.39) satisfy all the boundary conditions in Section 2.3.8. The nondimensional initial deflection equations are same as the dimensional ones expect that the parameter l in (2.38) and (2.39) does not appear.

The initial value for the axial variable u is obtained from the constraint equation (2.1) as:

$$\frac{\partial u}{\partial x} = -1 + \sqrt{1 - \left(\frac{\partial v}{\partial x}\right)^2 - \left(\frac{\partial w}{\partial x}\right)^2} \qquad (2.40)$$

where the positive square root is selected. The value of u is obtained using numerical

integration. Further, the initial values of λ are assumed to be zero because the above initial deformation field already satisfies the algebraic constraint. Figures 2.4 and 2.5 show graphical depictions of the initial values for $u, v,$ and w and their higher order derivatives for dimensional and nondimensional cases respectively. The figures also reveal that all the boundary conditions corresponding to u, v, and w given in Section 2.3.8 are satisfied.

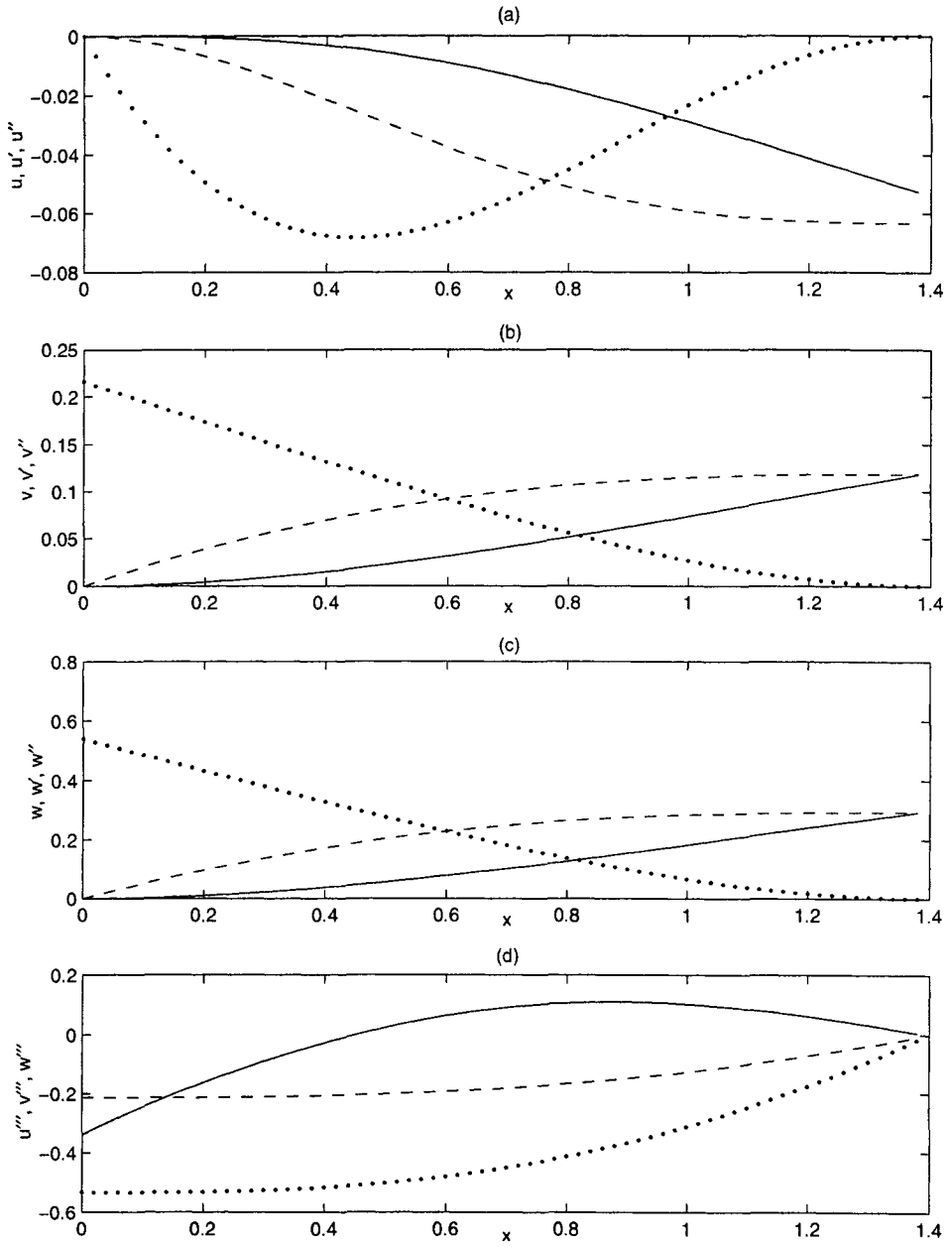

Figure 2.4: Initial values (a) (-)u, (- -)u', (...)u'', (b) (-)v, (- -)v', (...)v'', (c) (-)w, (- -)w', (...)w'', (d) (-)u''', (- -)v''', (...)w'''. u, v and w are in m, u', v' and w' are in rad, u'', v'' and w'' are in $1/m$, u''', v''' and w''' are in $1/m^2$.(dimensional case)

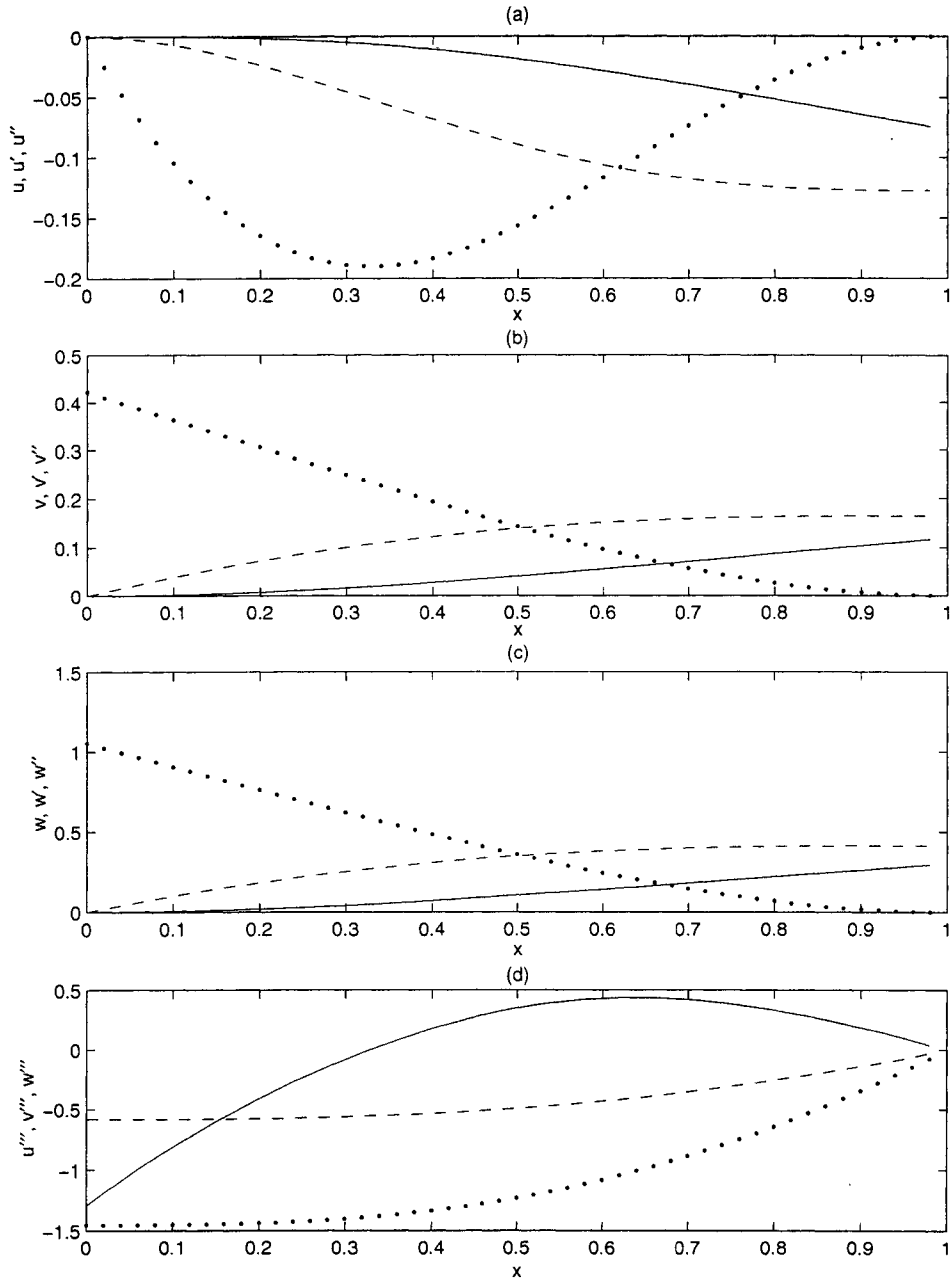

Figure 2.5: Initial values (a) (-)u, (- -)u', (...)u'', (b) (-)v, (- -)v', (...)v'', (c) (-)w, (- -)w', (...)w'', (d) (-)u''', (- -)v''', (...)w'''. (nondimensional case)

In this Chapter, equations of motion were developed for arbitrarily large dimensional and nondimensional oscillation models. In the following chapters strategies will be discussed to discretize, solve, and simulate the obtained governing equations and a vibration suppression strategy can be therefore developed.

Chapter 3

Spatial Discretization

The equations of motion obtained are nonlinear partial differential equations. The focus of this chapter is on reducing the obtained equations to ordinary differential equations using Galerkin method. The reduction of PDEs in space and time to ODEs in space coordinates alone is referred to as semi-discretization process. The resulting ODEs are expressed in terms of time dependent coefficient functions and spatial basis functions. It is important to choose the right type and sufficient number of basis functions in the discretization process so that the solution of the semi-discretized ordinary differential equations converges to the solution of the original partial differential equations. To this end, basis functions are chosen such that the resulting approximation satisfies the continuity requirements and boundary conditions of the partial differential equations. Since the highest spatial derivative of the beam is of fourth order, it implies that the solution must have continuous fourth derivative, which is very difficult to achieve. To reduce the continuity requirement, integration by parts is employed when applying the Galerkin method.

This approach not only reduces the continuity requirement but also incorporates the natural boundary conditions in the process.

In this work, the eigenfunctions corresponding to the cantilever beam are used as basis functions.

3.1 Symmetric Formulation

Following the Galerkin's approach [8, 9] the equations of motion in Section 2.3.7 are first multiplied by a weighting function $p(x)$ and then integrated by parts twice. The integration by parts renders the equations symmetrically. The natural boundary conditions in Section 2.3.8 are combined into the equations of motion during the integration by parts process. Applying the relationship between the angles θ_y, θ_z and the elastic deformations u, v, w (see equation (2.1)) yields the following symmetric equations of motion in dimensional form:

u variation:

$$\int_0^l \left\{ p\,A\,\rho\left(u_{,tt} - 2\,\Omega\,v_{,t} - \Omega^2 u\right) + E\left(\left(u_{,xx}\right) I_y - \frac{1}{2\left(1-\left(w_{,x}\right)^2\right)^2}\left(I_z + I_y\right)\right.\right.$$
$$\left(v_{,x}\right)\left(\left(1+u_{,x}\right)v_{,xx} - \left(v_{,x}\right)u_{,xx}\right) - \frac{1}{2\left(1-\left(w_{,x}\right)^2\right)}\left(I_z - 3\,I_y\right)\left(v_{,x}\right)$$
$$\left(\left(1+u_{,x}\right)v_{,xx} - \left(v_{,x}\right)u_{,xx}\right)\right) p_{,xx} + E\left(-\frac{I_y\left(1+u_{,x}\right)\left(w_{,xx}\right)^2}{1-\left(w_{,x}\right)^2}\right.$$
$$-\frac{1}{2\left(1-\left(w_{,x}\right)^2\right)^3}\left(I_z + I_y\right)\left(\left(1+u_{,x}\right)\left(\left(\left(v_{,x}\right)u_{,xx} - \left(1+u_{,x}\right)v_{,xx}\right)^2\right.\right.$$
$$\left.\left.+\left(v_{,x}\right)\left(v_{,xx}\right)\left(w_{,x}\right)w_{,xx}\right) - \left(v_{,x}\right)^2\left(u_{,xx}\right)\left(w_{,x}\right)w_{,xx}\right) - \frac{1}{2\left(1-\left(w_{,x}\right)^2\right)^2}$$
$$\left(I_z - 3\,I_y\right)\left(\left(v_{,x}\right)\left(v_{,xx}\right)\left(w_{,x}\right)\left(w_{,xx}\right)\left(1+u_{,x}\right) - \left(v_{,x}\right)^2\left(u_{,xx}\right)\left(w_{,x}\right)w_{,xx}\right)$$
$$+\frac{1}{2\left(1-\left(w_{,x}\right)^2\right)}\left(I_y - I_z\right)\left(1+u_{,x}\right)\left(\left(v_{,x}\right)u_{,xx} - \left(1+u_{,x}\right)v_{,xx}\right)^2$$
$$\left.\left.+\frac{\lambda}{E}\left(1+u_{,x}\right)\right) p_{,x}\right\} dx = 0 \qquad (3.1)$$

v variation:

$$\int_0^l \Big\{ p\,A\,\rho\left(v_{,tt} + 2\,\Omega\,u_{,t} - \Omega^2 v\right) + E\left(\left(v_{,xx}\right) I_y + \frac{1}{2\left(1-\left(w_{,x}\right)^2\right)^2}\left(I_z + I_y\right)\right.$$
$$\left(1+u_{,x}\right)\left(\left(1+u_{,x}\right)v_{,xx} - \left(v_{,x}\right)u_{,xx}\right) + \frac{1}{2\left(1-\left(w_{,x}\right)^2\right)}\left(I_z - 3\,I_y\right)$$
$$\left(1+u_{,x}\right)\left(\left(1+u_{,x}\right)v_{,xx} - \left(v_{,x}\right)u_{,xx}\right)\Big)p_{,xx} + E\left(-\frac{I_y\left(v_{,x}\right)\left(w_{,xx}\right)^2}{1-\left(w_{,x}\right)^2}\right.$$
$$-\frac{1}{2\left(1-\left(w_{,x}\right)^2\right)^3}\left(I_z + I_y\right)\Big(\left(v_{,x}\right)\Big(\left(\left(v_{,x}\right)u_{,xx} - \left(1+u_{,x}\right)v_{,xx}\right)^2$$
$$+\left(1+u_{,x}\right)\left(u_{,xx}\right)\left(w_{,x}\right)w_{,xx}\Big) - \left(1+u_{,x}\right)^2\left(v_{,xx}\right)\left(w_{,x}\right)w_{,xx}\Big) +$$
$$\frac{1}{2\left(1-\left(w_{,x}\right)^2\right)^2}\left(I_z - 3\,I_y\right)\Big(\left(1+u_{,x}\right)^2\left(v_{,xx}\right)\left(w_{,x}\right)w_{,xx} - \left(1+u_{,x}\right)\left(v_{,x}\right)$$
$$\left(u_{,xx}\right)\left(w_{,x}\right)w_{,xx}\Big) + \frac{1}{2\left(1-\left(w_{,x}\right)^2\right)}\left(I_y - I_z\right)\left(v_{,x}\right)\Big(\left(v_{,x}\right)u_{,xx}$$
$$\left.\left.-\left(1+u_{,x}\right)v_{,xx}\right)^2 + \frac{\lambda}{E}v_{,x}\right)p_{,x}\Big\}\,dx = 0 \qquad (3.2)$$

w variation:

$$\int_0^l \left[p\,A\,\rho w_{,tt} + E I_y\left(w_{,xx}\right)p_{,xx} + E\left(\frac{\lambda}{E}w_{,x} - \frac{I_y\left(w_{,x}\right)\left(w_{,xx}\right)^2}{1-w_{,x}^2}\right.\right.$$
$$\left.\left.-\frac{1}{2}\frac{\left(I_z - I_y\right)\left(w_{,x}\right)\left(\left(v_{,x}\right)u_{,xx} - \left(1+u_{,x}\right)v_{,xx}\right)^2}{1-w_{,x}^2}\right)p_{,x}\right]\,dx = 0 \qquad (3.3)$$

λ variation

$$-\frac{1}{2}\int_0^l \left[\left(1+u_{,x}\right)^2 + \left(v_{,x}\right)^2 + \left(w_{,x}\right)^2 - 1\right]\,dx = 0 \qquad (3.4)$$

Likewise, the nondimensional symmetric form of equations of motion are obtained which are given in the Appendix A.3 (See equations (A.18)-(A.21)).

In (3.1)-(3.4), the dependent variables $u(x,t)$, $v(x,t)$, $w(x,t)$ and $p(x)$ have the same highest order of derivative, which implies that the formulation is symmetric.

3.2 Spatial Discretization

To apply Galerkin method, the following approximations are assumed:

$$\begin{aligned} u(x,t) &= \sum_i \alpha_i(t)\phi_i(x) \\ v(x,t) &= \sum_i \beta_i(t)\phi_i(x) \\ w(x,t) &= \sum_i \gamma_i(t)\phi_i(x) \\ \lambda(x,t) &= \sum_i \lambda_i(t)\phi_i(x) \\ p(x) &= \sum_i p_i\phi_i(x) \end{aligned} \tag{3.5}$$

The summation in (3.5) is carried out over i from 1 to ∞. The continuity requirements for u, v, w and p have already been rendered the same in preceding section. Therefore the same basis functions ϕ_i can be chosen for u, v, w and p. Also the number of basis functions for u, v, w and p are assumed to be the same. The unknown parameters p_i in (3.5) are arbitrary and substituting (3.5) into the equations of motion (3.1)-(3.4) and setting p_i (the i^{th} value of p) to one and all other p_j ($j \neq i$ and the maxima of j is the same as i) to zero gives the i^{th} semi-discretized equations [27]. Consequently the following dimensional semi-discretized equations are obtained:

u equation:

$$\int_0^l \Big[EI_y \{\phi_i''\} \lfloor \phi_j'' \rfloor \{\alpha_j\} + [\phi_i' \phi_j] \{\lambda_j\} + A\rho [\phi_i \phi_j] \Big\{ \{\ddot{\alpha}_j\} - 2\Omega \Big\{ \dot{\beta}_j \Big\} - \Omega^2 \{\alpha_j\} \Big\} + \{\phi_i'\} \lfloor \phi_j \phi_k' \rfloor \{\lambda_j \alpha_k\} + \{\phi_i'\} \lfloor \phi_j'' \phi_k'' \rfloor \{-EI_z \{\beta_j \beta_k\} - EI_y \{\gamma_j \gamma_k\}\} + A\rho \{\phi_i\} \lfloor \phi_j \phi_k' \phi_l' \rfloor \Big\{ -3 \{\ddot{\alpha}_j \gamma_k \gamma_l\} + 6\Omega \Big\{ \dot{\beta}_j \gamma_k \gamma_l \Big\} + 3\Omega^2 \{\alpha_j \gamma_k \gamma_l\} \Big\} + \{\phi_i''\} \lfloor \phi_j' \phi_k' \phi_l'' \rfloor \{E(I_y - I_z) \{\alpha_j \beta_k \beta_l\} - E(I_y - I_z) \{\beta_j \beta_k \alpha_l\} - 3EI_y \{\gamma_j \gamma_k \alpha_l\}\} + \{\phi_i'\} \lfloor \phi_j' \phi_k'' \rfloor \{-3EI_z \{\alpha_j \beta_k \beta_l\} - EI_y \{\alpha_j \gamma_k \gamma_l\} + 2EI_z \{\beta_j \alpha_k \beta_l\}\} - 3 \{\phi_i'\} \lfloor \phi_j \phi_k' \phi_l' \rfloor \{\lambda_j \gamma_k \gamma_l\} \Big] dx = 0 \tag{3.6}$$

v equation:

$$\int_0^l \Big[EI_z [\phi_i'' \phi_j''] \{\beta_j\} + A\rho [\phi_i \phi_j] \Big\{ \Big\{ \ddot{\beta}_j \Big\} + 2\Omega \{\dot{\alpha}_j\} - \Omega^2 \{\beta_j\} \Big\} + \{\phi_i'\} \lfloor \phi_j \phi_k' \rfloor \{\lambda_j \beta_k\} + \{\phi_i''\} \lfloor \phi_j' \phi_k'' \rfloor \{-2E(I_y - I_z) \{\alpha_j \beta_k\} + E(I_y - I_z) \{\beta_j \alpha_k\}\} + A\rho \{\phi_i\} \lfloor \phi_j \phi_k' \phi_l' \rfloor \Big\{ -3 \Big\{ \ddot{\beta}_j \gamma_k \gamma_l \Big\} - 6\Omega \{\dot{\alpha}_j \gamma_k \gamma_l\} + 3\Omega^2 \{\beta_j \gamma_k \gamma_l\} \Big\} + \{\phi_i'\} \lfloor \phi_j' \phi_k'' \phi_l'' \rfloor \{-EI_z \{\beta_j \beta_k \beta_l\} - EI_y \{\beta_j \gamma_k \gamma_l\} - E(I_y - I_z) \{\gamma_j \beta_k \gamma_l\}\} + \{\phi_i''\} \lfloor \phi_j' \phi_k' \phi_l'' \rfloor \{-E(I_y - I_z) \{\alpha_j \alpha_k \beta_l\} + E(I_y - I_z) \{\alpha_j \beta_k \alpha_l\} - \frac{1}{2} E(3I_z + I_y) \{\gamma_j \gamma_k \beta_l\} \Big\} \Big] dx = 0 \tag{3.7}$$

w equation:

$$\int_0^l \left[EI_y \left[\phi_i'' \, \phi_j''\right] \{\gamma_j\} + A\rho \left[\phi_i \, \phi_j\right] \{\ddot{\gamma}_j\} + \{\phi_i'\} \lfloor \phi_j \, \phi_k' \rfloor \{\lambda_j \, \gamma_k\} \right.$$
$$-A\rho \, \{\phi_i\} \lfloor \phi_j \, \phi_k' \, \phi_l' \rfloor \{\ddot{\gamma}_j \, \gamma_k \, \gamma_l\} + \{\phi_i'\} \lfloor \phi_j' \, \phi_k'' \, \phi_l'' \rfloor \left\{ \frac{1}{2} E \left(I_y - I_z\right) \right.$$
$$\{\gamma_j \, \beta_k \, \beta_l\} - EI_y \, \{\gamma_j \, \gamma_k \, \gamma_l\}\}$$
$$\left. -EI_y \, \{\phi_i''\} \lfloor \phi_j' \, \phi_k' \, \phi_l'' \rfloor \{\gamma_j \, \gamma_k \, \gamma_l\} \right] dx = 0 \tag{3.8}$$

λ equation

$$\int_0^l \left[\left[\phi_i \, \phi_j'\right] \{\alpha_j\} + \{\phi_i\} \lfloor \phi_j' \, \phi_k' \rfloor \left\{ \frac{1}{2} \{\alpha_j \, \alpha_k\} + \frac{1}{2} \{\beta_j \, \beta_k\} \right.\right.$$
$$\left.\left. + \frac{1}{2} \{\gamma_j \, \gamma_k\} \right\} \right] dx = 0 \tag{3.9}$$

where $\lfloor \cdots \rfloor$ denote a row matrix, $\{\cdots\}$ denote a column matrix and $[\cdots]$ denote a square matrix. Thus, the obtained equations (3.6)-(3.9) are ordinary differential equations with both quadratic and cubic nonlinearities that can be directly used for numerical simulations in the following chapters. Also it can be seen from (3.6)-(3.9) that the number of equations of motion is decided by the number of basis functions ϕ_i used for the approximation. The basis functions are discussed in next section.

Following the same approach used for dimensional model, the nondimensional semi-discretized equations are obtained which are given in Appendix A.3 (See equations (A.22)-(A.25)).

3.3 Eigenfunction of a Cantilever Beam

As mentioned earlier, the eigenfunctions of a simple cantilever beam are chosen as basis functions in the Galerkin method. The basis functions have the desirable property of orthogonality so as to facilitate solving the initial value problem by producing diagonal matrices.

The cantilever beam eigenfunctions for the dimensional parameters used are as follows [8]:

$$\phi_i = \cosh(k_i x) - \cos(k_i x) - \frac{\cos(k_i l) + \cosh(k_i l)}{\sin(k_i l) + \sinh(k_i l)}(\sinh(k_i x) - \sin(k_i x)) \qquad (3.10)$$

where l denotes the length of the beam. For the first four modes, k_i have the following values:

$$k_1 = 1.3422 \quad k_2 = 3.3601 \quad k_3 = 5.6226 \quad k_4 = 7.8708$$

The four mode shapes are shown in Figure 3.1. The mass and stiffness matrices in (3.6)-(3.9) are obtained through integration of products of basis functions and their second derivatives over the length of the beam. All the integrations in (3.6)-(3.9) are carried out analytically using the symbolic manipulation program Maple. The

following mass and stiffness matrices are thus obtained for the dimensional model:

$$[M_{ij}] = \left[\int_0^l \phi_i \phi_j \, dx\right] = \begin{bmatrix} 1.397 & 0 & 0 & 0 \\ 0 & 1.397 & 0 & 0 \\ 0 & 0 & 1.397 & 0 \\ 0 & 0 & 0 & 1.397 \end{bmatrix} \tag{3.11}$$

$$[K_{ij}] = \left[\int_0^l \phi_i'' \phi_j'' \, dx\right]$$

$$= \begin{bmatrix} 4.5343 & 0 & 0 & 0 \\ 0 & 178.0807 & 0 & 0 \\ 0 & 0 & 1396.1815 & 0 \\ 0 & 0 & 0 & 5361.3869 \end{bmatrix} \tag{3.12}$$

The mass and stiffness matrices for the nondimensional parameters are similarly obtained. The basis functions and the matrices are given in the Appendix A.4.

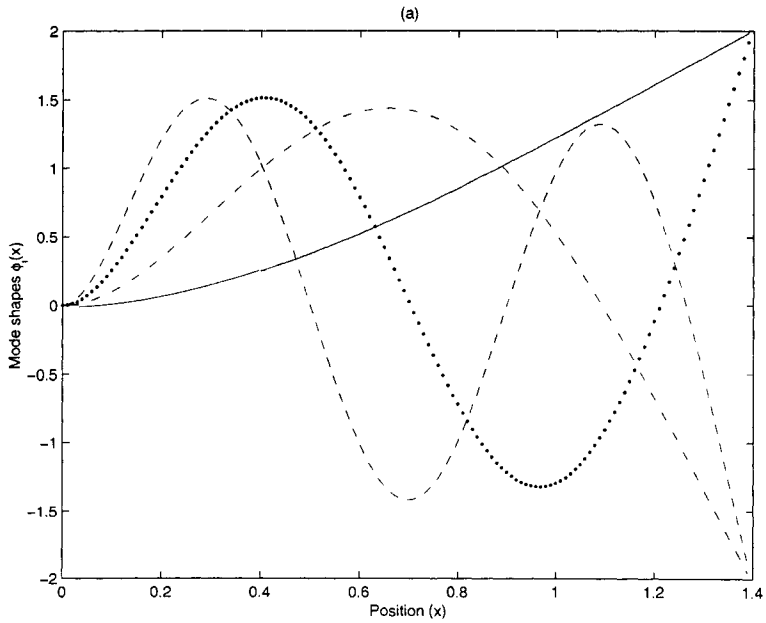

Figure 3.1: Dimensional mode shapes, (-) ϕ_1, (-.) ϕ_2, (...) ϕ_3, (- -) ϕ_4

Other terms in (3.6)-(3.9) are nonlinear and will require online assembly which is explained later in Chapter 5.

In the next Chapter, a vibration suppression strategy based on Internal Resonance state will be discussed and various types of IR ratio will be obtained.

Chapter 4

Vibration Suppression

The vibration suppression strategy used in this work is based on enhancing the modal coupling in the rotating Euler-Bernoulli beam using Internal Resonance (IR). The rotation of the beam coupled with the three vibratory modes results in gyroscopic coupling in the system. Internal resonance occurs when the three natural frequencies become commensurable, that is $a_1\omega_1 \pm a_2\omega_2 \pm a_3\omega_3 = 0$, where a_s are integral constants and ω_s are the three linear natural frequencies of the system [42]. The commensurable relationships of frequencies can lead to strong modal coupling and the gyroscopic beam may exhibit an amplitude modulated motion.

The coupling in the system is the basic reason for energy transfer between the modal amplitudes. When IR exists in the system, energy laid up initially in some particular modes will be continuously and rapidly exchanged among other resonant modes involved in that specific Internal Resonance. Different IR ratio can be chosen according to the type of coupling in the system. Gyroscopic system can exhibit both linear and nonlinear coupling. When the system has linear coupling,

it is possible to obtain 1:1 IR (any two frequencies in 1:1 ratio) through tuning its natural frequencies. When the system also has quadratic and cubic nonlinearities, 1:2 and 1:3 Internal Resonance ratios can be established. As mentioned in Chapter 1, tuning natural frequencies in this thesis implies tip displacement feedback control that is acquired by applying two P controllers to the gyroscopic system in any two out of the three directions u, v and w. For obtaining natural frequencies the nonlinear equations of motion are linearized about the equilibrium position using Taylor series expansion. To suppress vibration in the system, damping is introduced into the system through velocity feedback using two D controllers. Consequently, energy will be steadily exchanged and reduced. The implementation of IR control strategy is discussed in detail towards the end of this chapter.

4.1 Control Efforts

As discussed in Chapter 1, vibration suppression strategy used in this work is based on strengthening the modal coupling in the system through establishing Internal Resonance between the modes. To establish IR, the natural frequencies of the beam need to be calculated first. Also three P controller terms with gains K_{pu}, K_{pv} and K_{pw} are applied in u, v and w directions, respectively, to serve as displacement feedback for tuning the natural frequencies. The tuning efforts are added to the first mode shapes of the beam resulting in addition of the term $K_{pu}\alpha_1$ for u direction, $K_{pv}\beta_1$ for v direction and $K_{pw}\gamma_1$ for w direction. Here only first mode displacement feedback is considered because a low-pass filter can be used to remove those higher order modes physically. The position feedback controller

gains K_{pu}, K_{pv} and K_{pw} appear as components of stiffness matrix of the nonlinear gyroscopic beam equations.

4.2 Linearized Equations of Motion

In this section, the nonlinear equations of motion are linearized about equilibrium position to obtain natural frequencies of the system using Taylor series expansion.

4.2.1 Equilibrium Position

Equilibrium position is the position where both velocity and acceleration of the system are zero. Setting velocities and accelerations to zero in the first mode form of (3.6)-(3.9) gives the following equations for equilibrium value:

$$\begin{aligned}
(73115.9302 - 24.0033\,\Omega^2 + 3.7194\,\lambda)\,\alpha - 3219357.2730\,\beta^2 \\
-55827.0047\,\gamma^2 + 2.0\,\lambda = 0 \\
(2144733.9540 - 24.0033\,\Omega^2 + 3.7194\,\lambda + 1581765.1340\,\alpha)\,\beta = 0 \\
(73115.9302 + 3.7194\,\lambda)\,\gamma = 0 \\
2.0\,\alpha + 1.8597\,\alpha^2 + 1.8597\,\beta^2 + 1.8597\,\gamma^2 = 0
\end{aligned} \tag{4.1}$$

It can be seen from (4.1) that equilibrium positions are generally dependent on angular velocity Ω. The zero equilibrium position ($\alpha = 0$, $\beta = 0$, $\gamma = 0$, $\lambda = 0$) is the only equilibrium value that is independent of Ω. In this work, zero equilibrium position is selected to carry out the Taylor series expansion and obtain the linearized

equations and the characteristic values of the gyroscopic system. Therefore the following approximate equations of motion are obtained in the neighborhood of zero equilibrium point where α, β and γ represent motion about the equilibrium position:

$$\begin{bmatrix} A\rho\int_0^l \phi_1\phi_1 dx & 0 & 0 \\ 0 & A\rho\int_0^l \phi_1\phi_1 dx & 0 \\ 0 & 0 & A\rho\int_0^l \phi_1\phi_1 dx \end{bmatrix} \begin{bmatrix} \ddot{\alpha} \\ \ddot{\beta} \\ \ddot{\gamma} \end{bmatrix}$$

$$+ \begin{bmatrix} 0 & -2\Omega A\rho\int_0^l \phi_1\phi_1 dx & 0 \\ 2\Omega A\rho\int_0^l \phi_1\phi_1 dx & 0 & 0 \\ 0 & 0 & 0 \end{bmatrix} \begin{bmatrix} \dot{\alpha} \\ \dot{\beta} \\ \dot{\gamma} \end{bmatrix}$$

$$+ \begin{bmatrix} EI_y\int_0^l \phi_1''\phi_1'' dx - \Omega^2 A\rho\int_0^l \phi_1\phi_1 dx + K_{pu} & 0 & 0 \\ 0 & EI_z\int_0^l \phi_1''\phi_1'' dx - \Omega^2 A\rho\int_0^l \phi_1\phi_1 dx + K_{pv} & 0 \\ 0 & 0 & EI_y\int_0^l \phi_1''\phi_1'' dx + K_{pw} \end{bmatrix} \begin{bmatrix} \alpha \\ \beta \\ \gamma \end{bmatrix} = \begin{bmatrix} 0 \\ 0 \\ 0 \end{bmatrix} \tag{4.2}$$

In (4.2) the integral upper limit l is the length of the beam. Similarly, the nondimensional form of approximate equations of motion in the neighborhood of zero equilibrium point can be obtained which are shown in Appendix A.5 (See equations (A.29)).

4.2.2 Characteristic Equation

Based on the approximate equations of motions obtained in the previous section, the natural frequencies of the given system can be obtained. The following solutions are assumed for (4.2):

$$\begin{aligned} \alpha &= a_1 e^{j\omega t} \\ \beta &= a_2 e^{j\omega t} \\ \gamma &= a_3 e^{j\omega t} \end{aligned} \tag{4.3}$$

where a_1, a_2, a_3 and ω are in general complex. Substituting (4.3) into (4.2) yields the following system of linear algebraic equations:

$$\begin{bmatrix} c_2 - c_1\omega^2 & -jc_3\omega & 0 \\ jc_3\omega & c_4 - c_1\omega^2 & 0 \\ 0 & 0 & c_5 - c_1\omega^2 \end{bmatrix} \begin{Bmatrix} a_1 \\ a_2 \\ a_3 \end{Bmatrix} = \begin{Bmatrix} 0 \\ 0 \\ 0 \end{Bmatrix} \tag{4.4}$$

For dimensional model, c_1 to c_5 are as follows:

$$\begin{aligned} c_1 &= 24.0033 \\ c_2 &= 73115.9302 + 4.5343\,K_{pu} - 24.0033\,\Omega^2 \\ c_3 &= 48.0065\,\Omega \\ c_4 &= 2144733.9540 + 4.5343\,K_{pv} - 24.0033\,\Omega^2 \\ c_5 &= 73115.9302 + 4.5343\,K_{pw} \end{aligned} \tag{4.5}$$

where Ω represents angular velocity of the beam. Equations similar to (4.4) are obtained for the nondimensional model and the corresponding c values are given in Appendix A.30 (See (A.30)).

Finding the determinant of the characteristic matrix in (4.4) yields the same characteristic equation for dimensional and nondimensional models, which is given by:

$$\begin{aligned} & {c_1}^3\omega^6 + \left(-c_2\,{c_1}^2 - {c_1}^2 c_4 - {c_1}^2 c_5 - {c_3}^2 c_1\right)\omega^4 \\ & + \left(c_2\,c_4\,c_1 + c_2\,c_1\,c_5 + c_1\,c_4\,c_5 + {c_3}^2 c_5\right)\omega^2 - c_2\,c_4\,c_5 = 0 \end{aligned} \tag{4.6}$$

Equation (4.6) is a sixth order polynomial with six roots but the roots occur in complex conjugate pairs. The three positive roots ω_1, ω_2, and ω_3 are the linear natural frequencies of the system. Since the system is a gyroscopic and coupled system when the angular velocity $\Omega \neq 0$, the three linear natural frequencies will appear in the responses of u, v as well as w simultaneously. However, the first equation in (4.2) will disappear when $\Omega = 0$ because the foreshortening effect in u appears

only when gyroscopic effect is present and system is nonlinearly modelled. Also the linearized system will become uncoupled and v and w will become independent of each other when $\Omega = 0$. At this time, the two natural frequencies ω_1 and ω_2 are related to directions v and w, respectively. The expressions of the three natural frequencies for coupled system are the same for both dimensional and nondimensional models and given by:

$$\begin{aligned}
{\omega_1}^2 &= \frac{c_1\,c_2 + c_1\,c_4 + {c_3}^2 + \sqrt{(c_1\,c_2 + c_1\,c_4 + {c_3}^2)^2 - 4\,{c_1}^2\,c_2\,c_4}}{2\,{c_1}^2} \\
{\omega_2}^2 &= \frac{c_1\,c_2 + c_1\,c_4 + {c_3}^2 - \sqrt{(c_1\,c_2 + c_1\,c_4 + {c_3}^2)^2 - 4\,{c_1}^2\,c_2\,c_4}}{2\,{c_1}^2} \\
{\omega_3}^2 &= \frac{c_5}{c_1}
\end{aligned} \tag{4.7}$$

Equations (4.5), (A.30) and (4.7) show that the natural frequencies ω_1 and ω_2 are both dependent on tuning parameters K_{pu} and K_{pv}, the third natural frequency ω_3 is only dependent on tuning parameter K_{pw}. Therefore, by tuning K_{pu}, K_{pv} and K_{pw} any desired IR ratio can be established. It is important to note that the term K_{pu} is added to the u equation in (4.2) to serve two purposes: First, to account for the effect the P controller with gain K_{pw} applied in the w direction would have in the u direction when modelled properly. Secondly, to establish 1:2 IR, independent tuning is required in the u direction. This is achieved by another P controller applied in the u direction. To account for the first effect, the value of K_{pu} is chosen to be same as K_{pw} for 1:1 IR case where only one P controller in the w direction is needed. The reason for choosing K_{pu} to be same as K_{pw} is due to the fact that the term $K_{pw}\,\gamma$ behaves in exactly the manner as a stiffness term $EI_y \int_0^l \phi_1'' \phi_1'' dx$ and

the effect of $EI_y\phi_1''\phi_1''$ is same in the u direction as it is in the w direction.

4.2.3 Variation of Natural Frequencies

In this section 1:1 IR and 1:2 IR ratios are set up for the gyroscopic system by tuning different P controllers. From (4.5) and (4.7) one can see that the natural frequencies of the model are dependent on K_{pu}, K_{pv}, K_{pw} and angular velocity Ω.

Figure 4.1 shows the relationship between the system natural frequencies ω_1, ω_2 and the angular velocity Ω. The natural frequency ω_3 is not shown because it is independent of Ω. For simplicity sake, the parameter $\Omega = 50\ rad/s$ is assumed, which is actually the maximum angular velocity of the Rotor Experimental System mentioned in Chapter 2. In general the natural frequency of the system may or may not be naturally exhibiting an IR state. The vibration suppression strategy aims at establishing an Internal Resonance state by tuning the gains K_{pv} and K_{pw}.

Figure 4.2(a) shows the variation in ω_1 and ω_2 with K_{pu} indicating that it is possible to minimize the gap between the two roots and obtain an approximate 1:1 IR ratio when $K_{pu} = 4.57e5$. Figure 4.2(b) shows the variation in ω_1 and $2\omega_2$ with K_{pu} illustrating that an exact 1:2 ratio can be obtained when $K_{pu} = 1.524e5$. Variation in frequencies due to K_{pw} is not shown as it only affects ω_3. By varying K_{pw} ω_3 can be adjusted to any desired value.

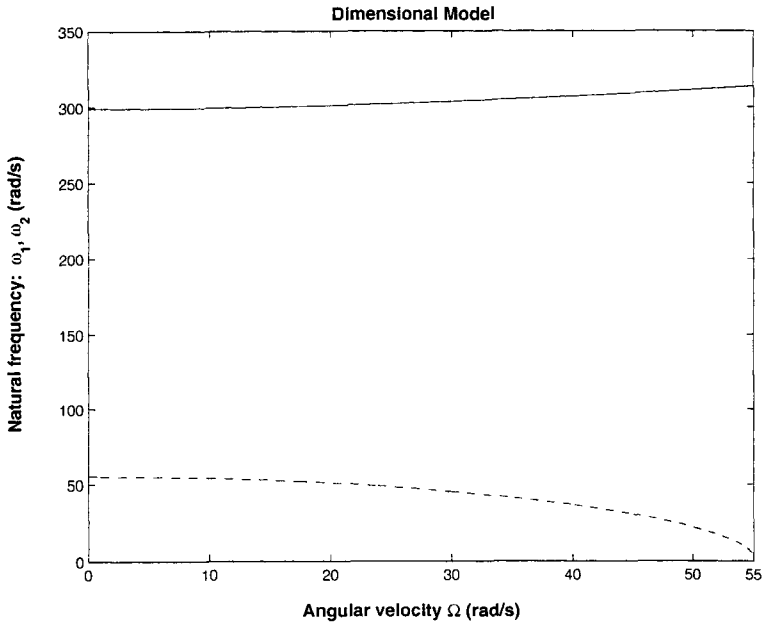

Figure 4.1: Variation in ω_1 and ω_2 with respect to Ω, (-) ω_1, (- -) ω_2

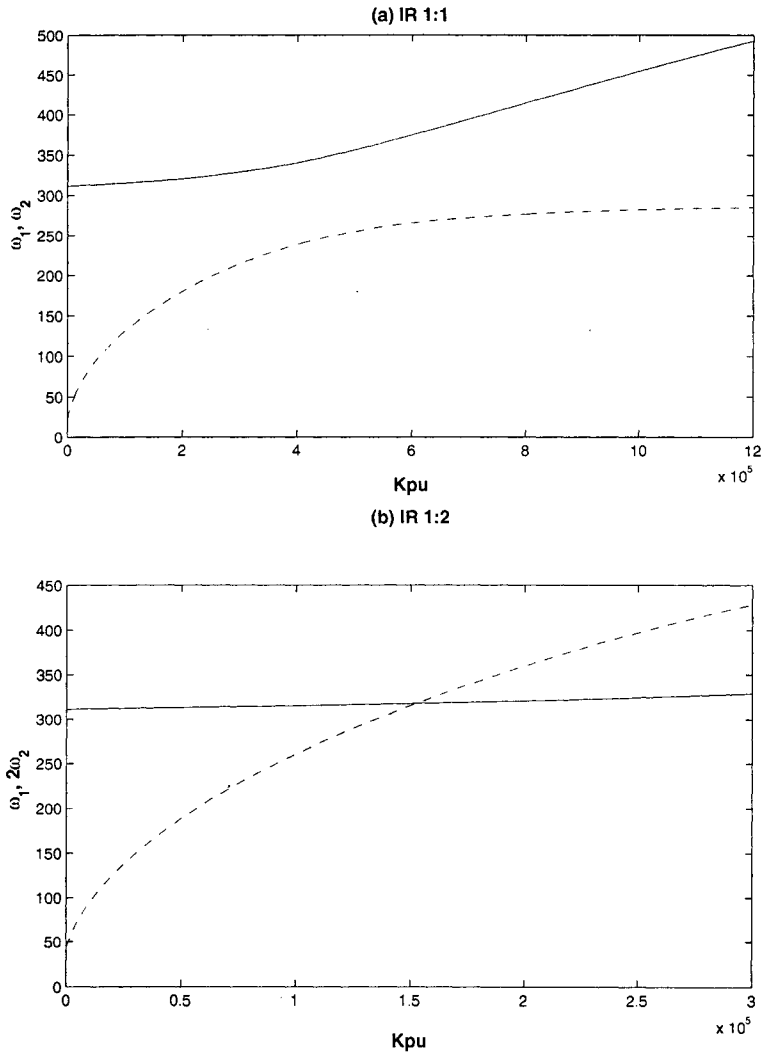

Figure 4.2: Variation in ω_1 and ω_2 with respect to K_{pu}, (a) 1:1 IR and (b) 1:2 IR, (-) ω_1, (- -) ω_2

It is also clear from Figure 4.2 that the gains required to tune the system is quite high. However, it should be realized that is not unusual because of the high frequencies of the system and the incorporation of the basis function parameter $\phi(l)$. The practical issue of achieving stability and robustness is a challenging task which is left as future work. The focus of the thesis is only to demonstrate the vibration suppression technique from a purely dynamics point of view.

Figure 4.3 shows that when $K_{pv} = 0$ the gap between ω_1 and ω_2 is the smallest indicating that it is possible to establish both 1:1 IR and 1:2 IR when $K_{pv} = 0$. Therefore, $K_{pv} = 0$ is chosen for all the numerical simulations in Chapter 5.

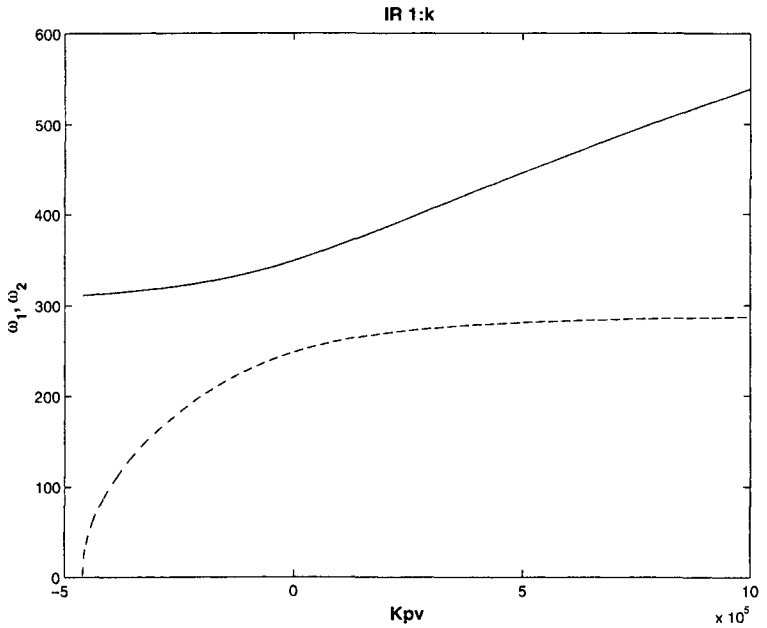

Figure 4.3: Variation in ω_1 and ω_2 with respect to K_{pv}, k is IR ratio, (-) ω_1, (- -) ω_2, k = 1 for 1:1 IR and k = 2 for 1:2 IR.

The values of the gains to establish 1:1 IR and 1:2 IR are given in Tables 4.1 and 4.2. The values for 1:1 IR correspond to the minimum difference between ω_1, ω_2 and

ω_3. The resonance ratios are established by tuning K_{pu} and K_{pw}. Results are summarized in Table 4.1 for the dimensional case and Table 4.2 for the nondimensional case.

Dimensional Model, $\Omega = 50$, $K_{pv} = 0$			
IR	K_{pu}	K_{pw}	Figure
1:1	4.57E+5	4.57E+5	4.2(a)
1:2	1.524E+5	5.183E+5	4.2(b)

Table 4.1: Tuning parameters for dimensional model

Nondimensional Model, $\Omega = 50$, $K_{pv} = 0$			
IR	K_{pu}	K_{pw}	Figure
1:1	2.6950	2.6950	A.2(a)
1:2	0.9110	3.0715	A.2(b)

Table 4.2: Tuning parameters for nondimensional model

The natural frequencies of the models are shown in the tables (4.3)-(4.4) for comparison.

Dimensional Model Single Mode Frequency	
IR	K_{pu}, K_{pw}, $\Omega = 50$
1:1	ω_1=348.9213, ω_2=248.9215, ω_3=298.9214
1:2	ω_1=317.7175, ω_2=158.8187, ω_3=317.6774

Table 4.3: Beam frequencies obtained using the dimensional single mode equations

Nondimensional Model Single Mode Frequency	
IR	K_{pu}, K_{pw}, $\Omega = 50$
1:1	ω_1=6.8731, ω_2=4.8731, ω_3=5.8731
1:2	ω_1=6.2564, ω_2=3.1268, ω_3=6.2550

Table 4.4: Beam frequencies obtained using the nondimensional single mode equations

4.3 Vibration Suppression

In this work, vibration suppression is implemented through velocity (derivatives) feedback control by applying K_{dv} and K_{dw} in directions v and w, respectively. Due to the contribution from tuning efforts which enhance the energy interaction among the coupled modes, one may apply only one velocity feedback controller in either direction v or direction w to suppress vibrations in all the three directions effectively and rapidly, which reveals the essence of IR control strategy.

4.4 Implementation of IR Control Strategy

In this section, the implementation of IR control strategy is discussed in a conceptual manner and should not be construed as a practical control system. For this, the actuators are assumed to be PZT actuators applied on the top and front planes of the rotating beam as shown in Figure 4.4. It is known that a piezo-electric element will distort when subjected to an electric field. This " Inverse Piezo-electric Effect " forms the basis for the operation of a piezo-electric actuator. In other words, if the displacement and velocity that are proportional to voltage signal are inputted to a piezo-electric actuator, it will apply a bending moment as output to the beam

that are proportional to the displacement, velocity or acceleration of the beam.

Modelling of PZT actuators attached to a beam has been discussed at length in the literatures, e.g. Oueini *et al.* [43] and Saguranrum *et al.* [44]. Oueini *et al.* [43] presented a Piezo-electric actuator as a nonlinear vibration absorber for a shaker based flexible one degree of freedom beam. The absorber in [43] is based on the saturation phenomenon exhibited by multidegree of freedom systems coupled with quadratic nonlinearities and possessing autoparametric (internal) resonances. They also set the controllers' natural frequencies to one-half the natural frequencies of the resonant modes and excited the system at a frequency close to its natural frequency. The nonlinear coupling terms created a unidirectional energy-transfer mechanism that saturated the response of the excited modes and suppressed their vibrations. The stiffening effect of the Piezo-electric actuators in [43] was neglected in deriving the equations of motion. Later Saguranrum *et al.* [44] went further on this topic by including the mass and Young's modulus of the Piezoceramic actuators in the derivation of governing equations of a uniform, cantilever beam subjected to a base excitation. They also employed saturation control strategy and fully included the resulting coupling between uniform, cantilever beam modes in the analytical model. In their investigation the nonuniformities due to the presence of piezoelectric actuators in the beam properties were included. The numerical simulation results in [44] show that the vibration response of a uniform, cantilever beam will be predicted with greater accuracy when the modal coupling terms that result from the presence of the Piezo-electric actuators are included in the mathematical model. Some other publications in this field are by Oueini and Golnaraghi [45] and Pai *et al.* [46].

In this thesis, the inertial and structural properties of Piezo-electric actuators are neglected because the emphasis is on control strategy and the detailed control techniques and experimental setup are both ignored.

The control logic is shown in Figure 4.5. Block 1 shows the control efforts applied to the nonlinear system using D feedback control technique based on IR state. The control signal to the system is issued in the form of force by two piezo-electric actuators applied on two planes of the beam as shown in Figure 4.4. Then accelerometer can be used to measure the output acceleration $a = [\ddot{u}, \ddot{v}, \ddot{w}]^T$. By integrating a once the corresponding velocity $v = [\dot{u}, \dot{v}, \dot{w}]^T$ can be obtained. Here velocity feedback (D controllers) is sent to the actuators to suppress vibrations in all the three directions. Finally, integrating v can give us the displacement $d = [u, v, w]^T$ that can be used as the displacement feedback (P controllers) to the actuators and as input to Block 2 to compute the response frequencies of the nonlinear beam.

Block 2 indicates the tuning process for obtaining P gain and establishing IR state as well. Taking an assumed K_p and angular velocity Ω as inputs, it first computes the 3 nominal natural frequencies (ω_1, ω_2, ω_3) of the beam around the equilibrium point $[0, 0, 0]$. Meanwhile the computer also takes the displacements from Block 1 as input signal and computes the real response frequencies of the beam using FFT, which contains many frequencies. In the vicinity of the three nominal natural frequencies, the computer will choose the three dominant real response frequencies ω_{r1}, ω_{r2}, ω_{r3} and compute the difference between ω_{r1} and $k\omega_{r2}$, where k is IR ratio ($k = 1$ for 1:1 IR and $k = 2$ for 1:2 IR, etc.). By minimizing the difference

between ω_{r1} and $k\omega_{r2}$ and placing ω_{r3} between ω_{r1} and $k\omega_{r2}$, the computer can thus tune K_p and use the updated K_p as input to compute the new nominal natural frequencies. At the same time, the K_p can serve as the P gain in Block 1 to obtain new displacement $d = [u, v, w]^T$. Using this new d as input, the computer in Block 2 can compute the new real response frequencies of the beam. The above iteration process goes on until the difference between ω_{r1} and $k\omega_{r2}$ is minimized and the IR state is thus established. Then through the process involved in Block 1, the vibration in u, v and w directions can be effectively and rapidly suppressed.

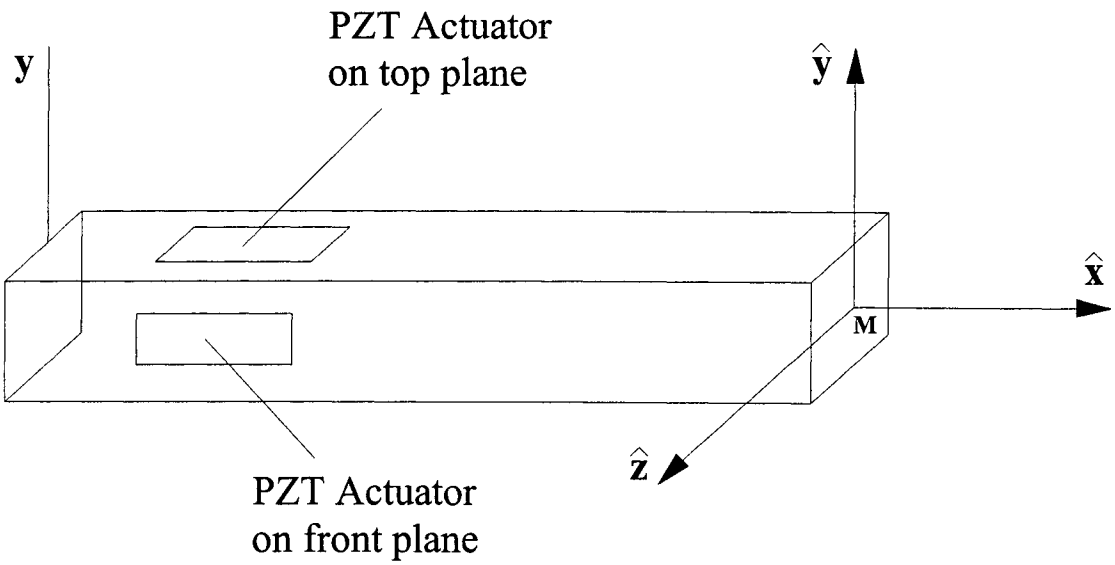

Figure 4.4: Conceptual view of actuators applied to the beam for setting up IR and suppress vibrations in u, v and w directions

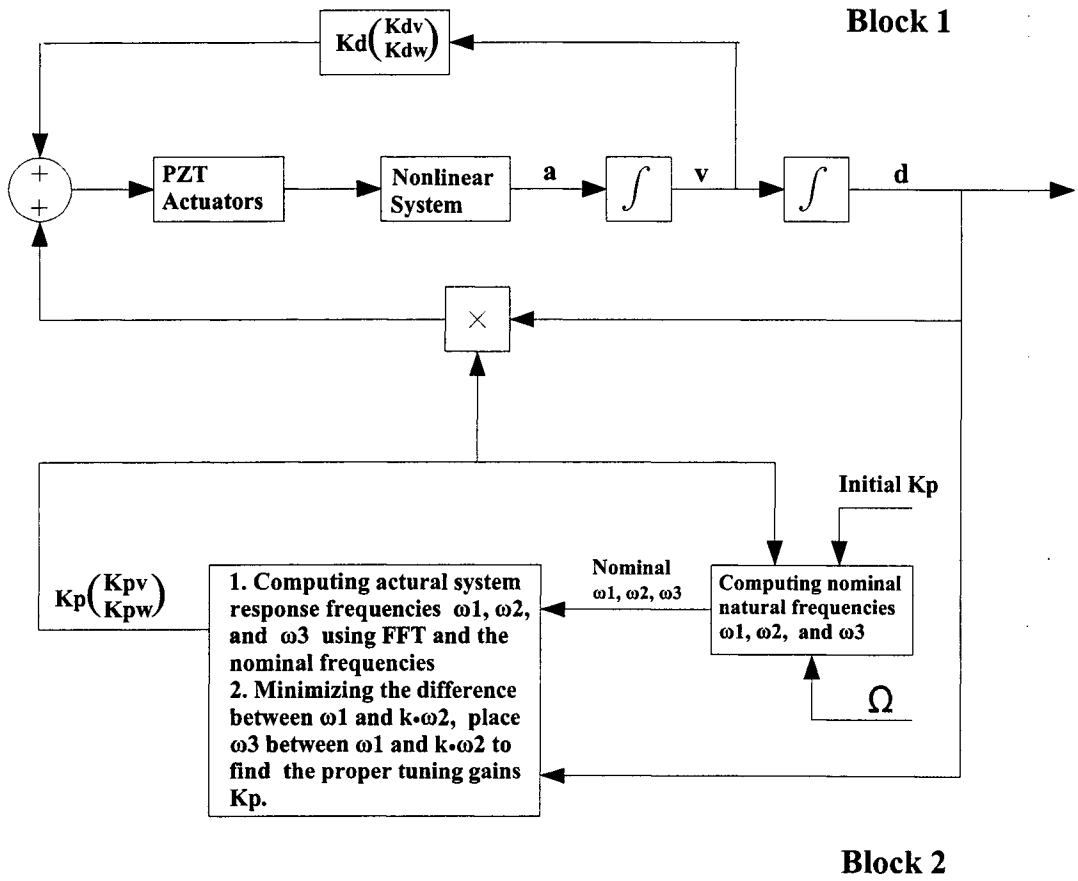

Figure 4.5: Control logic, k is the ratio of ω_1 to ω_2 for setting up 1:1 IR and 1:2 IR, **a** is acceleration vector, **v** is velocity vector and **d** is displacement vector. Ω stands for angular velocity.

In this chapter, a vibration suppression strategy is discussed and a conceptual view of how it can be implemented is presented. In the next chapter, the dimensional and nondimensional models will be simulated numerically. Supporting simulation results will also be presented according to the established IR cases in Chapter 5.

Chapter 5

Numerical Simulation

In this chapter, dynamics of the system are studied numerically in time domain and spectral domain and results are presented for the vibration suppression strategy developed in Chapter 4. The semi-discretized equations of motion obtained in Chapter 3 are Differential Algebraic Equations (DAEs) whose solutions are very difficult and challenging to obtain. In this chapter, two numerical approaches, namely, Runge-Kutta method and a new technique referred to as Average Acceleration Formulation (AAF), are applied to simulate the gyroscopic system. The results obtained using the two methods are also compared and analyzed.

5.1 Solution Techniques

In this section, the solution techniques based on Runge-Kutta method and Average Acceleration Formulation (AAF) are discussed in detail.

5.1.1 Runge-Kutta Method

First, an automatic ODEs solver, Adaptive Stepsize Runge-Kutta Method, is applied to solve the DAEs (3.6)-(3.9) for the dimensional model and (A.22)-(A.25) for the nondimensional model. Gear [47] gives an overview of the automatic ODE solvers dealing with such equations. As the equations to be solved are DAEs and not ODEs the approach used here is to differentiate the algebraic equation in the DAE system and then apply the ODE solver to obtain approximate solutions. A DAE solver SUNDIAL-IDA was tried but was not successful in obtaining the solution due to convergence problems. In Section 5.1.2, the AAF method mentioned earlier is developed to solve the equations. For the purpose of analysis, solutions for both single mode shape system and four mode shape system are developed and brought into comparison.

The underlying idea about adaptive stepsize control is to achieve some predetermined accuracy in the solution with minimum computational efforts. The Adaptive Stepsize Runge-Kutta Method is a commonly used numerical technique for solving initial value problems [48]. During the process, a solution is generated and improved over each time step by combining results from several Euler-style steps, and then using the information obtained to match a Taylor series expansion up to some higher order (see [48, 49]). The step size is adjusted according to an estimate of the truncation error. Simulation results using Runge-Kutta method are presented in Section 5.6.

5.1.2 Average Acceleration Formulation

The average acceleration formulation is a technique for solving equations of motion which arise in continuous dynamics problems where discretization of PDEs to ODEs through Rayleigh-Ritz or Galerkin method is involved. It was originally presented in [10] to solve multibody dynamics problems. The technique involves reducing system of ODE to an iterative problem involving Algebraic Equations (AE). The method is similar to the average acceleration method commonly used in solving equations arising in finite element problems. The difference in the formulation lies in the fact that the final equations are in terms of accelerations and not in terms of displacements as in the conventional average acceleration method. This is possible by using Taylor series in a direct way instead of the usual approach of deriving finite difference formula. The advantage of using this approach is that time step terms Δt appear in the numerator instead of denominator. Therefore, it gives better numerical stability. Additional details of the techniques can be found in [10]. Here only the application of the method to the problem at hand is shown.

5.1.3 Average Acceleration Method

Application of average acceleration method requires making the following finite difference approximations for displacements and velocities obtained using Taylor series expansion:

$$\begin{aligned} \dot{u}^{t+\Delta t} &= \dot{u}^t + \ddot{u}^t \Delta t \\ u^{t+\Delta t} &= u^t + \dot{u}^t \Delta t + \ddot{u}^t \frac{\Delta t^2}{2} \end{aligned} \tag{5.1}$$

where u represents the time dependent variables α_i, β_i, γ_i and λ_i, Δt is a small increment in time and the superscripts specify the time at which the term is evaluated. In addition, the following average acceleration assumption is also made:

$$\ddot{u}^t \Rightarrow \frac{\ddot{u}^{t+\Delta t} + \ddot{u}^t}{2} \tag{5.2}$$

where " $\Rightarrow$ " means replacement. Substituting (5.2) in (5.1) yields the following equations [10]:

$$\begin{aligned} \dot{u}^{t+\Delta t} &= \dot{u}^t + a_1\ddot{u}^t + a_2\ddot{u}^{t+\Delta t} \\ &= c1u(\dot{u}^t, \ddot{u}^t) + a_2\ddot{u}^{t+\Delta t} \\ u^{t+\Delta t} &= u^t + a_3\dot{u}^t + a_4\ddot{u}^t + a_5\ddot{u}^{t+\Delta t} \\ &= c2u(u^t, \dot{u}^t, \ddot{u}^t) + a_5\ddot{u}^{t+\Delta t} \end{aligned} \tag{5.3}$$

where the parameters a_i stand for:

$$\begin{aligned} a_1 = \tfrac{\Delta t}{2} \quad a_2 = \tfrac{\Delta t}{2} \quad a_3 = \Delta t \\ a_4 = \tfrac{\Delta t^2}{4} \quad a_5 = \tfrac{\Delta t^2}{4} \end{aligned} \tag{5.4}$$

and $c1u$ and $c2u$ represent the terms that will be evaluated at time t and are given by:

$$\begin{aligned} c1u &= \dot{u}^t + a_1\ddot{u}^t \\ c2u &= u^t + a_3\dot{u}^t + a_4\ddot{u}^t \end{aligned} \tag{5.5}$$

By applying (5.3) the DAEs (3.6)-(3.9) obtained in Chapter 3 are reduced to a set of nonlinear algebraic equations involving acceleration at $t + \Delta t$ and displacement, velocity and acceleration at time t.

5.1.4 Discretized Equations-Acceleration Formulation

By substituting (5.3) into (3.6)-(3.9), the following discretized equations are obtained:

u equation:

$$\int_0^l \left[EI_y \{\phi_i''\} \lfloor\phi_j''\rfloor \{a_5\ddot{\alpha}_j + c2\alpha_j\} + [\phi_i'\phi_j] \{\lambda_j\}\right.$$
$$+A\rho[\phi_i\,\phi_j]\left\{\{\ddot{\alpha}_j\} - 2\Omega\left\{\{a_2\ddot{\beta}_j + c1\beta_j\}\right\} - \Omega^2\{a_5\ddot{\alpha}_j + c2\alpha_j\}\right\}$$
$$+\{\phi_i'\}\lfloor\phi_j\,\phi_k'\rfloor\{\lambda_j\{a_5\ddot{\alpha}_k + c2\alpha_k\}\} + \{\phi_i'\}\lfloor\phi_j''\,\phi_k''\rfloor$$
$$\left\{-EI_z\left\{\{a_5\ddot{\beta}_j + c2\beta_j\}\{a_5\ddot{\beta}_k + c2\beta_k\}\right\} - EI_y\{\{a_5\ddot{\gamma}_j + c2\gamma_j\}\right.$$
$$\left.\{a_5\ddot{\gamma}_k + c2\gamma_k\}\}\right\} + A\rho\{\phi_i\}\lfloor\phi_j\,\phi_k'\,\phi_l'\rfloor\{-3\{\ddot{\alpha}_j\{a_5\ddot{\gamma}_k + c2\gamma_k\}$$
$$\{a_5\ddot{\gamma}_l + c2\gamma_l\}\} + 6\Omega\left\{\{a_2\ddot{\beta}_j + c1\beta_j\}\{a_5\ddot{\gamma}_k + c2\gamma_k\}\{a_5\ddot{\gamma}_l + c2\gamma_l\}\right\}$$
$$\left.+3\Omega^2\{\{a_5\ddot{\alpha}_j + c2\alpha_j\}\{a_5\ddot{\gamma}_k + c2\gamma_k\}\{a_5\ddot{\gamma}_l + c2\gamma_l\}\}\right\}$$
$$+\{\phi_i''\}\lfloor\phi_j'\,\phi_k'\,\phi_l''\rfloor\left\{E(I_y - I_z)\left\{\{a_5\ddot{\alpha}_j + c2\alpha_j\}\{a_5\ddot{\beta}_k + c2\beta_k\}\right.\right.$$
$$\left.\{a_5\ddot{\beta}_l + c2\beta_l\}\right\} - E(I_y - I_z)\left\{\{a_5\ddot{\beta}_j + c2\beta_j\}\{a_5\ddot{\beta}_k + c2\beta_k\}\right.$$
$$\{a_5\ddot{\alpha}_l + c2\alpha_l\}\} - 3EI_y\{\{a_5\ddot{\gamma}_j + c2\gamma_j\}\{a_5\ddot{\gamma}_k + c2\gamma_k\}$$
$$\{a_5\ddot{\alpha}_l + c2\alpha_l\}\}\} + \{\phi_i'\}\lfloor\phi_j'\,\phi_k''\rfloor\{-3EI_z\{\{a_5\ddot{\alpha}_j + c2\alpha_j\}$$
$$\{a_5\ddot{\beta}_k + c2\beta_k\}\{a_5\ddot{\beta}_l + c2\beta_l\}\} - EI_y\{\{a_5\ddot{\alpha}_j + c2\alpha_j\}$$
$$\{a_5\ddot{\gamma}_k + c2\gamma_k\}\{a_5\ddot{\gamma}_l + c2\gamma_l\}\} + 2EI_z\left\{\{a_5\ddot{\beta}_j + c2\beta_j\}\right.$$
$$\left.\left.\{a_5\ddot{\alpha}_k + c2\alpha_k\}\{a_5\ddot{\beta}_l + c2\beta_l\}\right\}\right\} - 3\{\phi_i'\}\lfloor\phi_j\,\phi_k'\,\phi_l'\rfloor\{\lambda_j$$
$$\left.\{a_5\ddot{\gamma}_k + c2\gamma_k\}\{a_5\ddot{\gamma}_l + c2\gamma_l\}\}\right]\,dx = 0 \tag{5.6}$$

v equation:

$$\int_0^l \Big[EI_z \left[\phi_i'' \, \phi_j''\right] \{a_5 \ddot{\beta}_j + c2\beta_j\} + A\rho \left[\phi_i \, \phi_j\right] \Big\{ \Big\{ \ddot{\beta}_j \Big\} + 2\Omega \, \{\{a_2 \ddot{\alpha}_j + c1\alpha_j\}\} - \Omega^2 \Big\{ \{a_5 \ddot{\beta}_j + c2\beta_j\} \Big\} \Big\} + \{\phi_i'\} \left\lfloor \phi_j \, \phi_k' \right\rfloor \Big\{ \lambda_j \, \{a_5 \ddot{\beta}_k + c2\beta_k\} \Big\} + \{\phi_i''\} \left\lfloor \phi_j' \, \phi_k'' \right\rfloor \{-2\, E\,(I_y - I_z) \, \{\{a_5 \ddot{\alpha}_j + c2\alpha_j\} \{a_5 \ddot{\beta}_k + c2\beta_k\} \Big\} + E\,(I_y - I_z) \Big\{ \{a_5 \ddot{\beta}_j + c2\beta_j\} \{a_5 \ddot{\alpha}_k + c2\alpha_k\} \Big\} \Big\} + A\rho \, \{\phi_i\} \left\lfloor \phi_j \, \phi_k' \, \phi_l' \right\rfloor \Big\{ -3 \Big\{ \ddot{\beta}_j \, \{a_5 \ddot{\gamma}_k + c2\gamma_k\} \{a_5 \ddot{\gamma}_l + c2\gamma_l\} \Big\} - 6\,\Omega \, \{\{a_2 \ddot{\alpha}_j + c1\alpha_j\} \{a_5 \ddot{\gamma}_k + c2\gamma_k\} \{a_5 \ddot{\gamma}_l + c2\gamma_l\}\} + 3\,\Omega^2 \Big\{ \{a_5 \ddot{\beta}_j + c2\beta_j\} \{a_5 \ddot{\gamma}_k + c2\gamma_k\} \{a_5 \ddot{\gamma}_l + c2\gamma_l\} \Big\} \Big\} + \{\phi_i'\} \left\lfloor \phi_j' \, \phi_k'' \, \phi_l'' \right\rfloor \Big\{ -EI_z \Big\{ \{a_5 \ddot{\beta}_j + c2\beta_j\} \{a_5 \ddot{\beta}_k + c2\beta_k\} \{a_5 \ddot{\beta}_l + c2\beta_l\} \Big\} - EI_y \Big\{ \{a_5 \ddot{\beta}_j + c2\beta_j\} \{a_5 \ddot{\gamma}_k + c2\gamma_k\} \{a_5 \ddot{\gamma}_l + c2\gamma_l\} \} - E\,(I_y - I_z) \Big\{ \{a_5 \ddot{\gamma}_j + c2\gamma_j\} \{a_5 \ddot{\beta}_k + c2\beta_k\} \{a_5 \ddot{\gamma}_l + c2\gamma_l\} \} \} + \{\phi_i''\} \left\lfloor \phi_j' \, \phi_k' \, \phi_l'' \right\rfloor \{-E\,(I_y - I_z) \Big\{ \{a_5 \ddot{\alpha}_j + c2\alpha_j\} \{a_5 \ddot{\alpha}_k + c2\alpha_k\} \{a_5 \ddot{\beta}_l + c2\beta_l\} \Big\} + E\,(I_y - I_z) \Big\{ \{a_5 \ddot{\alpha}_j + c2\alpha_j\} \{a_5 \ddot{\beta}_k + c2\beta_k\} \{a_5 \ddot{\alpha}_l + c2\alpha_l\} \Big\} - \frac{1}{2} E\,(3\,I_z + I_y) \Big\{ \{a_5 \ddot{\gamma}_j + c2\gamma_j\} \{a_5 \ddot{\gamma}_k + c2\gamma_k\} \{a_5 \ddot{\beta}_l + c2\beta_l\} \Big\} \Big\} \Big] \, dx \; = \; 0 \tag{5.7}$$

w equation:

$$\int_0^l \left[EI_y\left[\phi_i'' \phi_j''\right]\{a_5\ddot{\gamma}_j + c2\gamma_j\} + A\rho[\phi_i \phi_j]\{\ddot{\gamma}_j\} + \{\phi_i'\}\lfloor\phi_j \phi_k'\rfloor\right.$$
$$\{\lambda_j\{a_5\ddot{\gamma}_k + c2\gamma_k\}\} - A\rho\{\phi_i\}\lfloor\phi_j \phi_k' \phi_l'\rfloor\{\ddot{\gamma}_j\{a_5\ddot{\gamma}_k + c2\gamma_k\}$$
$$\{a_5\ddot{\gamma}_l + c2\gamma_l\}\} + \{\phi_i'\}\lfloor\phi_j' \phi_k'' \phi_l''\rfloor\left\{\frac{1}{2}E(I_y - I_z)\{\{a_5\ddot{\gamma}_j + c2\gamma_j\}\right.$$
$$\left.\{a_5\ddot{\beta}_k + c2\beta_k\}\{a_5\ddot{\beta}_l + c2\beta_l\}\right\} - EI_y\{\{a_5\ddot{\gamma}_j + c2\gamma_j\}$$
$$\{a_5\ddot{\gamma}_k + c2\gamma_k\}\{a_5\ddot{\gamma}_l + c2\gamma_l\}\}\} - EI_y\{\phi_i''\}\lfloor\phi_j' \phi_k' \phi_l''\rfloor$$
$$\left.\{\{a_5\ddot{\gamma}_j + c2\gamma_j\}\{a_5\ddot{\gamma}_k + c2\gamma_k\}\{a_5\ddot{\gamma}_l + c2\gamma_l\}\}\right] dx = 0 \tag{5.8}$$

λ equation

$$\int_0^l \left[[\phi_i \phi_j']\{a_5\ddot{\alpha}_j + c2\alpha_j\}\right.$$
$$+ \{\phi_i\}\lfloor\phi_j' \phi_k'\rfloor\left\{\frac{1}{2}\{\{a_5\ddot{\alpha}_j + c2\alpha_j\}\{a_5\ddot{\alpha}_k + c2\alpha_k\}\}\right.$$
$$+\frac{1}{2}\left\{\{a_5\ddot{\beta}_j + c2\beta_j\}\{a_5\ddot{\beta}_k + c2\beta_k\}\right\}$$
$$\left.\left.+\frac{1}{2}\{\{a_5\ddot{\gamma}_j + c2\gamma_j\}\{a_5\ddot{\gamma}_k + c2\gamma_k\}\}\right\}\right] dx = 0 \tag{5.9}$$

In the above equations, $c1\alpha_j$, $c2\alpha_j$, $c1\beta_j$, $c2\beta_j$, $c1\gamma_j$, $c2\gamma_j$ are defined as:

$$\begin{aligned}
c1\alpha_j &= \dot{\alpha_j}^t + a_1\ddot{\alpha}_j^t \\
c2\alpha_j &= \alpha_j{}^t + a_3\dot{\alpha}_j^t + a_4\ddot{\alpha}_j^t \\
\\
c1\beta_j &= \dot{\beta_j}^t + a_1\ddot{\beta}_j^t \\
c2\beta_j &= \beta_j{}^t + a_3\dot{\beta}_j^t + a_4\ddot{\beta}_j^t \\
\\
c1\gamma_j &= \dot{\gamma_j}^t + a_1\ddot{\gamma}_j^t \\
c2\gamma_j &= \gamma_j{}^t + a_3\dot{\gamma}_j^t + a_4\ddot{\gamma}_j^t
\end{aligned} \tag{5.10}$$

Following the same approach, the nondimensional form of discretized equations are obtained which are given in Appendix A.7 (See equations (A.31)-(A.34)).

5.2 Solution of Nonlinear Algebraic Equations

The conventional way of solving systems of nonlinear algebraic equations is Newton's method or its variants which require computing the system Jacobian. When the system of equations is large, numerical stability and computational effort becomes a major issue and the method fails. In this work an automatic DAE solver package SUNDIAL-IDA, which is based on Newton's method, was first tried without success. To solve the resulting nonlinear algebraic equations of motion (5.6)-(5.9) an iterative scheme is adopted and employed which was originally presented in [10].

The technique involves direct iteration of the nonlinear algebraic equations of motion without the need to find the Jacobian explicitly. To apply this approach the obtained nonlinear algebraic equations are reorganized in the following way [10]:

$$[A]_n^{t+\Delta t}\{u\}_{n+1}^{t+\Delta t} + \{N\}_n^{t+\Delta t} = \{0\} \tag{5.11}$$

where u_i (elements of $\{u\}$) represents the accelerations. The matrix $[A]$ is computed using the values of u_i at the n^{th} iteration step, then by solving the linear system (5.11) improved estimates of u_i are obtained. In this method the approach used for formulating the linear system (5.11) from the original nonlinear algebraic equations is the key to successful convergence of the iterative scheme. It involves extracting the linear variables u_i not only from the linear terms in the discretized algebraic equations, but also from bilinear and multilinear terms (terms linear in any u_i). The linear terms in u_i are written in the $[A]\{u\}$ form in (5.11) and the remaining nonlinear terms and constants are written in the $\{N\}$ matrix (see [10]). Bilinear (or multilinear) terms are accounted for twice (or as many times as the number of linear variables) in the matrix $[A]$ and all the additional terms introduced by Bilinear (or multilinear) terms in A are subtracted in the $\{N\}$ matrix to keep the equations the same.

To illustrate the iterative scheme formulation, the nonlinear terms in the alge-

braic equations in Section 5.1.4 are rewritten as follows to fit the form (5.11):

$$\phi_i'\phi_j\phi_k'\lambda_j(a_5\ddot{\alpha}_k + c2\alpha_k) =$$
$$\lambda_{\mathbf{j}}\phi_i'\phi_j\phi_k'(a_5\ddot{\alpha}_k + c2\alpha_k) + \ddot{\alpha}_{\mathbf{j}}a_5\phi_i'\phi_j'\phi_k\lambda_k - \phi_i'\phi_j\phi_k'a_5\lambda_j\ddot{\alpha}_k \tag{5.12}$$

$$\phi_i'\phi_j''\phi_k''(a_5\ddot{\alpha}_j + c2\alpha_j)(a_5\ddot{\alpha}_k + c2\alpha_k) =$$
$$\ddot{\alpha}_{\mathbf{j}}2a_5\phi_i'\phi_j''\phi_k''((1-\delta_{jk})a_5\ddot{\alpha}_k + c2\alpha_k)$$
$$+\phi_i'\phi_j''\phi_k''(\delta_{jk}{a_5}^2\ddot{\alpha}_j\ddot{\alpha}_k - (1-\delta_{jk}){a_5}^2\ddot{\alpha}_j\ddot{\alpha}_k + c2\alpha_j c2\alpha_k) \tag{5.13}$$

$$\phi_i''\phi_j'\phi_k''(a_5\ddot{\beta}_j + c2\beta_j)(a_5\ddot{\beta}_k + c2\beta_k) =$$
$$\ddot{\beta}_{\mathbf{j}}a_5(\phi_i''\phi_j''\phi_k' + \phi_i''\phi_j'\phi_k'')((1-\delta_{jk})a_5\ddot{\beta}_k + c2\beta_k)$$
$$+\phi_i''\phi_j'\phi_k''(\delta_{jk}{a_5}^2\ddot{\beta}_j\ddot{\beta}_k - (1-\delta_{jk}){a_5}^2\ddot{\beta}_j\ddot{\beta}_k + c2\beta_j c2\beta_k) \tag{5.14}$$

$$\phi_i''\phi_j'\phi_k''(a_5\ddot{\alpha}_j + c2\alpha_j)(a_5\ddot{\beta}_k + c2\beta_k) =$$
$$\ddot{\alpha}_{\mathbf{j}}a_5\phi_i''\phi_j'\phi_k''(a_5\ddot{\beta}_j + c2\beta_j) + \ddot{\beta}_{\mathbf{j}}a_5\phi_i''\phi_j''\phi_k'(a_5\ddot{\alpha}_j + c2\alpha_j)$$
$$+\phi_i''\phi_j'\phi_k''(-{a_5}^2\ddot{\alpha}_j\ddot{\beta}_k + c2\alpha_j c2\beta_k) \tag{5.15}$$

In the above formulation the terms with bold type face $\ddot{\alpha}_{\mathbf{j}}$, $\ddot{\beta}_{\mathbf{j}}$, $\ddot{\gamma}_{\mathbf{j}}$ and $\ddot{\lambda}_{\mathbf{j}}$ should be kept in the u matrix with the remaining terms being kept in the column matrix N. The Lagrange multipliers λ_j are treated as accelerations because its time derivatives do not exist in the equations of motion. It should be noted that in the formulation (5.12)-(5.15) index summation notation and the Kronecker delta are both used to

select or eliminate nonlinear terms from the products of type $\alpha_i\alpha_j\alpha_k$ and $\alpha_i\alpha_j\alpha_k\alpha_l$. All the other terms in 5.1.4 are expanded in a similar way.

The complete algorithm to obtain numerical solutions based on the iterative scheme formulation can be found in [10].

5.3 Numerical Algorithms

Dynamics of the system is studied using results obtained from different models. Time response and power spectrum are compared and analyzed. To study the system dynamics four algorithms are used: (1) Adaptive Runge-Kutta method for time response using approximate ODE system [48], (2) AAF algorithm for time response using actual DAE system [10], (3) Power Spectrum algorithm [48], (4) Polynomial Interpolation algorithm [48]. The Polynomial Interpolation algorithm is used for obtaining evenly spaced data from the unevenly spaced data obtained from the adaptive Runge-Kutta solver. The step size of obtained data files using AAF is constant and hence can be directly used to analyze the power spectrum.

To obtain the power spectrum the Discrete Fourier Transform (DFT) of the time series is computed. Hann window function is applied to the time series to reduce leakage in the first place and secondly, Fast Fourier Transform (FFT) algorithm is applied to implement the DFT. To reduce the variance, the data points are segmented and overlapped and the resulting FFTs are averaged. Then the power spectral density (PSD) is carried out by taking the mean squared amplitude of the transformed FFTs. All the power spectrums in this chapter are obtained in the same manner.

5.4 Excitation in Different Directions

The first set of simulation compares the effect of exciting the system by giving initial values in different directions. The four mode dimensional model (3.6)-(3.9) is used for all the simulations in this section. For initial values, (2.38) is used for v direction and (2.39) is used for w direction.

Figure 5.1 indicates the effect of exciting the system in the w direction. It can be seen clearly from the figure that exciting in w direction results in strong vibrations in all the other directions. The transfer of energy from w to the other directions occurs due to IR coupling as indicated by the characteristic beating motion.

Figure 5.1 also shows that the response in the u direction is less than or equal to zero ($u(l,t) \leq 0$). This phenomenon is due to the inextensionality constraint. From the algebraic constraints (3.9) and (A.25) in Chapter 3, the following constraint equation is applied:

$$\int_0^l \Big[[\phi_1 \; \phi_1'] \{\alpha_1\} + \frac{1}{2} \{\phi_1\} \lfloor \phi_1' \; \phi_1' \rfloor \{\{\alpha_1\}^2 + \{\beta_1\}^2 + \{\gamma_1\}^2\} \Big] \, dx = 0 \tag{5.16}$$

from (5.16) it can easily be seen that $\alpha_1 \leq 0$, which implies that the u tip deflection $u(l,t) \leq 0$ because $u(l,t) = \phi_1(l)\alpha_1(t)$ and here $\phi_1(l) = 2$.

Figure 5.2 shows the effect of exciting the system in the v direction alone. This figure shows coupling between u and v directions. However the coupling with the w direction is very weak. The coupling between u and v directions is not due to IR but is due to the fact that when an initial value is given in the v direction or

w direction it automatically results in an initial value for u direction due to the constraint (2.1). Therefore for all simulations in this thesis the system is excited in the w direction alone.

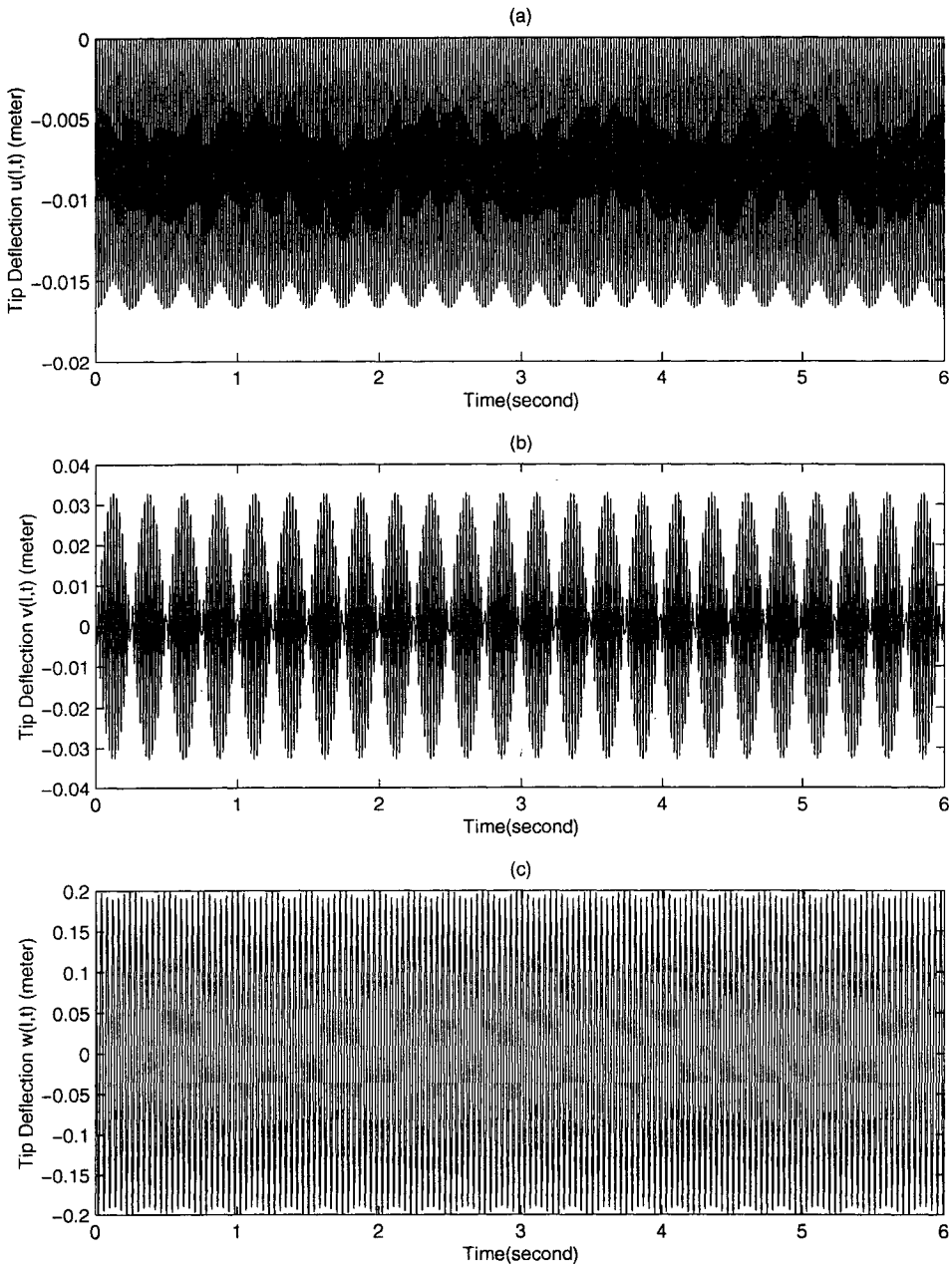

Figure 5.1: Four mode shape dimensional system response obtained by exciting in w direction only, AAF Method is applied. $\Omega = 50$, $w_{t0} = 0.2$, 1:2 IR, (a), (b) and (c) are time responses in u, v, and w directions respectively.

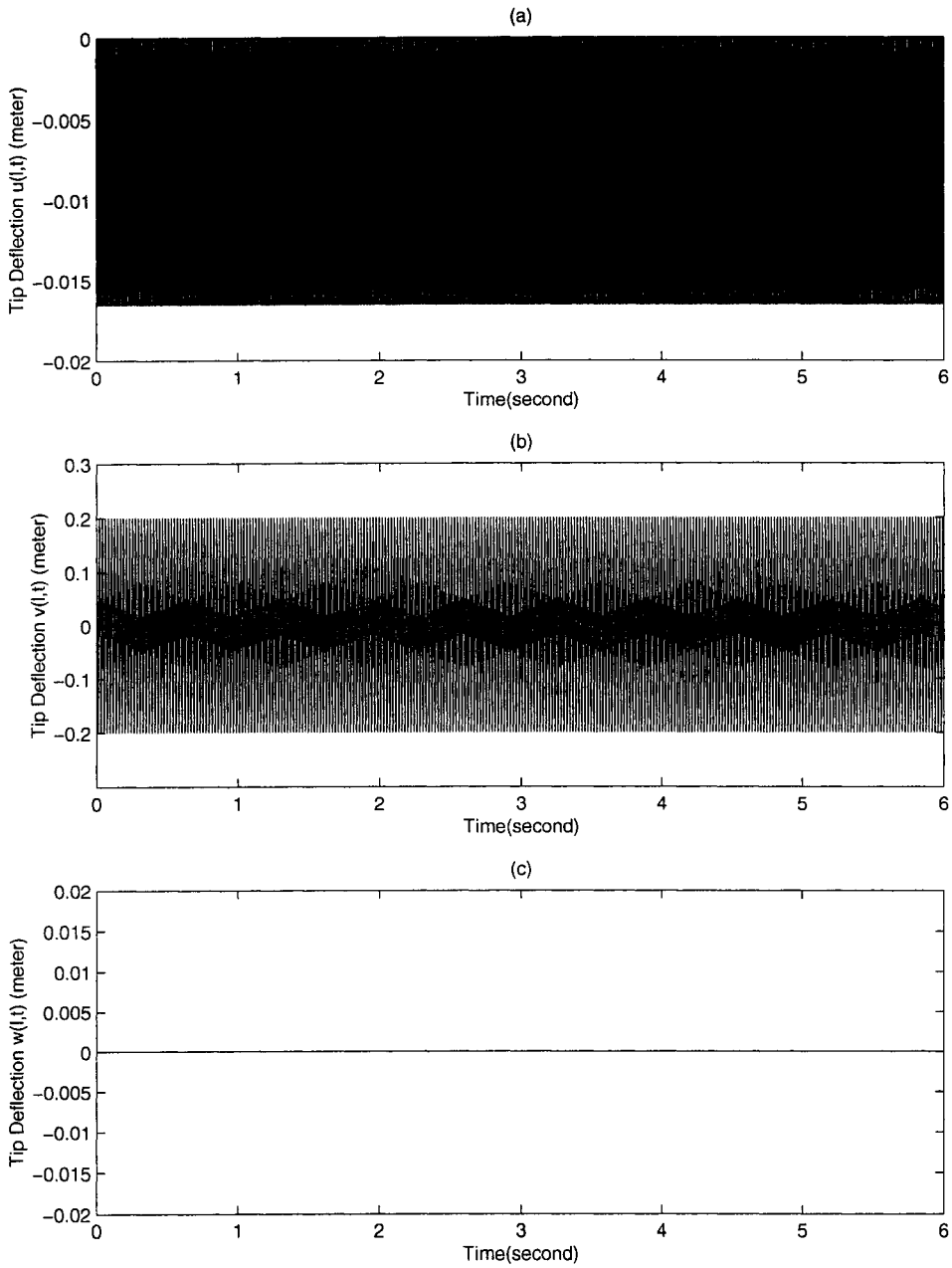

Figure 5.2: Four mode shape dimensional system response obtained by exciting in v direction only, AAF Method is applied. $\Omega = 50$, $v_{t0} = 0.2$, (a), (b) and (c) are time responses in u, v, and w directions respectively.

5.5 Non-Resonant Response Using AAF Method

To illustrate the advantage of IR based control strategy, the Non-Resonant responses of four mode shape dimensional model is obtained using AAF method. Since the modelling of dimensional system is accomplished according to the real parameters of NASA Army Aeroelastic Rotor Experimental System (ARES) [41] which is inherently in the state of modal coupling, the system needs to be detuned through K_{pu}, K_{pv} or K_{pw} such that its three eigenvalues are far apart from each other. Consequently $K_{pv} = 1e + 5$ and $K_{pw} = -1.6124e4$ are chosen for this purpose which results in a detuned system. The corresponding simulation result is shown in Figure 5.3. Comparing Figure 5.3 with Figure 5.1 clearly illustrates the difference between non-resonant and resonant responses. Under IR conditions the system is strongly coupled and the motion undergoes amplitude modulation. For the non-resonant response shown in Figure 5.3 the motion in u and v directions is similar to the linear oscillators without coupling between them.

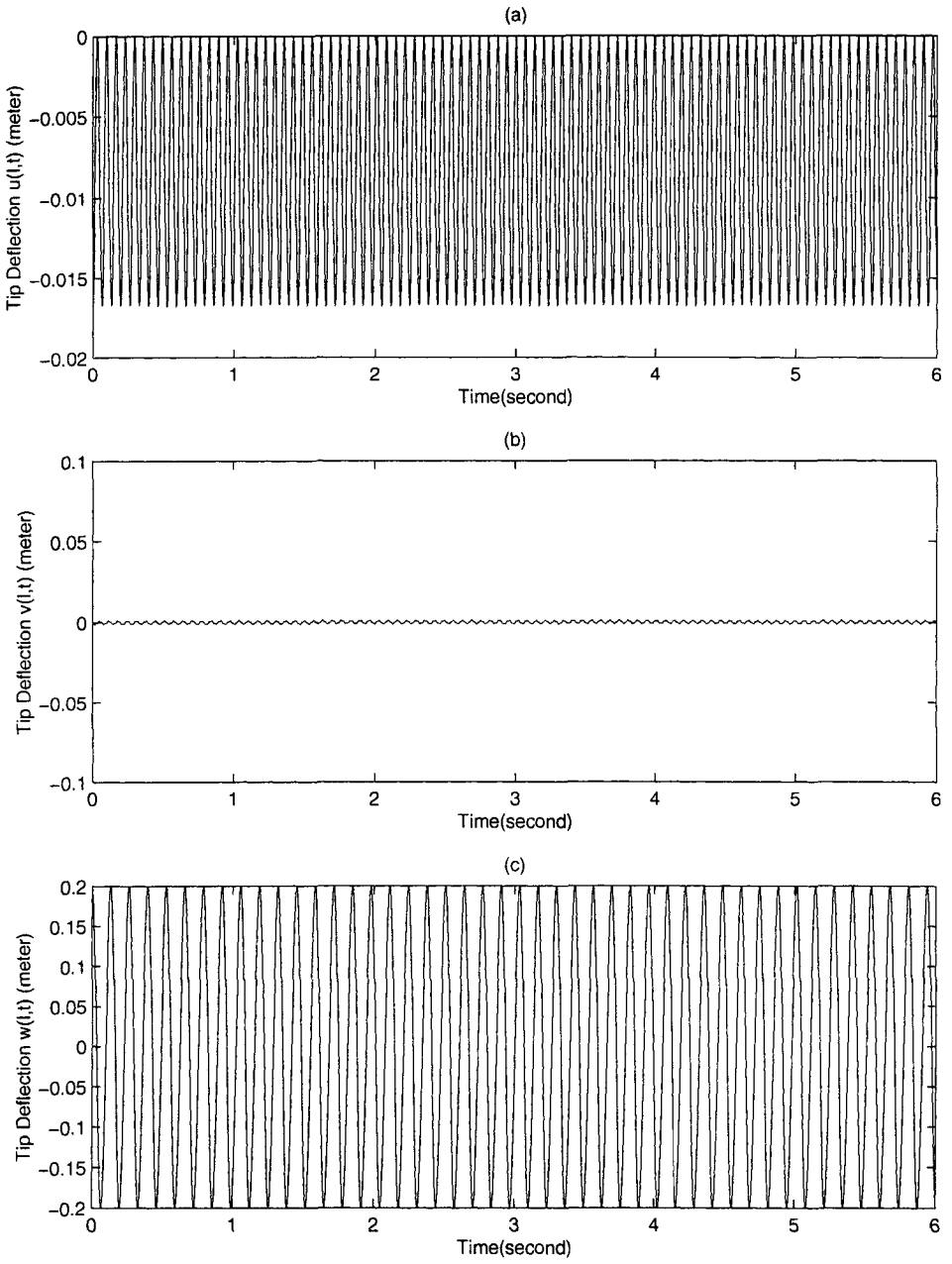

Figure 5.3: Four mode shape dimensional system response away from internal resonance, AAF Method is applied. Ω= 50, $w_{t0} = 0.2$, $K_{pu} = 0, K_{pv} = 1e + 5, K_{pw} = -1.6124e4$. (a), (b) and (c) are time responses in u, v, and w directions respectively.

5.6 Comparison of Runge-Kutta Method and AAF Method

In this section, time and spectral responses are compared using Runge-Kutta solver and AAF method. The first set of simulations are for dimensional case. The figures and parameters are tabulated in Table 5.1.

Dimensional Model 1:2 IR, $\Omega = 50$, $w_{t0} = 0.2$, $K_{pu} = 1.524e5$, $K_{pv} = 0$, $K_{pw} = 5.183e5$			
Single Mode Shape		Four Mode Shape	
Runge-Kutta	AAF	Runge-Kutta	AAF
5.4	5.5	5.6	5.7

Table 5.1: Comparison between Runge-Kutta and AAF method for dimensional model

In general there are minor differences in the amplitudes obtained using the two methods as can be seen by comparing Figure 5.4 and 5.5. This is due to the fact that the model for Runge-Kutta method is approximate as discussed in Section 5.1.1. The amplitudes for the four mode shape models however match well as shown in Figures 5.6 and 5.7. The power spectrums show all the main peaks. It can be seen by comparing the power spectrums that the main response frequencies match well. With regard to the power spectrums it should be noted that in the case of Runge-Kutta method, polynomial interpolation is used to generate evenly spaced data as mentioned earlier in Section 5.3.

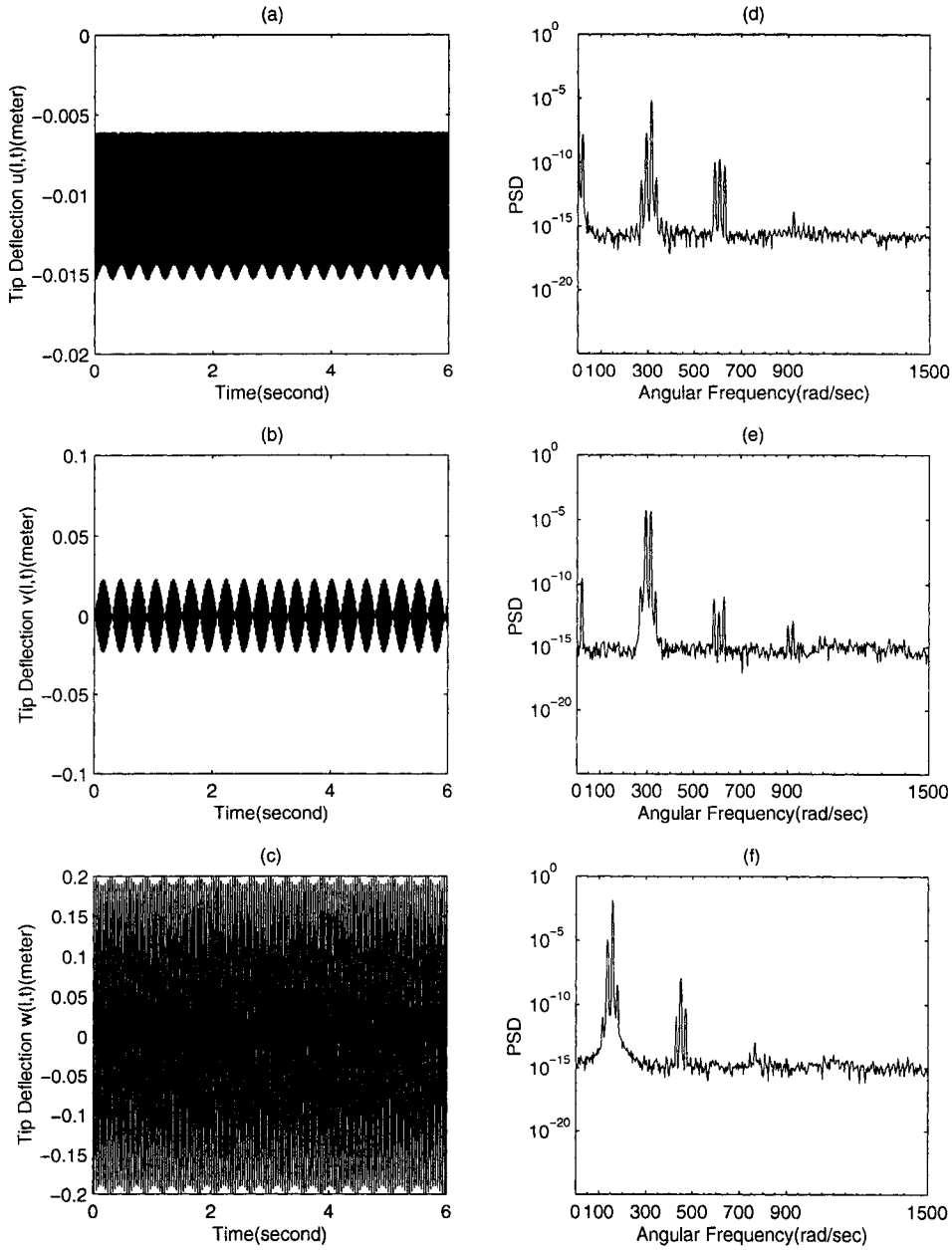

Figure 5.4: Single mode shape dimensional system response, 1:2 IR by tuning K_{pu} and K_{pw}, Runge-Kutta Method is applied. (a), (b) and (c) are time responses in u, v, and w directions respectively, (d), (e) and (f) are power spectrums in u, v, and w directions respectively

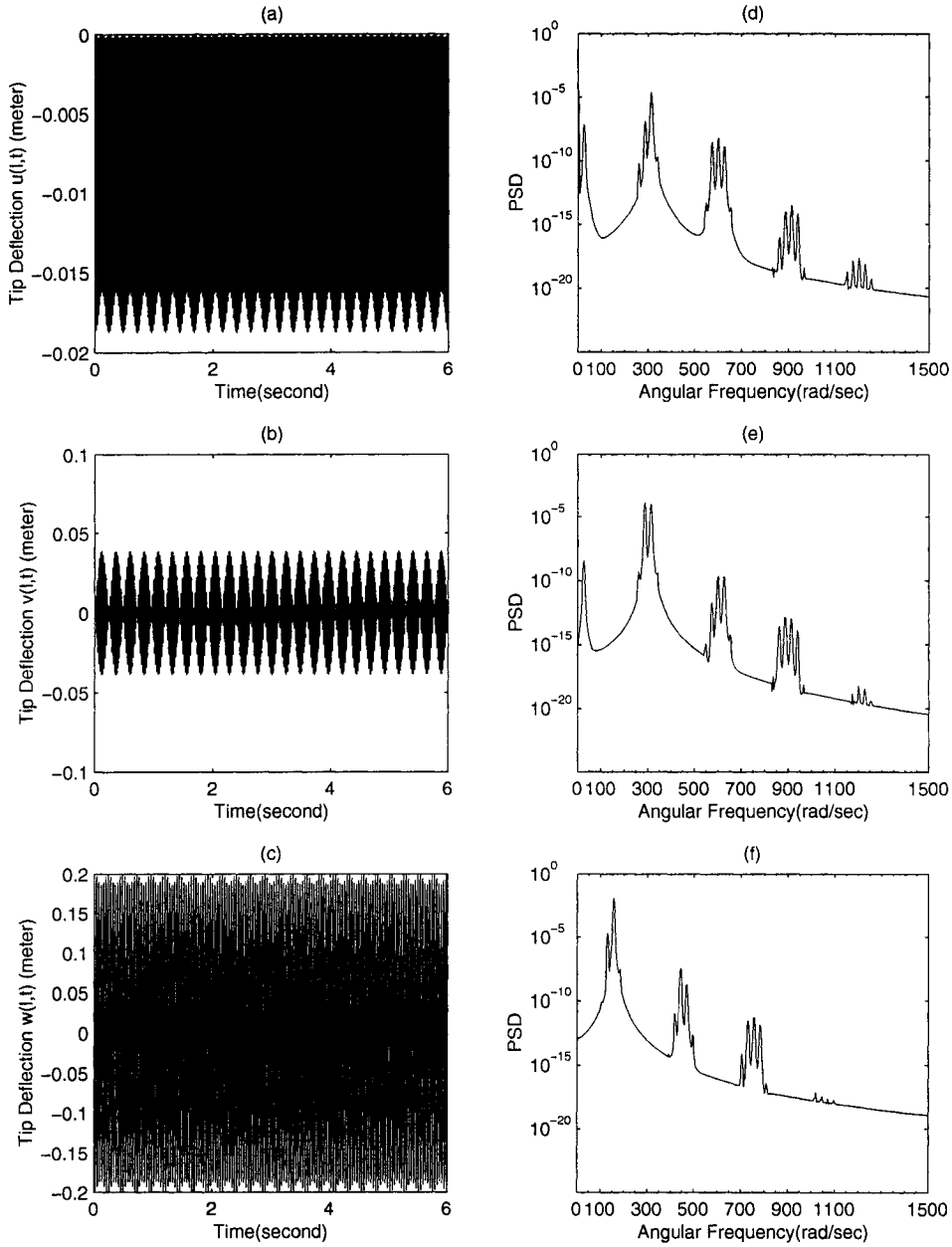

Figure 5.5: Single mode shape dimensional system response, 1:2 IR by tuning K_{pu} and K_{pw}, AAF Method is applied. (a), (b) and (c) are time responses in u, v, and w directions respectively, (d), (e) and (f) are power spectrums in u, v, and w directions respectively

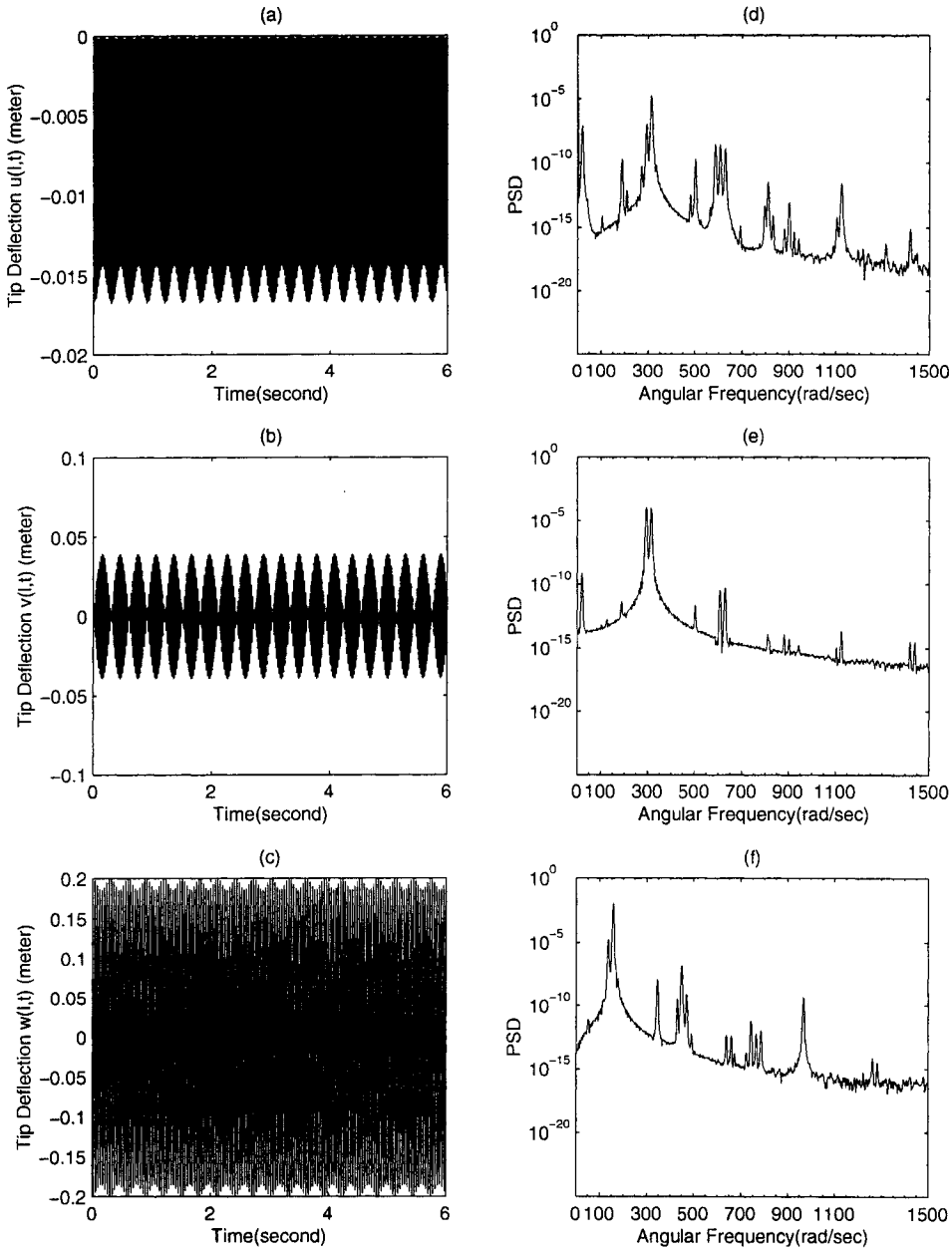

Figure 5.6: Four mode shape dimensional system response, 1:2 IR by tuning K_{pu}^{*} and K_{pw}^{*}, Runge-Kutta Method is applied. (a), (b) and (c) are time responses in u, v, and w directions respectively, (d), (e) and (f) are power spectrums in u, v, and w directions respectively

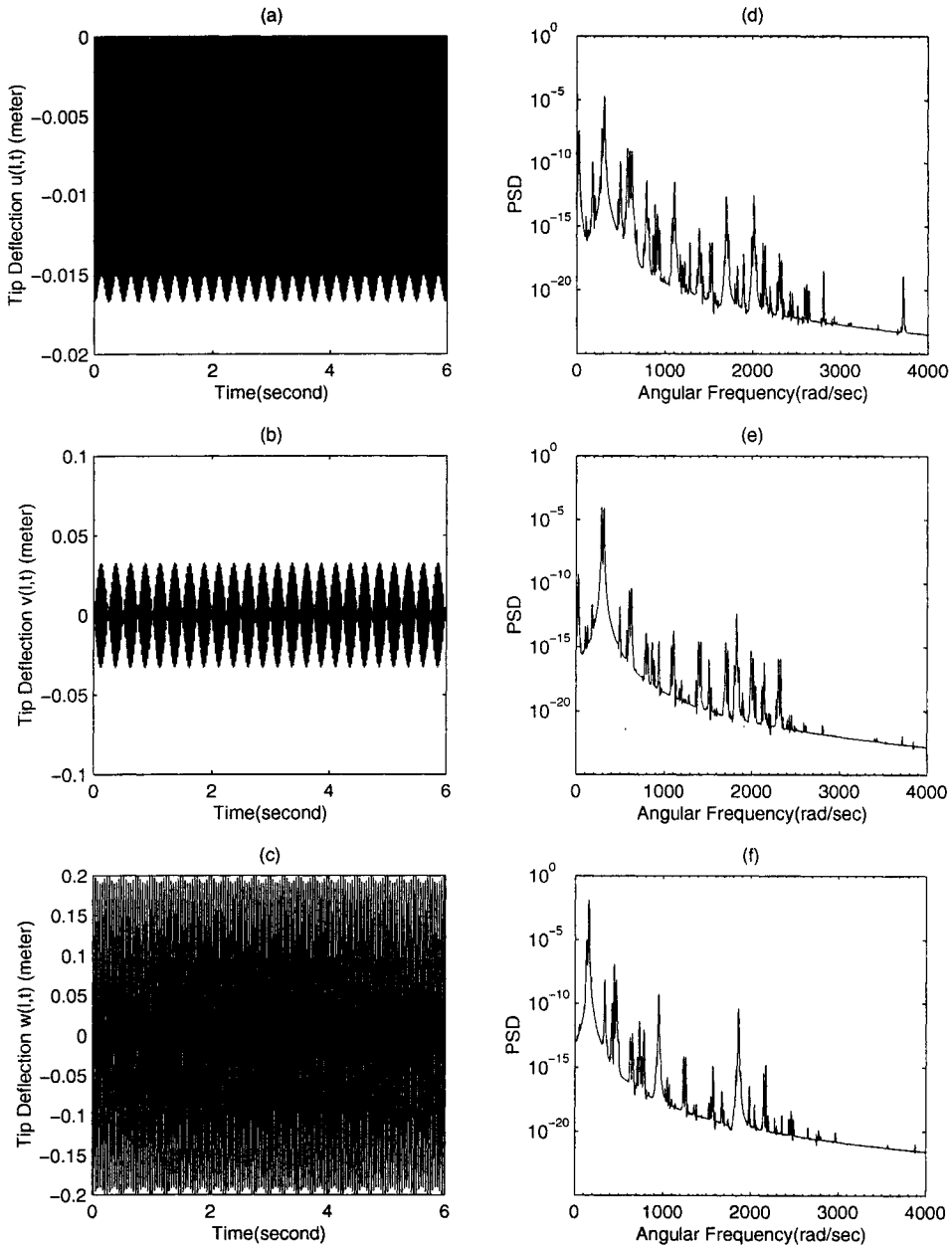

Figure 5.7: Four mode shape dimensional system response, 1:2 IR by tuning K_{pu} and K_{pw}, AAF Method is applied. (a), (b) and (c) are time responses in u, v, and w directions respectively, (d), (e) and (f) are power spectrums in u, v, and w directions respectively.

The results obtained using the two methods show remarkable differences when the time range is increased. The nondimensional model is used to illustrate these differences. The figures and parameters for this set of simulation are tabulated in Table 5.2.

Nondimensional Model 1:2 IR, $\Omega = 50$, $w_{t0} = 0.1432$, $K_{pu} = 0.9110$, $K_{pv} = 0$, $K_{pw} = 3.0715$			
Single Mode Shape		Four Mode Shape	
Runge-Kutta	AAF	Runge-Kutta	AAF
5.8	5.9	5.10	5.11

Table 5.2: Difference between Runge-Kutta and AAF for nondimensional model

Comparing the time responses in Figure 5.8 with Figure 5.9 and Figure 5.10 with Figure 5.11 shows that the Runge-Kutta method is diverging. This is clearly due to numerical instability.

The spectral response is not shown for the Runge-Kutta case as the results are diverging.

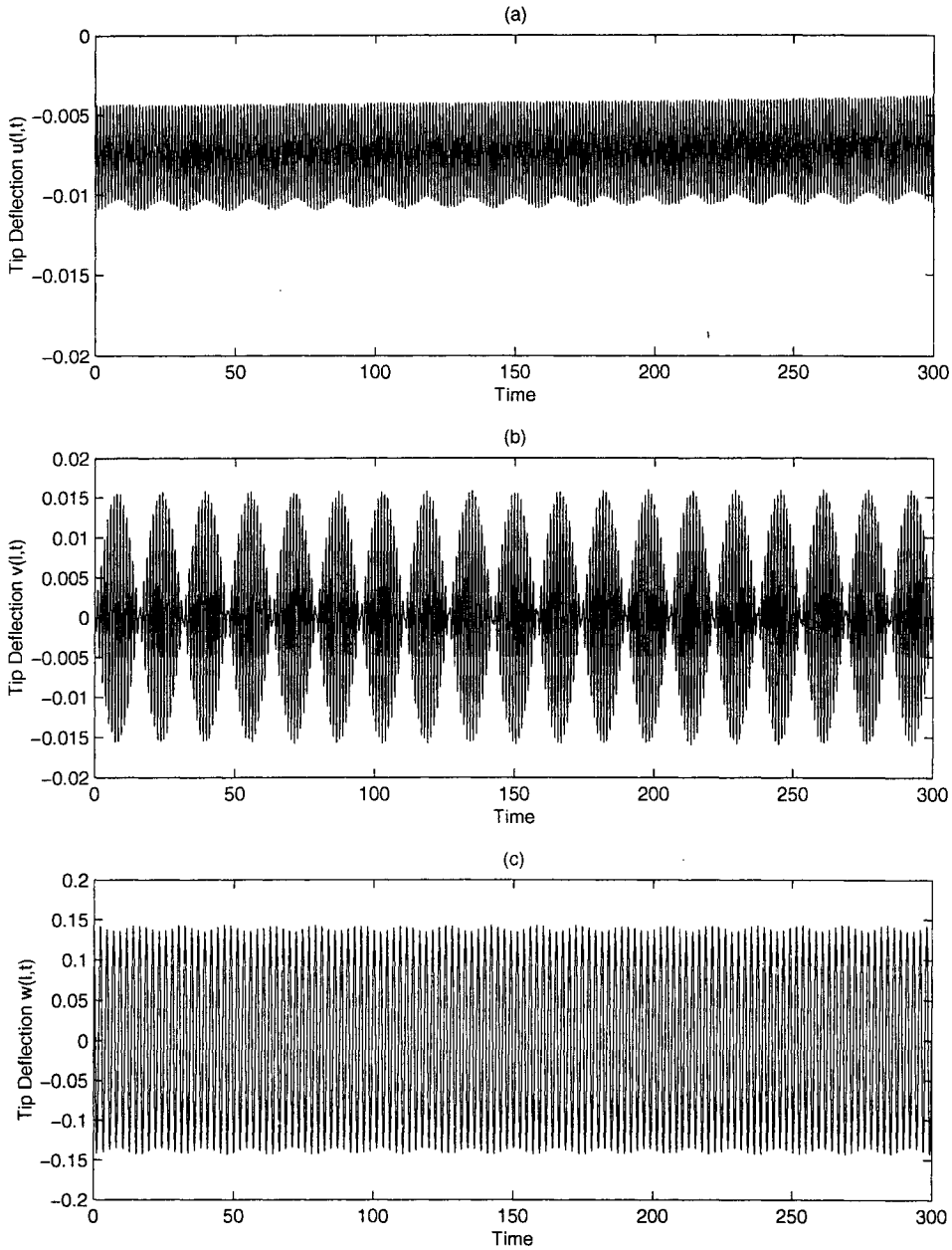

Figure 5.8: Single mode shape nondimensional system response, 1:2 IR by tuning K_{pu} and K_{pw}, Runge-Kutta Method is applied. (a), (b) and (c) are time responses in u, v, and w directions respectively.

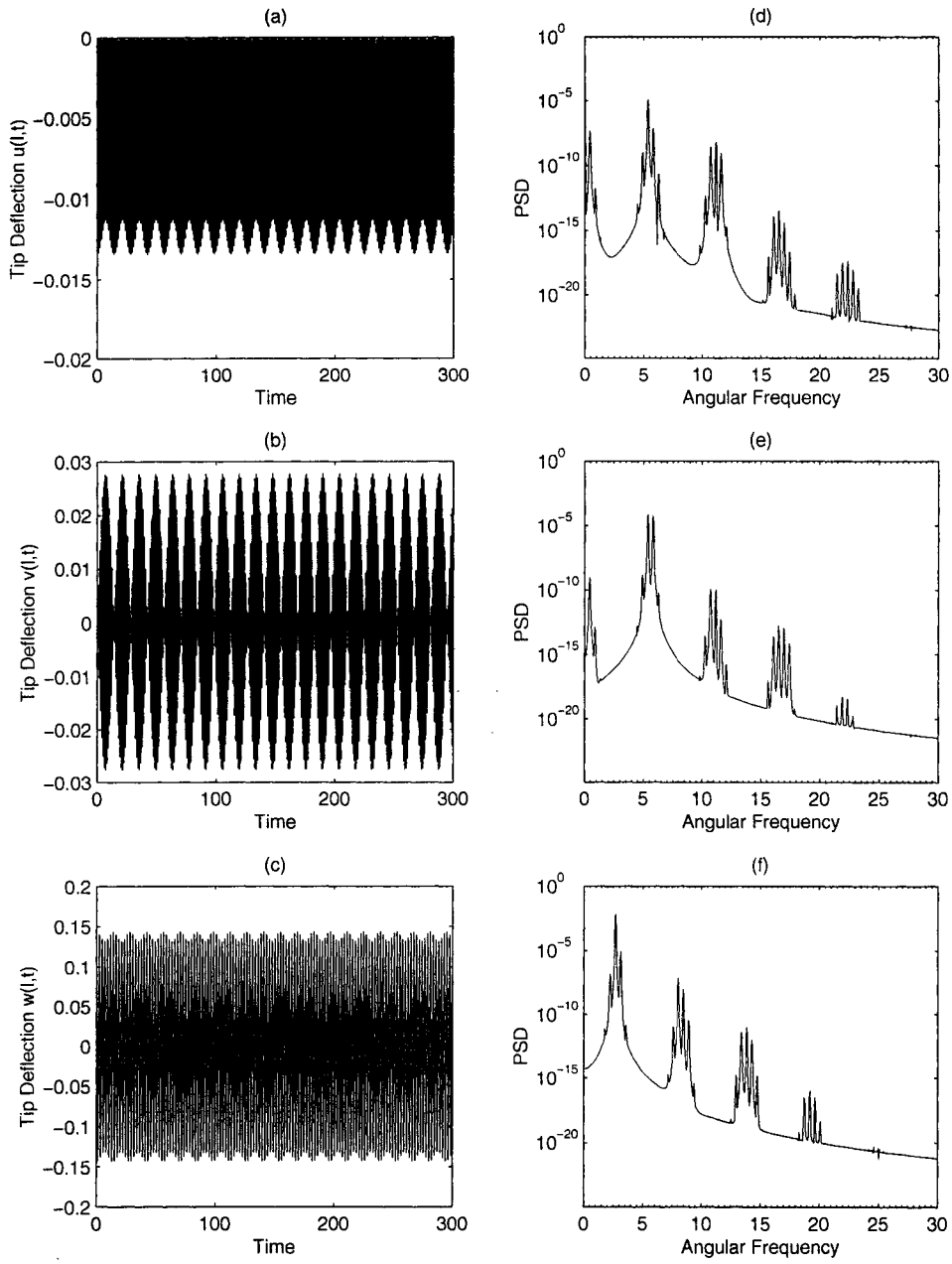

Figure 5.9: Single mode shape nondimensional system response, 1:2 IR by tuning K_{pu} and K_{pw}, AAF Method is applied. (a), (b) and (c) are time responses in u, v, and w directions respectively, (d), (e) and (f) are power spectrums in u, v, and w directions respectively

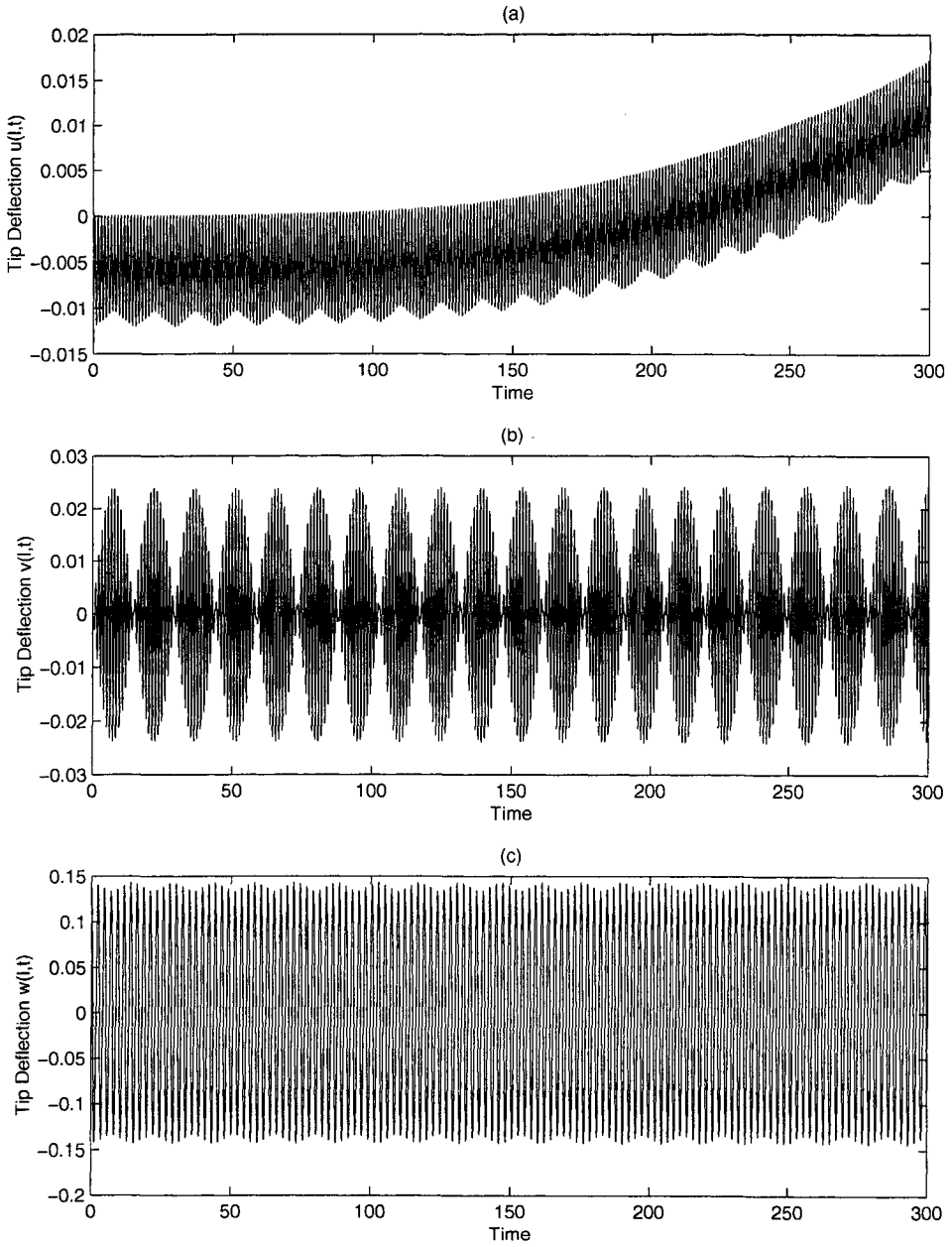

Figure 5.10: Four mode shape nondimensional system response, 1:2 IR by tuning K_{pu} and K_{pw}, Runge-Kutta Method is applied. (a), (b) and (c) are time responses in u, v, and w directions respectively.

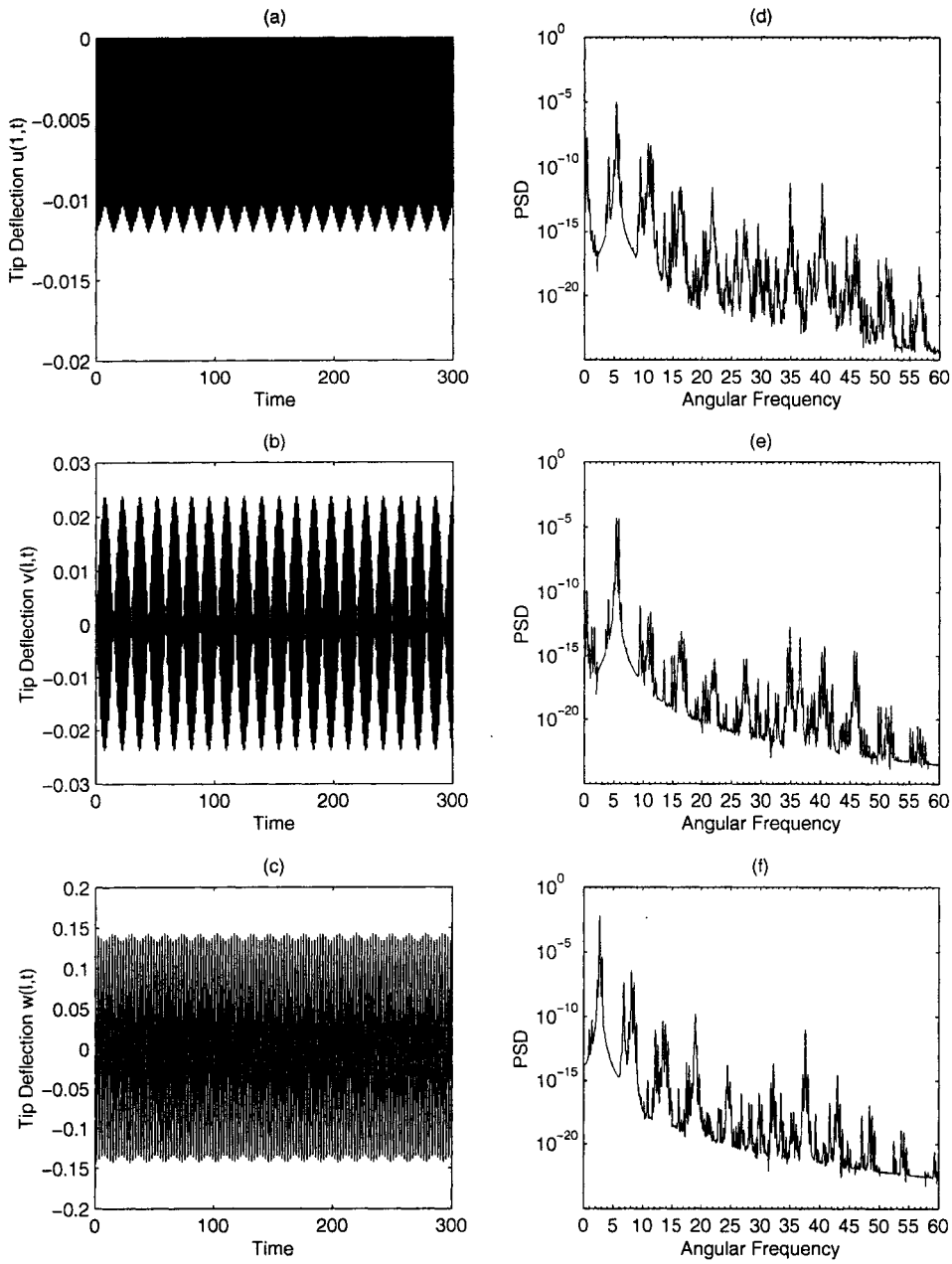

Figure 5.11: Four mode shape nondimensional system response, 1:2 IR by tuning K_{pu} and K_{pw}, AAF Method is applied. (a), (b) and (c) are time responses in u, v, and w directions respectively, (d), (e) and (f) are power spectrums in u, v, and w directions respectively.

In addition to providing good numerical stability, the AAF method employs the actual DAE system and hence the results are more accurate. Further, the AAF algorithm produces evenly spaced data with desired accuracy when compared to the variable step sizes in the adaptive step size Runge-Kutta algorithm. The advantage of having evenly spaced data is that spectral analysis can be implemented directly without any interpolation which necessarily introduces errors.

5.7 Comparison of Single Mode Shape Model and Four Mode Shape Model

For the comparison of the single mode model and four mode model systems the simulations that have already been presented will be used. The figures used for this comparison are tabulated in Table 5.3.

AAF Method 1:2 IR, $\Omega = 50$			
Dimensional Model		Nondimensional Model	
Single Mode	Four Mode	Single Mode	Four Mode
5.5	5.7	5.9	5.11

Table 5.3: Comparison between single mode shape and four mode shape models

By comparing the time response for the single mode shape and four mode shape models it can be seen that there are small differences in the amplitudes. In particular the amplitudes for the single mode shape are slightly larger than the four mode shape models. This is expected because in the four mode shape model there is interaction between higher frequencies which is not present in the single mode

shape model. The interaction between the higher frequencies results in some energy transfer from the lower frequencies to the higher frequencies, which explains the smaller amplitudes of the lower frequencies. The frequency interaction can be seen from the presence of peaks at higher frequencies in the four mode shape model response shown in Figures 5.7 and 5.11. The higher frequencies do not appear in the single mode shape system response as shown in Figures 5.5 and 5.9. This phenomenon is also observed in the 1:1 IR case. The simulation set for 1:1 IR case is tabulated in Table 5.4.

AAF Method 1:1 IR, $\Omega = 50$			
Dimensional Model		Nondimensional Model	
Single Mode	Four Mode	Single Mode	Four Mode
5.12	5.13	5.14	5.15

Table 5.4: Comparison between single mode shape and four mode shape models

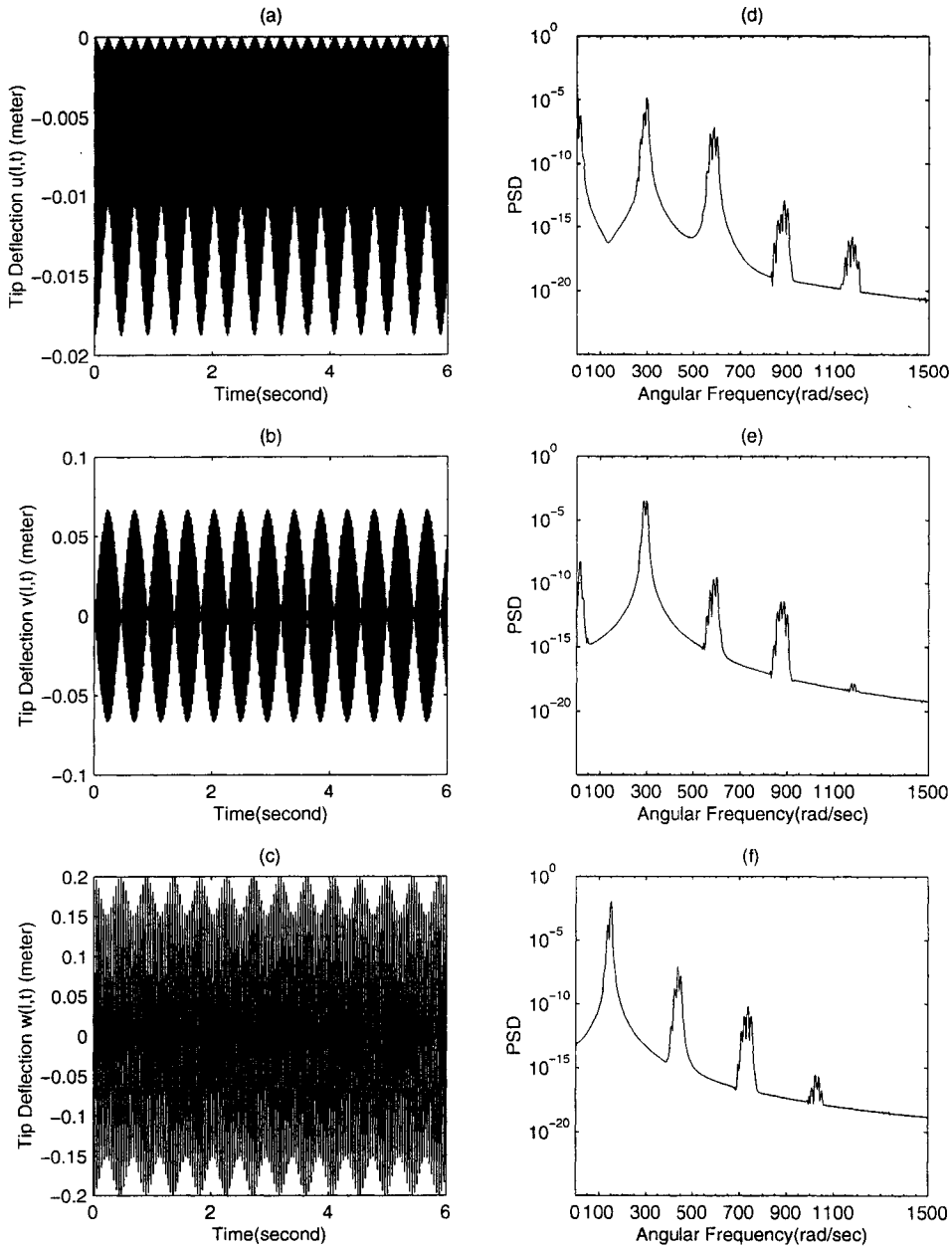

Figure 5.12: Single mode shape dimensional system response, 1:1 IR by tuning K_{pu} and K_{pw}, AAF Method is applied. (a), (b) and (c) are time responses in u, v, and w directions respectively, (d), (e) and (f) are power spectrums in u, v, and w directions respectively.

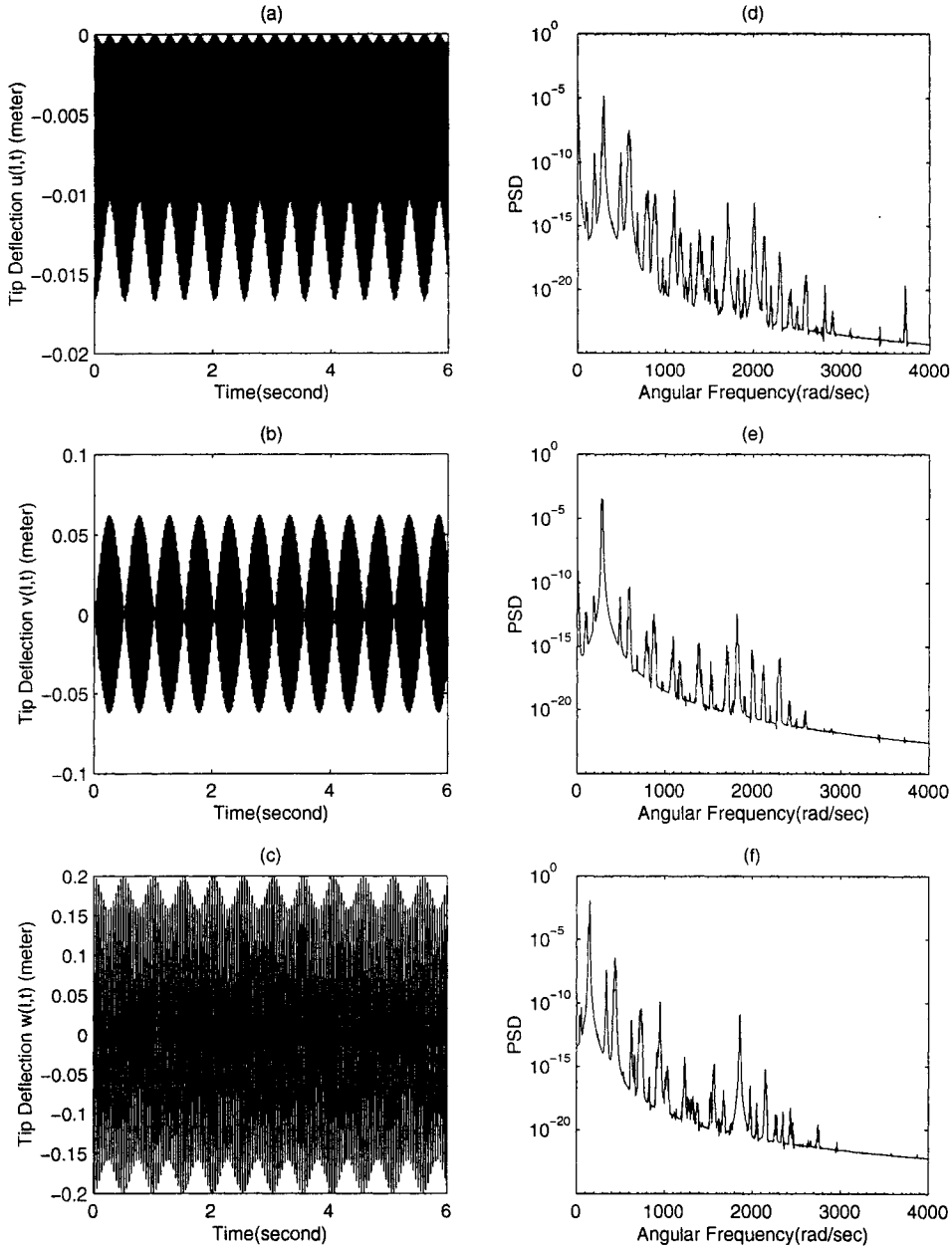

Figure 5.13: Four mode shape dimensional system response, 1:1 IR by tuning K_{pu} and K_{pw}, AAF Method is applied. (a), (b) and (c) are time responses in u, v, and w directions respectively, (d), (e) and (f) are power spectrums in u, v, and w directions respectively.

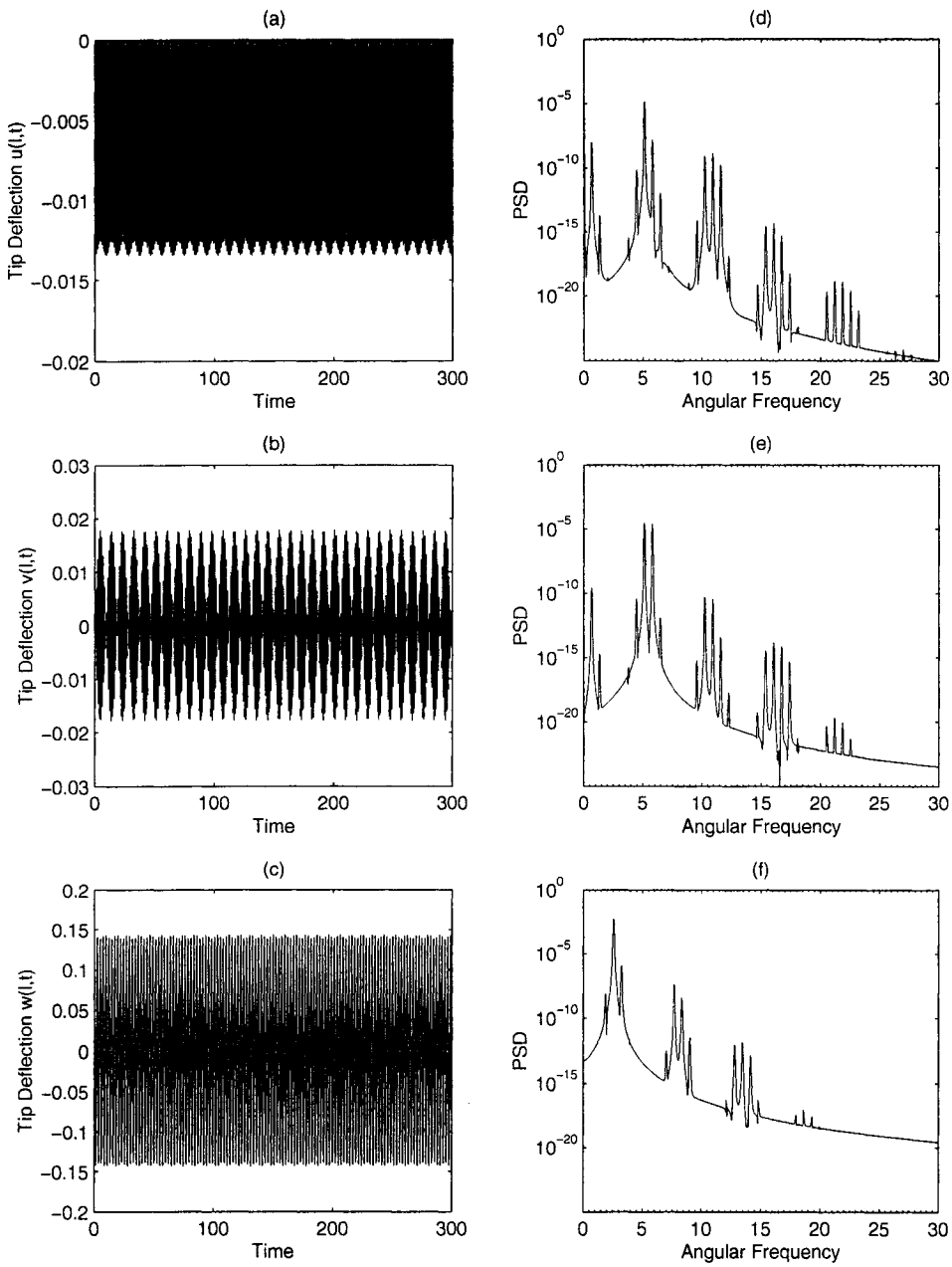

Figure 5.14: Single mode shape nondimensional system response, 1:1 IR by tuning K_{pu} and K_{pw}, AAF Method is applied. (a), (b) and (c) are time responses in u, v, and w directions respectively, (d), (e) and (f) are power spectrums in u, v, and w directions respectively.

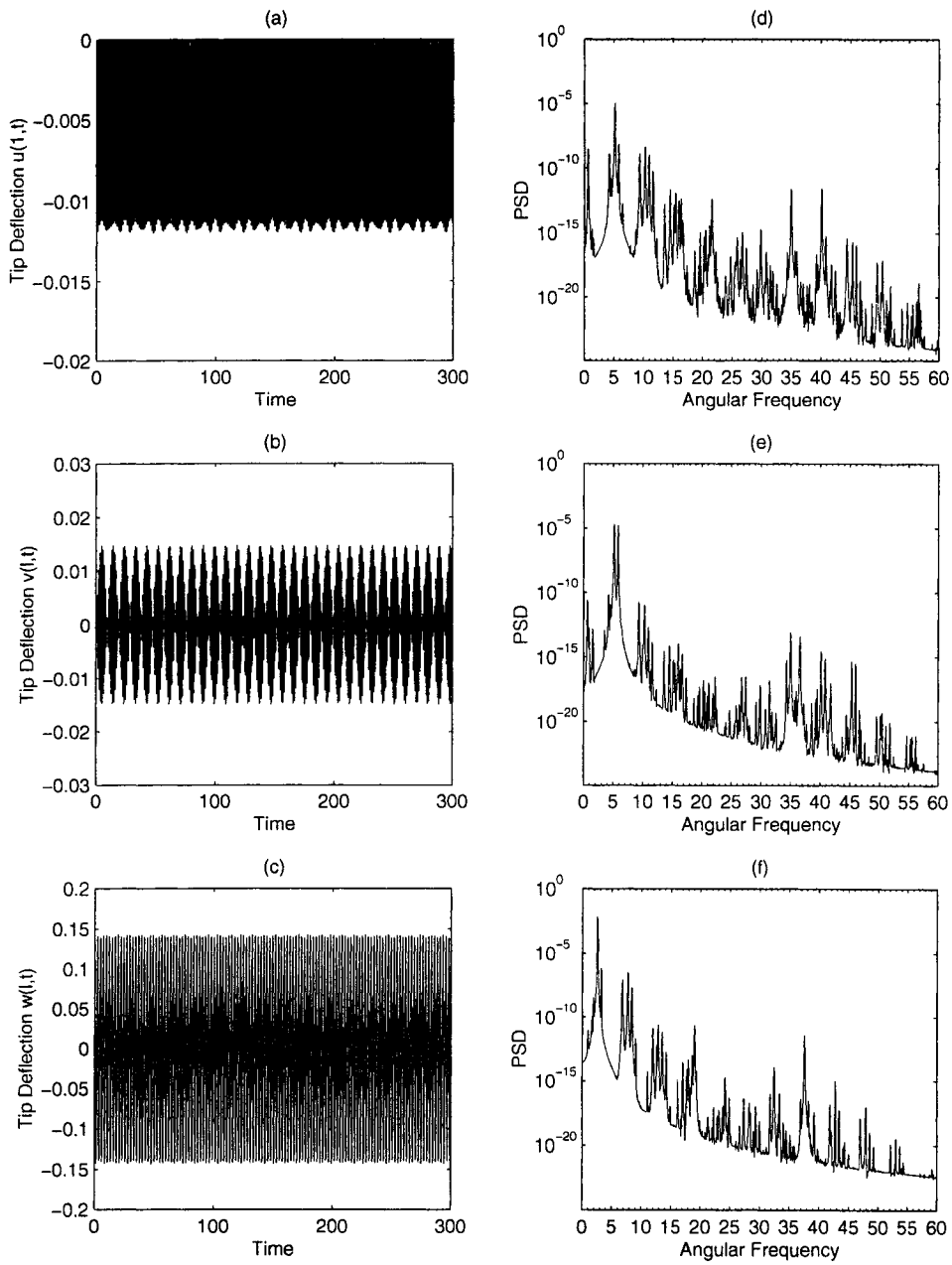

Figure 5.15: Four mode shape nondimensional system response, 1:1 IR by tuning K_{pu} and K_{pw}, AAF Method is applied. (a), (b) and (c) are time responses in u, v, and w directions respectively, (d), (e) and (f) are power spectrums in u, v, and w directions respectively.

5.8 Comparison of 1:1 IR and 1:2 IR

The simulations that have already been presented in the previous sections will be used for the comparison of 1:1 IR and 1:2 IR cases. The figures used for this comparison are tabulated in Table 5.5.

Dimensional Model, $\Omega = 50$, $w_{t0} = 0.2$			
Single Mode Shape		Four Mode Shape	
1:1 IR	1:2 IR	1:1 IR	1:2 IR
5.12	5.5	5.13	5.7

Table 5.5: Comparison between 1:1 IR and 1:2 IR cases

By comparing the system response for 1:1 IR and 1:2 IR (e.g. Figures 5.5 and 5.12) it can be seen that there are slight differences in the spectrums. A careful examination shows that these differences occur in the side bands. The differences in the side bands correspond to the different modulating frequencies (beating frequencies) for the two cases. The different modulating frequencies can be seen by a closer examination of the number of peaks in the time responses for the 1:1 IR and 1:2 IR cases. The number of peaks for 1:2 IR case should be exactly twice the number of peaks for 1:1 IR case. In Figure 5.13(a) for example, the number of peaks for 1:1 IR case is approximately 12.5 and the number of peaks for 1:2 IR case in Figure 5.7(a) is 25. This phenomenon is shown more clearly in Figure 5.16.

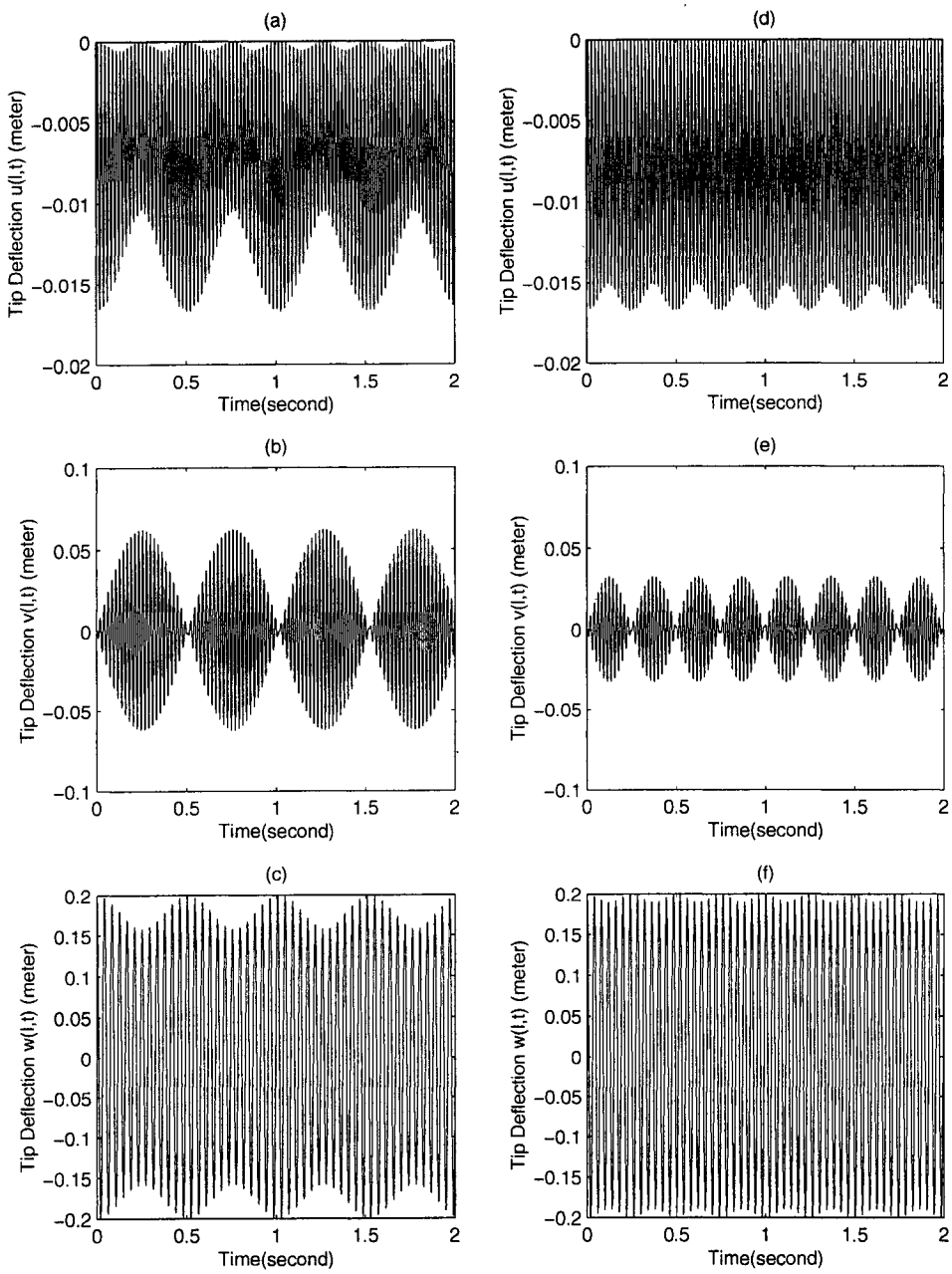

Figure 5.16: Four mode shape dimensional system response, 1:1 IR and 1:2 IR by tuning K_{pu} and K_{pw}, AAF Method is applied. (a), (b) and (c) are time responses in u, v, and w directions respectively for 1:1 IR, (d), (e) and (f) are time responses in u, v, and w directions respectively for 1:2 IR.

5.9 Vibration Suppression Results

As discussed in Section 4.3, vibration suppression is implemented through velocity feedback control by applying velocity feedback in either direction v (K_{dv}) or direction w (K_{dw}), after IR state is established. The control results with only one D controller applied are summarized in Table 5.6.

Dimensional Model 1:1 IR and 1:2 IR, $\Omega = 50$, $w_{t0} = 0.2, K_{dv} = 600, K_{dw} = 0$	
Single Mode Shape	Four Mode Shape
5.17	5.18

Table 5.6: Vibration suppression results with only K_{dv} applied

Good control results are expected for the different tuning techniques and different IR ratios as shown in the Figures 5.17 and 5.18. It is also clear that in direction w, there is a stripe in the steady state response due to the linear oscillator in the system. Since every system has natural damping either due to internal material damping or due to air drag that can remove the steady state stripe, a D controller K_{pw} in direction w was introduced to account for the natural damping effect of the system. The control results with two D controllers applied are summarized in Table 5.7.

Dimensional Model 1:1 IR and 1:2 IR, $\Omega = 50$, $w_{t0} = 0.2, K_{dv} = 15, K_{dw} = 10$	
Single Mode Shape	Four Mode Shape
5.19	5.20

Table 5.7: Vibration suppression results

In other words, after establishing IR state and applying two controllers in direction v and direction w, vibrations can be successfully and rapidly suppressed.

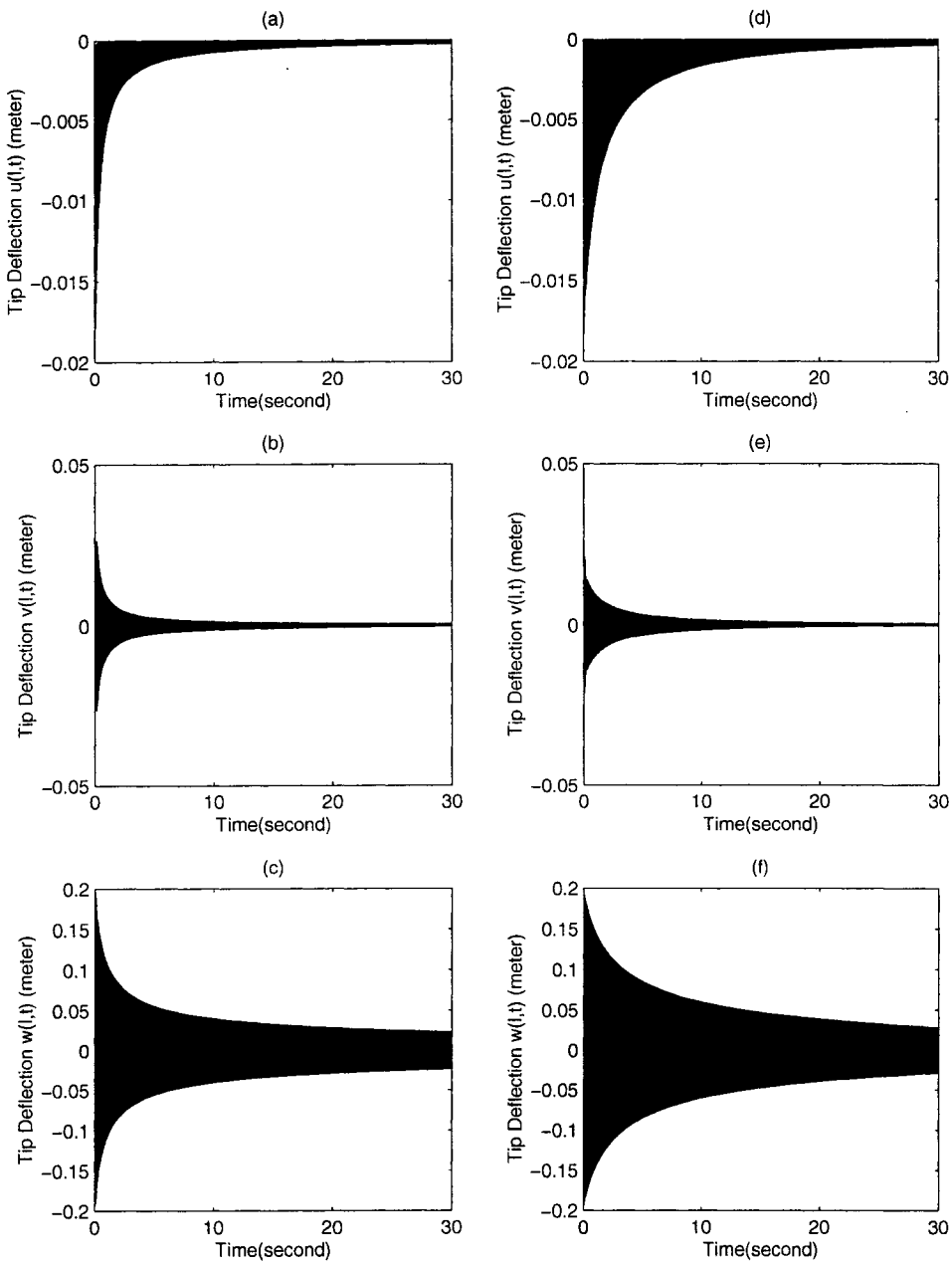

Figure 5.17: Single mode shape dimensional system with damping K_{dv} only, (a), (b) and (c) are time responses for 1:1 IR in u, v, and w directions respectively by tuning K_{pu} and k_{pw}. (d), (e) and (f) are time responses for 1:2 IR in u, v, and w directions respectively by tuning K_{pu} and k_{pw}. AAF Method is applied.

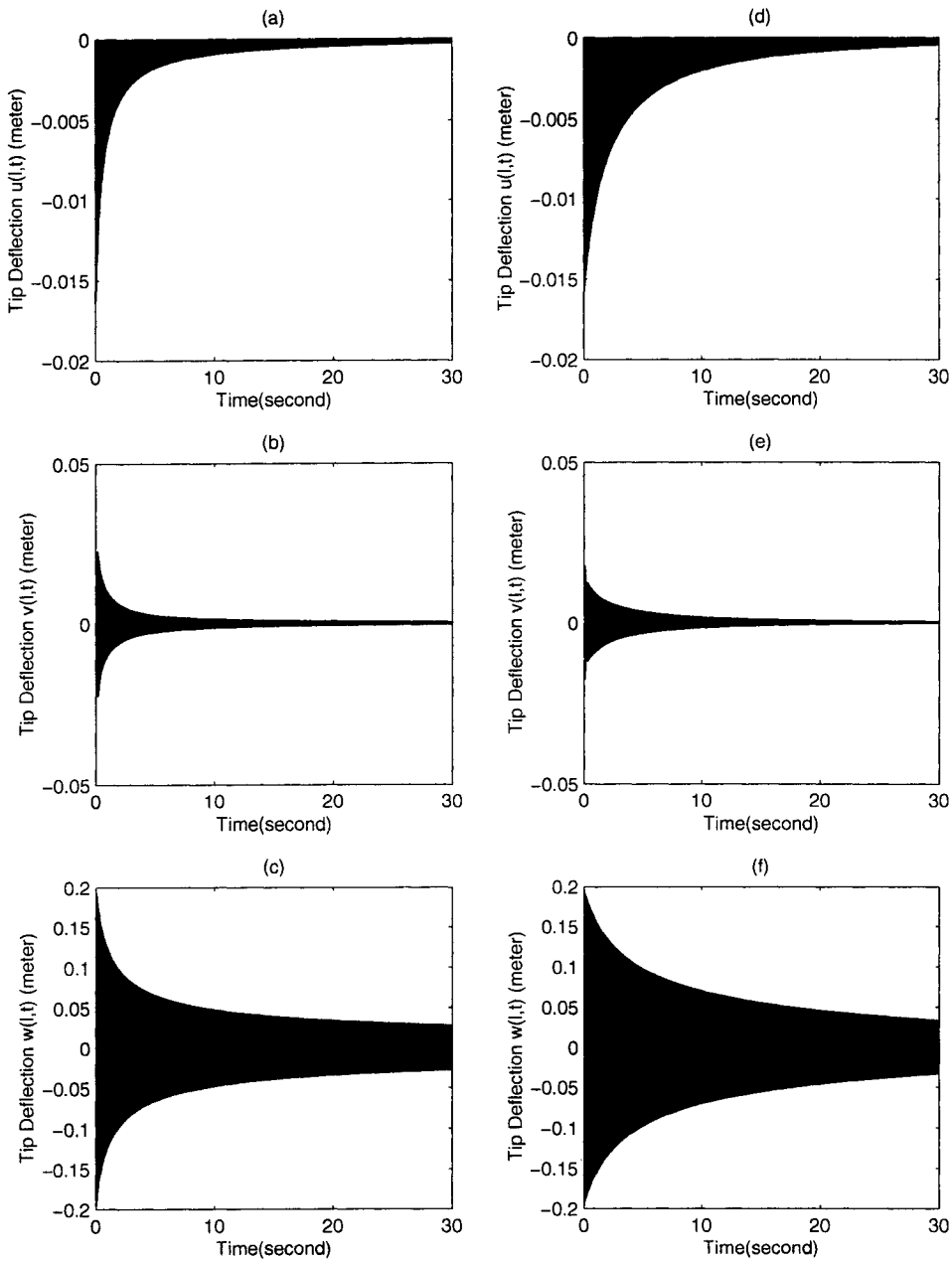

Figure 5.18: Four mode shape dimensional system with damping K_{dv} only, (a), (b) and (c) are time responses for 1:1 IR in u, v, and w directions respectively by tuning K_{pu} and k_{pw}. (d), (e) and (f) are time responses for 1:2 IR in u, v, and w directions respectively by tuning K_{pu} and k_{pw}. AAF Method is applied.

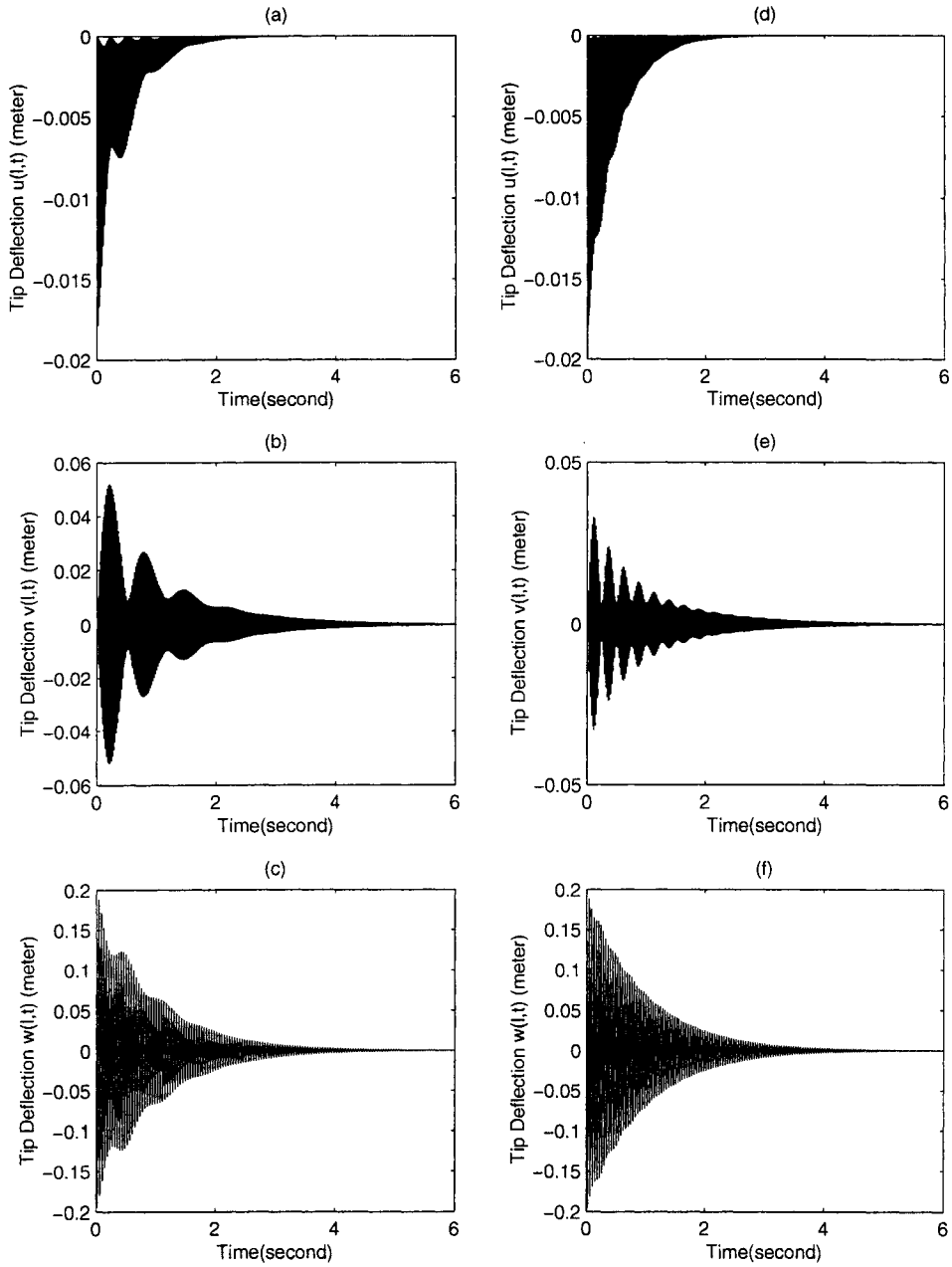

Figure 5.19: Single mode shape dimensional system with damping, (a), (b) and (c) are time responses for 1:1 IR in u, v, and w directions respectively by tuning K_{pu} and k_{pw}. (d), (e) and (f) are time responses for 1:2 IR in u, v, and w directions respectively by tuning K_{pu} and k_{pw}. AAF Method is applied.

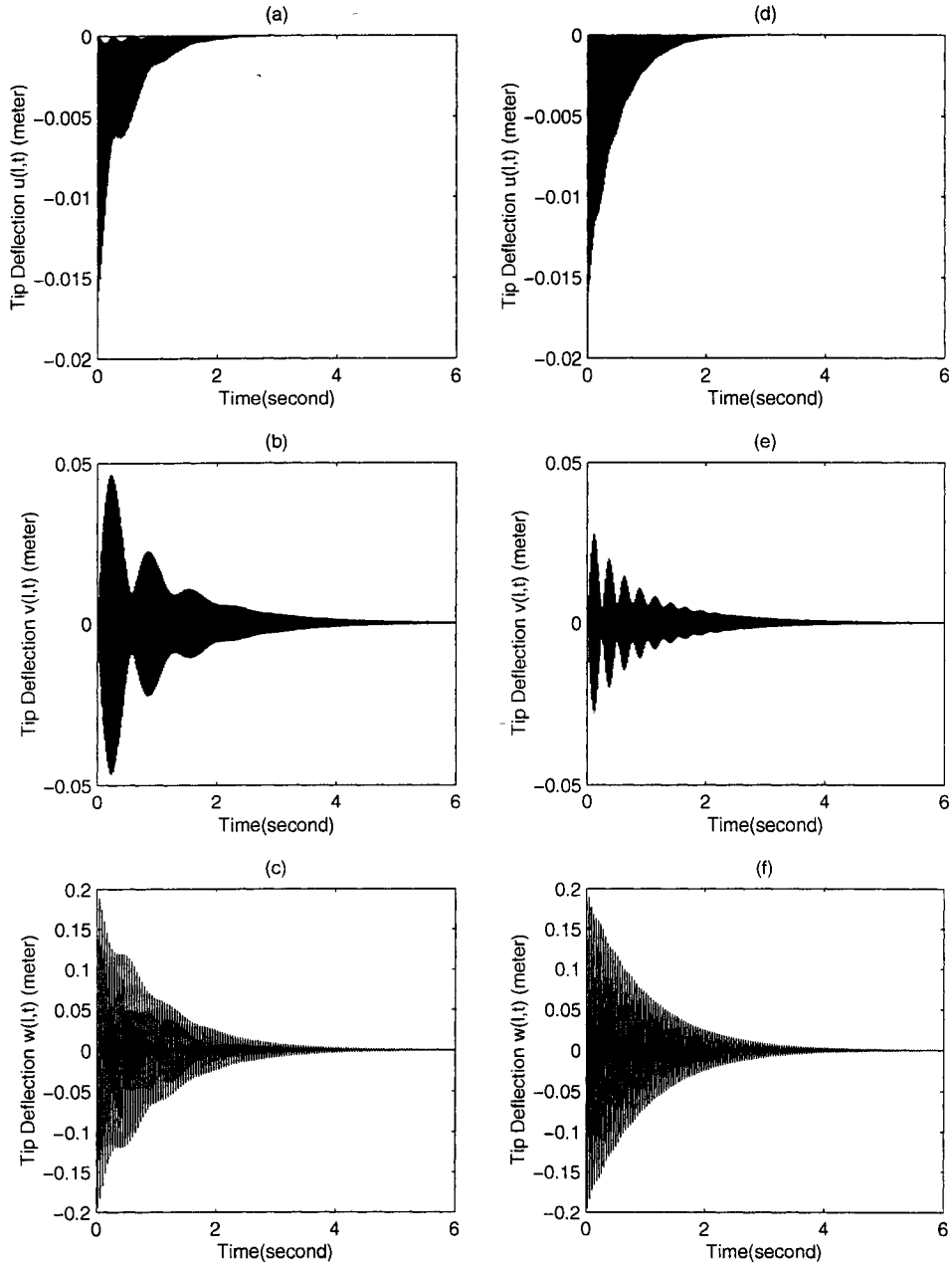

Figure 5.20: Four mode shape dimensional system with damping, (a), (b) and (c) are time responses for 1:1 IR in u, v, and w directions respectively by tuning K_{pu} and k_{pw}. (d), (e) and (f) are time responses for 1:2 IR in u, v, and w directions respectively by tuning K_{pu} and k_{pw}. AAF Method is applied.

In this chapter, two different simulation approaches are presented and their pros and cons are also illustrated through simulation results. The dynamics of the system is also investigated in both time domain and spectral domain and some important aspects of the research are compared. In next chapter, some conclusions will be drawn for this thesis and some future works will also be outlined.

Chapter 6

Conclusion and Future Work

6.1 Conclusion

This thesis has made the following contributions: developing a model for continuous gyroscopic system, the applications of the AAF method, Runge-Kutta method and IR based control strategy for continuous gyroscopic system, and system response analysis.

A typical continuous gyroscopic system is modelled using variational approach based on Hamilton's principle, which yields the governing nonlinear Partial Differential Equations of motion.

To study the dynamics of such a continuous gyroscopic system, a spacial discretization process is implemented using the Galerkin method to reduce the obtained PDEs to ODEs while simultaneously incorporating the natural boundary conditions. Two numerical solvers, an ODEs solver based on Runge-Kutta method and an DAEs solver based on Average Acceleration Formulation (AAF), are used

to simulate the nonlinear gyroscopic system. The Power Spectrum Density (PSD) is computed using FFT to facilitate the system response investigation.

Vibration suppression of the beam is carried out using Internal Resonance (IR) control strategy. Once IR state is established, coupling and energy transaction among the three directions u, v and w of the beam is greatly enhanced. Accordingly, damping (velocity feedback) is introduced into the system to suppress the vibrations. The IR control strategy is implemented through the design of IR based PD controllers.

To set up Internal Resonance, linear natural frequencies of the system is first computed to approximate the response frequencies of the nonlinear system. The approximate natural frequencies are tuned and made commensuable by adjusting the stiffness of the nonlinear beam using position feedback.

The numerical simulation results from different solvers, models and IR states and under different circumstances have been brought into comparisons that yield some important conclusions.

In general there are minor differences between the Runge-Kutta method and AAF for the dimensional model. As for nondimensional model, Runge-Kutta method is diverging due to numerical instability when the time range is increased, whereas AAF remains very stable. In addition to good numerical stability, the AAF method employs the actual DAE system and hence yields more accurate results. Further, the AAF algorithm produces evenly spaced data with desired accuracy.

There are small differences in the amplitudes for the single mode shape and four mode shape models. In particular the amplitudes for the single mode shape are

slightly larger than the four mode shape models.

Finally, by comparing the system response for 1:1 IR and 1:2 IR cases it is observed that there are slight differences in the spectrums. However, large differences exist in the amplitude for v. These differences are due to different modulating frequencies.

6.2 Future Work

This thesis focused on vibration suppression of a gyroscopic beam that undergoes flapwise and chordwise elastic deformations. One of the possible future research topics is the introduction of torsional elastic motion into the beam. In the spatial discretization, the eigenfunctions of a cantilever beam are chosen as the basis function when applying Galerkin method, the use of Finite Element shape function as the orthogonal basis function and using finite element based acceleration method to change the resulting ODEs into nonlinear algebraic equations is worth examining. When modelling the system, piezo-electric actuator can also be taken into account. Another future research goal is to use perturbation method to investigate the continuous gyroscopic system.

Appendix A

Nondimensional Model

In this Appendix, the nondimensional form of equations of motion, their corresponding spatial discretization and numerical simulation are presented through the nondimensionalizing process.

A.1 Nondimensional Parameters

To derive the nondimensional equations of motion, the length of the beam l and the angular velocity Ω are both used to nondimensionalize the system parameters and the following nondimensional parameters are therefore obtained:

$$\begin{array}{llll} \hat{x} = \frac{x}{l} & \hat{u} = \frac{u}{l} & \hat{v} = \frac{v}{l} & \hat{w} = \frac{w}{l} \\ \hat{A} = \frac{A}{l^2} & \hat{I}_y = \frac{I_y}{Al^2} & \hat{I}_z = \frac{I_z}{Al^2} & \hat{E} = \frac{E}{\rho A \Omega^2} \\ \hat{t} = \Omega t & \hat{\lambda} = \frac{\lambda}{EA} & & \end{array} \tag{A.1}$$

For convenience sake, the (ˆ)s are dropped in the following sections.

A.2 Nondimensional Equations of Motion

Using the nondimensional parameters in Section A.1, the following nondimensional form of equations of motion are obtained:

u variation:

$$\int_0^1 \{(-2\,v_{,t} - u + u_{,tt}) - E\,A\,[\lambda\,(1+u_{,x}) + \sin(\theta_y)\cos(\theta_z)\,I_y\,\theta_{y,xx} - \frac{1}{2}\frac{\sin(\theta_z)\left((\cos(\theta_y))^2(I_y - I_z) - I_y - I_z\right)\theta_{z,xx}}{\cos(\theta_y)} - \frac{1}{2}(I_y - I_z)(\sin(\theta_y))^2\cos(\theta_y)\cos(\theta_z)(\theta_{z,x})^2 + \sin(\theta_y)\sin(\theta_z)(I_y - I_z)\,\theta_{y,x}\theta_{z,x}]_{,x}\} dx = 0 \tag{A.2}$$

v variation:

$$\int_0^1 \{(2\,u_{,t} - v + v_{,tt}) - E\,A\,[\lambda\,v_{,x} + \sin(\theta_y)\sin(\theta_z)\,I_y\,\theta_{y,xx} + \frac{1}{2}\frac{\cos(\theta_z)\left((\cos(\theta_y))^2(I_y - I_z) - I_y - I_z\right)\theta_{z,xx}}{\cos(\theta_y)} - \frac{1}{2}(I_y - I_z)(\sin(\theta_y))^2\cos(\theta_y)\sin(\theta_z)(\theta_{z,x})^2 - \sin(\theta_y)\cos(\theta_z)(I_y - I_z)\,\theta_{y,x}\theta_{z,x}]_{,x}\} dx = 0 \tag{A.3}$$

w variation:

$$\int_0^1 \left[w_{,tt} - E\,A\left(\frac{1}{2}(\cos(\theta_y))^2\sin(\theta_y)(\theta_{z,x})^2(I_z - I_y) + \cos(\theta_y)(\theta_{y,xx})\,I_y + \lambda\,w_{,x}\right)_{,x}\right] dx = 0 \tag{A.4}$$

λ variation

$$-\frac{1}{2}\int_0^l \left[(1+u_{,x})^2+(v_{,x})^2+(w_{,x})^2-1\right]dx = 0 \tag{A.5}$$

the derivations for $\delta\theta_y$ and $\delta\theta_z$ are as follows:

1. From the trigonometric relations between $\delta\theta_y$, $\delta\theta_z$, u, v and w, we have:

$$\tan\theta_y = -\frac{w'}{\sqrt{(1+u')^2+v'^2}} \tag{A.6}$$

$$\tan\theta_z = \frac{v'}{1+u'} \tag{A.7}$$

$$\sin\theta_y = -w' \tag{A.8}$$

$$\cos\theta_y = \sqrt{(1+u')^2+v'^2} \tag{A.9}$$

$$\sin\theta_z = \frac{v'}{\sqrt{(1+u')^2+v'^2}} \tag{A.10}$$

$$\cos\theta_z = \frac{1+u'}{\sqrt{(1+u')^2+v'^2}} \tag{A.11}$$

$$v' = \cos\theta_y \sin\theta_z \tag{A.12}$$

$$1+u' = \cos\theta_y \cos\theta_z \tag{A.13}$$

2. For $F(x,y,y')$, its first variation is given by:

$$\delta^{(1)}F = \frac{\partial F}{\partial y}\delta y + \frac{\partial F}{\partial y'}\delta y' \tag{A.14}$$

3. Apply (A.14) to (A.7) and use the relations in (A.12) and (A.13), the following equation is obtained:

$$\begin{aligned} \frac{1}{\cos^2\theta_z}\delta\theta_z &= -\frac{v'}{(1+u')^2}\delta u' + \frac{1}{1+u'}\delta v' \\ &= -\frac{\cos\theta_y \sin\theta_z}{\cos^2\theta_y \cos^2\theta_z}\delta u' + \frac{1}{\cos\theta_y \cos\theta_z}\delta v' \end{aligned} \tag{A.15}$$

4. From (A.15), the equation for $\delta\theta_z$ is obtained as:

$$\delta\theta_z = -\frac{\sin\theta_z}{\cos\theta_y}\,\delta u' + \frac{\cos\theta_z}{\cos\theta_y}\,\delta v' \tag{A.16}$$

5. Following the same approach, the equation for $\delta\theta_y$ is given by:

$$\delta\theta_y = -\cos\theta_y\,\delta w' - \cos\theta_z \sin\theta_y\,\delta u' - \sin\theta_z \sin\theta_y\,\delta v' \tag{A.17}$$

A.3 Spatial Discretization

In this section, the nondimensional process of spatial discritization is presented.

A.3.1 Symmetric Form

The nondimensional symmetric form of equations of motion are given by:

u variation:

$$\int_0^1 \left\{ p\left(u_{,tt} - 2v_{,t} - u\right) + EA\left(\left(u_{,xx}\right) I_y - \frac{1}{2\left(1-\left(w_{,x}\right)^2\right)^2}\left(I_z + I_y\right) \right.\right.$$
$$\left(v_{,x}\right)\left(\left(1+u_{,x}\right)v_{,xx} - \left(v_{,x}\right)u_{,xx}\right) - \frac{1}{2\left(1-\left(w_{,x}\right)^2\right)}\left(I_z - 3I_y\right)\left(v_{,x}\right)$$
$$\left(\left(1+u_{,x}\right)v_{,xx} - \left(v_{,x}\right)u_{,xx}\right)\right) p_{,xx} + EA\left(-\frac{I_y\left(1+u_{,x}\right)\left(w_{,xx}\right)^2}{1-\left(w_{,x}\right)^2} \right.$$
$$-\frac{1}{2\left(1-\left(w_{,x}\right)^2\right)^3}\left(I_z + I_y\right)\left(\left(1+u_{,x}\right)\left(\left(\left(v_{,x}\right)u_{,xx} - \left(1+u_{,x}\right)v_{,xx}\right)^2\right.\right.$$
$$\left.\left. + \left(v_{,x}\right)\left(v_{,xx}\right)\left(w_{,x}\right)w_{,xx}\right) - \left(v_{,x}\right)^2\left(u_{,xx}\right)\left(w_{,x}\right)w_{,xx}\right) - \frac{1}{2\left(1-\left(w_{,x}\right)^2\right)^2}$$
$$\left(I_z - 3I_y\right)\left(\left(v_{,x}\right)\left(v_{,xx}\right)\left(w_{,x}\right)\left(w_{,xx}\right)\left(1+u_{,x}\right) - \left(v_{,x}\right)^2\left(u_{,xx}\right)\left(w_{,x}\right)w_{,xx}\right)$$
$$+\frac{1}{2\left(1-\left(w_{,x}\right)^2\right)}\left(I_y - I_z\right)\left(1+u_{,x}\right)\left(\left(v_{,x}\right)u_{,xx} - \left(1+u_{,x}\right)v_{,xx}\right)^2$$
$$\left.\left. +\lambda\left(1+u_{,x}\right)\right)p_{,x}\right\}dx = 0 \qquad \text{(A.18)}$$

v variation:

$$\int_0^1 \Bigg\{ p\left(v_{,tt} + 2\,u_{,t} - v\right) + EA\left(\left(v_{,xx}\right) I_y + \frac{1}{2\left(1-\left(w_{,x}\right)^2\right)^2}\left(I_z + I_y\right) \right.$$
$$\left(1+u_{,x}\right)\left(\left(1+u_{,x}\right)v_{,xx} - \left(v_{,x}\right)u_{,xx}\right) + \frac{1}{2\left(1-\left(w_{,x}\right)^2\right)}\left(I_z - 3\,I_y\right)$$
$$\left(1+u_{,x}\right)\left(\left(1+u_{,x}\right)v_{,xx} - \left(v_{,x}\right)u_{,xx}\right)\Big) p_{,xx} + EA\left(-\frac{I_y\left(v_{,x}\right)\left(w_{,xx}\right)^2}{1-\left(w_{,x}\right)^2} \right.$$
$$-\frac{1}{2\left(1-\left(w_{,x}\right)^2\right)^3}\left(I_z + I_y\right)\Big(\left(v_{,x}\right)\Big(\left(\left(v_{,x}\right)u_{,xx} - \left(1+u_{,x}\right)v_{,xx}\right)^2$$
$$+\left(1+u_{,x}\right)\left(u_{,xx}\right)\left(w_{,x}\right)w_{,xx}\Big) - \left(1+u_{,x}\right)^2\left(v_{,xx}\right)\left(w_{,x}\right)w_{,xx}\Big) +$$
$$\frac{1}{2\left(1-\left(w_{,x}\right)^2\right)^2}\left(I_z - 3\,I_y\right)\Big(\left(1+u_{,x}\right)^2\left(v_{,xx}\right)\left(w_{,x}\right)w_{,xx} - \left(1+u_{,x}\right)\left(v_{,x}\right)$$
$$\left(u_{,xx}\right)\left(w_{,x}\right)w_{,xx}\Big) + \frac{1}{2\left(1-\left(w_{,x}\right)^2\right)}\left(I_y - I_z\right)\left(v_{,x}\right)\Big(\left(v_{,x}\right)u_{,xx}$$
$$\left.\left. -\left(1+u_{,x}\right)v_{,xx}\right)^2 + \lambda\, v_{,x}\right) p_{,x} \Bigg\}\, dx = 0 \qquad \text{(A.19)}$$

w variation:

$$\int_0^1 \left[p\,w_{,tt} + EA\,I_y\,\left(w_{,xx}\right)p_{,xx} + EA\left(\lambda\, w_{,x} - \frac{I_y\left(w_{,x}\right)\left(w_{,xx}\right)^2}{1-w_{,x}^2} \right.\right.$$
$$\left.\left. -\frac{1}{2}\,\frac{\left(I_z - I_y\right)\left(w_{,x}\right)\left(\left(v_{,x}\right)u_{,xx} - \left(1+u_{,x}\right)v_{,xx}\right)^2}{1-w_{,x}^2}\right) p_{,x} \right] dx = 0 \qquad \text{(A.20)}$$

λ variation

$$-\frac{1}{2}\int_0^l \left[\left(1+u_{,x}\right)^2 + \left(v_{,x}\right)^2 + \left(w_{,x}\right)^2 - 1\right] dx = 0 \qquad \text{(A.21)}$$

A.3.2 Discretized Equations of Motion

The nondimensional discretized equations of motion are as follows:

u equation:

$$\int_0^1 \Big[EAI_y \{\phi_i''\} \lfloor \phi_j'' \rfloor \{\alpha_j\} + [\phi_i' \phi_j] \{\lambda_j\} + [\phi_i \, \phi_j] \left\{ \{\ddot{\alpha}_j\} - 2 \left\{ \dot{\beta}_j \right\} \right.$$
$$\left. - \{\alpha_j\} \right\} + \{\phi_i'\} \lfloor \phi_j \, \phi_k' \rfloor \{\lambda_j \, \alpha_k\} + \{\phi_i'\} \lfloor \phi_j'' \, \phi_k''' \rfloor \{-EAI_z \{\beta_j \, \beta_k\}$$
$$-EAI_y \{\gamma_j \, \gamma_k\}\} + \{\phi_i\} \lfloor \phi_j \, \phi_k' \, \phi_l' \rfloor \left\{ -3 \{\ddot{\alpha}_j \, \gamma_k \, \gamma_l\} + 6 \left\{ \dot{\beta}_j \, \gamma_k \, \gamma_l \right\} \right.$$
$$\left. +3 \{\alpha_j \, \gamma_k \, \gamma_l\} \right\} + \{\phi_i''\} \lfloor \phi_j' \, \phi_k' \, \phi_l'' \rfloor \{EA \, (I_y - I_z) \{\alpha_j \, \beta_k \, \beta_l\}$$
$$-EA \, (I_y - I_z) \{\beta_j \, \beta_k \, \alpha_l\} - 3 \, EAI_y \{\gamma_j \, \gamma_k \, \alpha_l\}\} + \{\phi_i'\} \lfloor \phi_j' \, \phi_k'' \rfloor$$
$$\{-3 \, EAI_z \{\alpha_j \, \beta_k \, \beta_l\} - EAI_y \{\alpha_j \, \gamma_k \, \gamma_l\} + 2 \, EAI_z \{\beta_j \, \alpha_k \, \beta_l\}\}$$
$$-3 \{\phi_i'\} \lfloor \phi_j \, \phi_k' \, \phi_l' \rfloor \{\lambda_j \, \gamma_k \, \gamma_l\}] \, dx = 0 \qquad \text{(A.22)}$$

v equation:

$$\int_0^1 \Big[EAI_z \, [\phi_i'' \, \phi_j''] \{\beta_j\} + [\phi_i \, \phi_j] \left\{ \left\{ \ddot{\beta}_j \right\} + 2 \{\dot{\alpha}_j\} - \{\beta_j\} \right\}$$
$$+ \{\phi_i'\} \lfloor \phi_j \, \phi_k' \rfloor \{\lambda_j \, \beta_k\} + \{\phi_i''\} \lfloor \phi_j' \, \phi_k'' \rfloor \{-2 \, EA \, (I_y - I_z) \{\alpha_j \, \beta_k\}$$
$$+EA \, (I_y - I_z) \{\beta_j \, \alpha_k\}\} + \{\phi_i\} \lfloor \phi_j \, \phi_k' \, \phi_l' \rfloor \left\{ -3 \left\{ \ddot{\beta}_j \, \gamma_k \, \gamma_l \right\} \right.$$
$$\left. -6 \{\dot{\alpha}_j \, \gamma_k \, \gamma_l\} + 3 \{\beta_j \, \gamma_k \, \gamma_l\} \right\} + \{\phi_i'\} \lfloor \phi_j' \, \phi_k'' \, \phi_l'' \rfloor \{-EAI_z \{\beta_j \, \beta_k \, \beta_l\}$$
$$-EAI_y \{\beta_j \, \gamma_k \, \gamma_l\} - EA \, (I_y - I_z) \{\gamma_j \, \beta_k \, \gamma_l\}\} + \{\phi_i''\} \lfloor \phi_j' \, \phi_k' \, \phi_l'' \rfloor$$
$$\{-EA \, (I_y - I_z) \{\alpha_j \, \alpha_k \, \beta_l\} + EA \, (I_y - I_z) \{\alpha_j \, \beta_k \, \alpha_l\}$$
$$\left. -\frac{1}{2} EA \, (3 \, I_z + I_y) \{\gamma_j \, \gamma_k \, \beta_l\} \right\} \Big] \, dx = 0 \qquad \text{(A.23)}$$

w equation:

$$\int_0^1 \left[EAI_y \left[\phi_i'' \, \phi_j''\right] \{\gamma_j\} + \left[\phi_i \, \phi_j\right] \{\ddot{\gamma}_j\} + \{\phi_i'\} \lfloor \phi_j \, \phi_k' \rfloor \{\lambda_j \, \gamma_k\} \right.$$
$$- \{\phi_i\} \lfloor \phi_j \, \phi_k' \, \phi_l' \rfloor \{\ddot{\gamma}_j \, \gamma_k \, \gamma_l\} + \{\phi_i'\} \lfloor \phi_j' \, \phi_k'' \, \phi_l'' \rfloor \left\{ \frac{1}{2} EA \left(I_y - I_z\right) \right.$$
$$\{\gamma_j \, \beta_k \, \beta_l\} - EAI_y \, \{\gamma_j \, \gamma_k \, \gamma_l\}\}$$
$$\left. -EAI_y \, \{\phi_i''\} \lfloor \phi_j' \, \phi_k' \, \phi_l'' \rfloor \{\gamma_j \, \gamma_k \, \gamma_l\} \right] dx \, = \, 0 \tag{A.24}$$

λ equation

$$\int_0^1 \left[\left[\phi_i \, \phi_j'\right] \{\alpha_j\} + \{\phi_i\} \lfloor \phi_j' \, \phi_k' \rfloor \left\{ \frac{1}{2} \, \{\alpha_j \, \alpha_k\} + \frac{1}{2} \, \{\beta_j \, \beta_k\} \right.\right.$$
$$\left.\left. + \frac{1}{2} \, \{\gamma_j \, \gamma_k\} \right\} \right] dx \, = \, 0 \tag{A.25}$$

A.4 Basis Functions and the Matrices

The nondimensional eigenfunctions of cantilever beam are given by:

$$\phi_i = \cosh(k_i x) - \cos(k_i x) - \frac{\cos(k_i) + \cosh(k_i)}{\sin(k_i) + \sinh(k_i)} (\sinh(k_i x) - \sin(k_i x)) \tag{A.26}$$

For the first four modes, k_i have the following values:

$$k_1 = 1.875104069 \quad k_2 = 4.694091133 \quad k_3 = 7.854757438 \quad k_4 = 10.99554073$$

The four mode shapes for nondimensional model are shown in Figure A.1, and the corresponding mass and stiffness matrices are given by:

$$[M_{ij}] = \left[\int_0^l \phi_i \phi_j \, dx\right] = \begin{bmatrix} 1 & 0 & 0 & 0 \\ 0 & 1 & 0 & 0 \\ 0 & 0 & 1 & 0 \\ 0 & 0 & 0 & 1 \end{bmatrix} \tag{A.27}$$

$$[K_{ij}] = \left[\int_0^l \phi_i'' \phi_j'' \, dx\right]$$

$$= \begin{bmatrix} 12.36236340 & 0 & 0 & 0 \\ 0 & 485.5185211 & 0 & 0 \\ 0 & 0 & 3806.546524 & 0 \\ 0 & 0 & 0 & 14617.25610 \end{bmatrix} \tag{A.28}$$

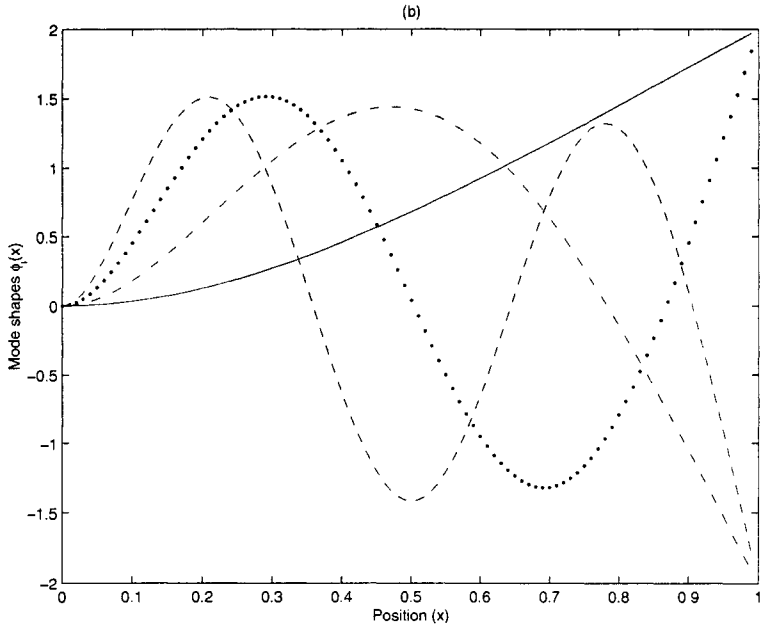

Figure A.1: Nondimensional mode shapes, (-) ϕ_1, (-.) ϕ_2, (...) ϕ_3, (- -) ϕ_4

In next section, linearized equations of motion will be presented.

A.5 Linearized Equations of Motion

The nondimensional form of linearized equations of motion are given as:

$$\begin{bmatrix} \int_0^1 \phi_1\phi_1 dx & 0 & 0 \\ 0 & \int_0^1 \phi_1\phi_1 dx & 0 \\ 0 & 0 & \int_0^1 \phi_1\phi_1 dx \end{bmatrix} \begin{bmatrix} \ddot{\alpha} \\ \ddot{\beta} \\ \ddot{\gamma} \end{bmatrix}$$

$$+ \begin{bmatrix} 0 & -2\int_0^1 \phi_1\phi_1 dx & 0 \\ 2\int_0^1 \phi_1\phi_1 dx & 0 & 0 \\ 0 & 0 & 0 \end{bmatrix} \begin{bmatrix} \dot{\alpha} \\ \dot{\beta} \\ \dot{\gamma} \end{bmatrix}$$

$$+ \begin{bmatrix} EAI_y \int_0^1 \phi_1''\phi_1'' dx - \int_0^1 \phi_1\phi_1 dx + K_{pu} & 0 & 0 \\ 0 & EAI_z \int_0^1 \phi_1''\phi_1'' dx - \int_0^1 \phi_1\phi_1 dx + K_{pv} & 0 \\ 0 & 0 & EAI_y \int_0^1 \phi_1''\phi_1'' dx + K_{pw} \end{bmatrix} \begin{bmatrix} \alpha \\ \beta \\ \gamma \end{bmatrix} = \begin{bmatrix} 0 \\ 0 \\ 0 \end{bmatrix} \tag{A.29}$$

where the integral upper limit is 1.

A.6 Coefficients in Nondimensional Linear Algebraic Equations

The nondimensional form of the coefficients for (4.4) are as follows:

$$\begin{aligned} c_1 &= 1 \\ c_2 &= 2939.813383\,\Omega^{-2} + 12.36236338\,K_{pu} - 1.0 \\ c_3 &= 2 \\ c_4 &= 86235.42346\,\Omega^{-2} + 12.36236338\,K_{pv} - 1.0 \\ c_5 &= 2939.813383\,\Omega^{-2} + 12.36236338\,K_{pw} \end{aligned} \tag{A.30}$$

A.7 Discretized Equations of Motion

The nondimensional form of discretized equations of motion are given by:

u equation:

$$\int_0^1 \left[EAI_y \{\phi_i''\} \lfloor\phi_j''\rfloor \{a_5\ddot{\alpha}_j + c2\alpha_j\} + EA\,[\phi_i'\phi_j]\,\{\lambda_j\}\right.$$
$$+[\phi_i\,\phi_j]\left\{\{\ddot{\alpha}_j\} - 2\left\{\{a_2\ddot{\beta}_j + c1\beta_j\}\right\} - \{a_5\ddot{\alpha}_j + c2\alpha_j\}\right\}$$
$$+EA\,\{\phi_i'\}\,\lfloor\phi_j\,\phi_k'\rfloor\,\{\lambda_j\,\{a_5\ddot{\alpha}_k + c2\alpha_k\}\} + \{\phi_i'\}\,\lfloor\phi_j''\,\phi_k''\rfloor$$
$$\left\{-EAI_z\left\{\{a_5\ddot{\beta}_j + c2\beta_j\}\,\{a_5\ddot{\beta}_k + c2\beta_k\}\right\} - EAI_y\,\{\{a_5\ddot{\gamma}_j + c2\gamma_j\}\right.$$
$$\{a_5\ddot{\gamma}_k + c2\gamma_k\}\}\} + \{\phi_i\}\,\lfloor\phi_j\,\phi_k'\,\phi_l'\rfloor\,\{-3\,\{\ddot{\alpha}_j\,\{a_5\ddot{\gamma}_k + c2\gamma_k\}$$
$$\{a_5\ddot{\gamma}_l + c2\gamma_l\}\} + 6\left\{\{a_2\ddot{\beta}_j + c1\beta_j\}\,\{a_5\ddot{\gamma}_k + c2\gamma_k\}\,\{a_5\ddot{\gamma}_l + c2\gamma_l\}\right\}$$
$$+3\,\{\{a_5\ddot{\alpha}_j + c2\alpha_j\}\,\{a_5\ddot{\gamma}_k + c2\gamma_k\}\,\{a_5\ddot{\gamma}_l + c2\gamma_l\}\}\}$$
$$+\{\phi_i''\}\,\lfloor\phi_j'\,\phi_k'\,\phi_l''\rfloor\left\{EA\,(I_y - I_z)\left\{\{a_5\ddot{\alpha}_j + c2\alpha_j\}\,\{a_5\ddot{\beta}_k + c2\beta_k\}\right.\right.$$
$$\left.\{a_5\ddot{\beta}_l + c2\beta_l\}\right\} - EA\,(I_y - I_z)\left\{\{a_5\ddot{\beta}_j + c2\beta_j\}\,\{a_5\ddot{\beta}_k + c2\beta_k\}\right.$$
$$\{a_5\ddot{\alpha}_l + c2\alpha_l\}\} - 3\,EAI_y\,\{\{a_5\ddot{\gamma}_j + c2\gamma_j\}\,\{a_5\ddot{\gamma}_k + c2\gamma_k\}$$
$$\{a_5\ddot{\alpha}_l + c2\alpha_l\}\}\} + \{\phi_i'\}\,\lfloor\phi_j'\,\phi_k''\rfloor\,\{-3\,EAI_z\,\{\{a_5\ddot{\alpha}_j + c2\alpha_j\}$$
$$\{a_5\ddot{\beta}_k + c2\beta_k\}\,\{a_5\ddot{\beta}_l + c2\beta_l\}\} - EAI_y\,\{\{a_5\ddot{\alpha}_j + c2\alpha_j\}$$
$$\{a_5\ddot{\gamma}_k + c2\gamma_k\}\,\{a_5\ddot{\gamma}_l + c2\gamma_l\}\} + 2\,EAI_z\left\{\{a_5\ddot{\beta}_j + c2\beta_j\}\right.$$
$$\left.\left.\{a_5\ddot{\alpha}_k + c2\alpha_k\}\,\{a_5\ddot{\beta}_l + c2\beta_l\}\right\}\right\} - 3EA\,\{\phi_i'\}\,\lfloor\phi_j\,\phi_k'\,\phi_l'\rfloor\,\{\lambda_j$$
$$\left.\{a_5\ddot{\gamma}_k + c2\gamma_k\}\,\{a_5\ddot{\gamma}_l + c2\gamma_l\}\}\right]\,dx \;=\; 0 \qquad \text{(A.31)}$$

v equation:

$$\int_0^1 \Big[EAI_z\,[\phi_i''\,\phi_j'']\{a_5\ddot{\beta}_j + c2\beta_j\} + [\phi_i\,\phi_j]\left\{\left\{\ddot{\beta}_j\right\}\right.$$
$$+2\,\{\{a_2\ddot{\alpha}_j + c1\alpha_j\}\} - \left.\left\{\{a_5\ddot{\beta}_j + c2\beta_j\}\right\}\right\} + EA\,\{\phi_i'\}\,\lfloor\phi_j\,\phi_k'\rfloor$$
$$\left\{\lambda_j\,\{a_5\ddot{\beta}_k + c2\beta_k\}\right\} + \{\phi_i''\}\,\lfloor\phi_j'\,\phi_k''\rfloor\,\{-2\,EA\,(I_y - I_z)\,\{\{a_5\ddot{\alpha}_j + c2\alpha_j\}$$
$$\{a_5\ddot{\beta}_k + c2\beta_k\}\Big\} + EA\,(I_y - I_z)\left\{\{a_5\ddot{\beta}_j + c2\beta_j\}\,\{a_5\ddot{\alpha}_k + c2\alpha_k\}\right\}\Big\}$$
$$+\{\phi_i\}\,\lfloor\phi_j\,\phi_k'\,\phi_l'\rfloor\left\{-3\left\{\ddot{\beta}_j\,\{a_5\ddot{\gamma}_k + c2\gamma_k\}\,\{a_5\ddot{\gamma}_l + c2\gamma_l\}\right\}\right.$$
$$-6\,\{\{a_2\ddot{\alpha}_j + c1\alpha_j\}\,\{a_5\ddot{\gamma}_k + c2\gamma_k\}\,\{a_5\ddot{\gamma}_l + c2\gamma_l\}\}$$
$$\left.+3\left\{\{a_5\ddot{\beta}_j + c2\beta_j\}\,\{a_5\ddot{\gamma}_k + c2\gamma_k\}\,\{a_5\ddot{\gamma}_l + c2\gamma_l\}\right\}\right\}$$
$$+\{\phi_i'\}\,\lfloor\phi_j'\,\phi_k''\,\phi_l''\rfloor\left\{-EAI_z\left\{\{a_5\ddot{\beta}_j + c2\beta_j\}\,\{a_5\ddot{\beta}_k + c2\beta_k\}\right.\right.$$
$$\left.\{a_5\ddot{\beta}_l + c2\beta_l\}\right\} - EAI_y\left\{\{a_5\ddot{\beta}_j + c2\beta_j\}\,\{a_5\ddot{\gamma}_k + c2\gamma_k\}\right.$$
$$\{a_5\ddot{\gamma}_l + c2\gamma_l\}\} - EA\,(I_y - I_z)\left\{\{a_5\ddot{\gamma}_j + c2\gamma_j\}\,\{a_5\ddot{\beta}_k + c2\beta_k\}\right.$$
$$\{a_5\ddot{\gamma}_l + c2\gamma_l\}\}\} + \{\phi_i''\}\,\lfloor\phi_j'\,\phi_k'\,\phi_l''\rfloor\,\{-EA\,(I_y - I_z)$$
$$\left\{\{a_5\ddot{\alpha}_j + c2\alpha_j\}\,\{a_5\ddot{\alpha}_k + c2\alpha_k\}\,\{a_5\ddot{\beta}_l + c2\beta_l\}\right\} + EA\,(I_y - I_z)$$
$$\left\{\{a_5\ddot{\alpha}_j + c2\alpha_j\}\,\{a_5\ddot{\beta}_k + c2\beta_k\}\,\{a_5\ddot{\alpha}_l + c2\alpha_l\}\right\} - \frac{1}{2}\,EA\,(3\,I_z + I_y)$$
$$\left.\left\{\{a_5\ddot{\gamma}_j + c2\gamma_j\}\,\{a_5\ddot{\gamma}_k + c2\gamma_k\}\,\{a_5\ddot{\beta}_l + c2\beta_l\}\right\}\right\}\Big]\,dx\;=\;0 \qquad \text{(A.32)}$$

w equation:

$$\int_0^1 \left[EAI_y\,[\phi_i''\,\phi_j'']\{a_5\ddot{\gamma}_j + c2\gamma_j\} + [\phi_i\,\phi_j]\,\{\ddot{\gamma}_j\} + EA\,\{\phi_i'\}\,\lfloor\phi_j\,\phi_k'\rfloor\right.$$
$$\{\lambda_j\,\{a_5\ddot{\gamma}_k + c2\gamma_k\}\} - \{\phi_i\}\,\lfloor\phi_j\,\phi_k'\,\phi_l'\rfloor\,\{\ddot{\gamma}_j\,\{a_5\ddot{\gamma}_k + c2\gamma_k\}$$
$$\{a_5\ddot{\gamma}_l + c2\gamma_l\}\} + \{\phi_i'\}\,\lfloor\phi_j'\,\phi_k''\,\phi_l''\rfloor\left\{\frac{1}{2}\,EA\,(I_y - I_z)\,\{\{a_5\ddot{\gamma}_j + c2\gamma_j\}\right.$$
$$\left.\{a_5\ddot{\beta}_k + c2\beta_k\}\,\{a_5\ddot{\beta}_l + c2\beta_l\}\right\} - EAI_y\,\{\{a_5\ddot{\gamma}_j + c2\gamma_j\}$$
$$\{a_5\ddot{\gamma}_k + c2\gamma_k\}\,\{a_5\ddot{\gamma}_l + c2\gamma_l\}\}\} - EAI_y\,\{\phi_i''\}\,\lfloor\phi_j'\,\phi_k'\,\phi_l''\rfloor$$
$$\left.\{\{a_5\ddot{\gamma}_j + c2\gamma_j\}\,\{a_5\ddot{\gamma}_k + c2\gamma_k\}\,\{a_5\ddot{\gamma}_l + c2\gamma_l\}\}\right]\,dx = 0 \qquad \text{(A.33)}$$

λ equation

$$\int_0^1 \left[[\phi_i\,\phi_j']\{a_5\ddot{\alpha}_j + c2\alpha_j\}\right.$$
$$+ \{\phi_i\}\,\lfloor\phi_j'\,\phi_k'\rfloor\left\{\frac{1}{2}\,\{\{a_5\ddot{\alpha}_j + c2\alpha_j\}\,\{a_5\ddot{\alpha}_k + c2\alpha_k\}\}\right.$$
$$+\frac{1}{2}\left\{\{a_5\ddot{\beta}_j + c2\beta_j\}\,\{a_5\ddot{\beta}_k + c2\beta_k\}\right\}$$
$$\left.\left.+\frac{1}{2}\,\{\{a_5\ddot{\gamma}_j + c2\gamma_j\}\,\{a_5\ddot{\gamma}_k + c2\gamma_k\}\}\right\}\right]\,dx = 0 \qquad \text{(A.34)}$$

A.8 Variation of Natural Frequencies

As discussed in Chapter 4, the variation of natural frequencies for nondimensional model are shown in Figure A.2-A.3

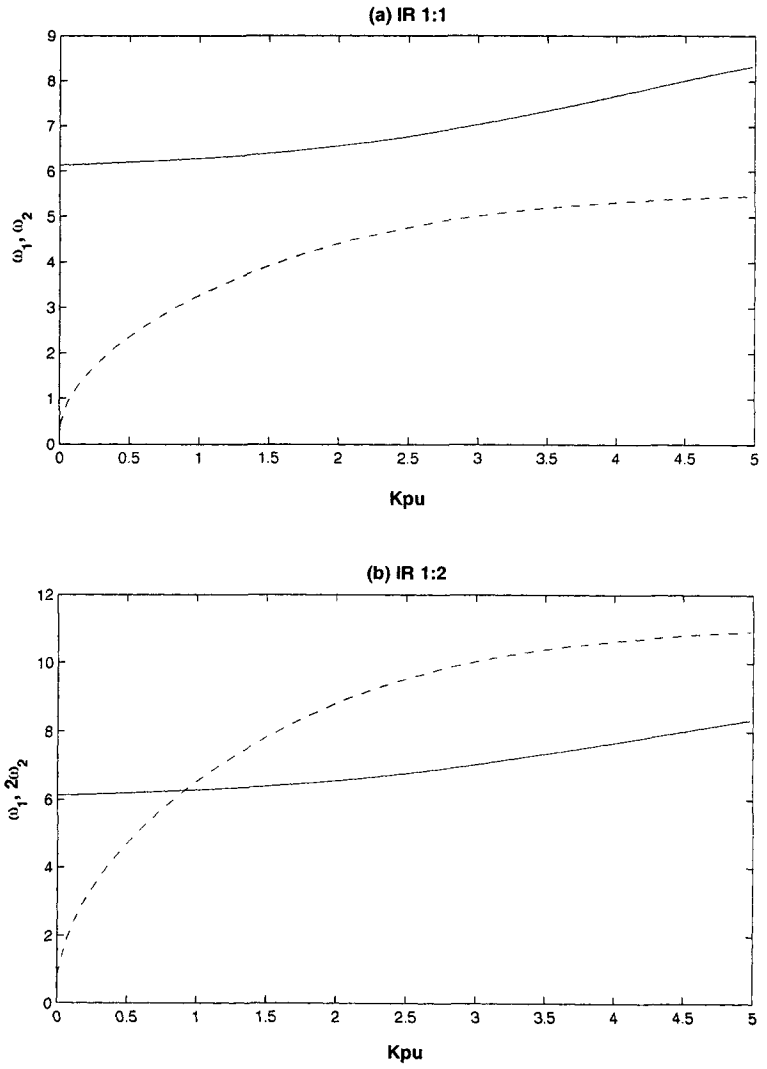

Figure A.2: Variation in ω_1 and ω_2 with respect to K_{pu}, (a) 1:1 IR and (b) 1:2 IR, (-) ω_1, (- -) ω_2

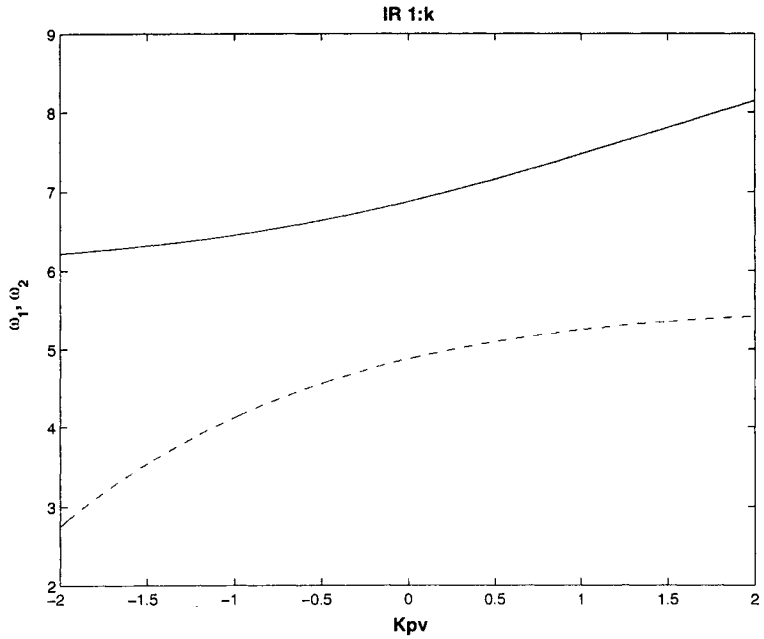

Figure A.3: Variation in ω_1 and ω_2 with respect to K_{pv}, k is IR ratio, (-) ω_1, (- -) ω_2

Bibliography

[1] S. A. Q. Siddiqui. Vibration suppression and stability in gyroscopic systems. Master's thesis, Department of Mechanical Engineering, University of Waterloo, Ontario, Canada, 1994.

[2] S. A. Q. Siddiqui and M. F. Golnaraghi. Vibration suppression in a flexible gyroscopic system using modal coupling strategies. *Journal of Mathematical Problems in Engineering*, 2:107–129, 1996.

[3] S. A. Q. Siddiqui and M. F. Golnaraghi. A new vibration regulation strategy and stability analysis for a flexible gyroscopic system. *Journal of Sound and Vibration*, 193(2):465–481, 1996.

[4] A. H. Nayfeh, J. F. Nayfeh, and D. T. Mook. On methods for continuous systems with quadratic and cubic nonlinearities. *Nonlinear Dynamics*, 3:145–162, 1992.

[5] S. Hsieh, S. W. Shaw, and C. Pierre. Normal modes for large amplitude vibration of a cantilever beam. *International Journal of Solids Structures*, 31(14):1981–2014, 1994.

[6] S. W. Shaw and C. Pierre. Normal modes of vibration for nonlinear continuous systems. *Journal of Sound and Vibration*, 169(3):319–347, 1994.

[7] C. L. Zartezky and Crespo da Silva. Experimental investigation of nonlinear modal coupling in the response of cantilever beams. *Journal of Sound and Vibration*, 174(2):145–167, 1994.

[8] I. H. Shames and C. L. Dym. *Energy and Finite Element Methods in Structural Mechanics.* Hemisphere Publishing Corporation, Taylor & Francis, Bristol, Pasadena, USA, 1985.

[9] Y. C. Fung. *Foundations of Solid Mechanics.* Prentice-Hall, INC., Englewood Cliffs, New Jersey, 1995.

[10] S. A. Q. Siddiqui. *Nonlinear Beam Behaviour with a Moving Mass.* PhD thesis, Department of Mechanical Engineering, University of Waterloo, Ontario, Canada, December 1998.

[11] A.R.S. Bramwell. *Helicopter Dynamics.* Edward Arnold Ltd., London, United Kingdom, 1976.

[12] Mark W. Spong and M. Vidyasagar. *Robot Dynamics and Control.* John Wiley & Sons Inc., 1988.

[13] K. E. Bishopp and D. C. Drucker. Large deflection of cantilever beams. *Quarterly of Applied Mechanics*, 3(3):272–275, 1945.

[14] A. V. Srinivasan. Large amplitude free oscillations of beams and plates. *AIAA Journal*, 3(10):1951–1952, October 1965.

[15] K. Bathe and S. Bolourchi. Large displacement analysis of three dimensional beam structures. *International Journal for Numerical Methods in Engineering*, 14:961–986, 1979.

[16] M. R. M. Crespo da Silva. Equations for nonlinear analysis of 3d motions of beams. *Applied Mechanics Reviews*, 44(11):s51–s59, November 1991.

[17] M. R. M. Crespo da Silva. Nonlinear flexural-flexural-torsional-extensional dynamics of beams–2. response analysis. *International Journal of Solids and Structures*, 24(12):1235–1242, 1988.

[18] M. R. M. Crespo da Silva. Nonlinear flexural-flexural-torsional-extensional dynamics of beams–1. formulation. *International Journal of Solids and Structures*, 24(12):1225–1234, 1988.

[19] M. R. M. Crespo da Silva and C. C. Glynn. Nonlinear flexural-flexural-torsional dynamics of inextensional beams. 1. equations of motion. *Journal of Structural Mechanics*, 6(4):437–448, 1978.

[20] M. R. M. Crespo da Silva and C. C. Glynn. Nonlinear flexural-flexural-torsional dynamics of inextensional beams. 2. forced motions. *Journal of Structural Mechanics*, 6(4):449–461, 1978.

[21] E. Pestel. Dynamic stiffness matrix formulation by means of hermitian polynomials. In J. S. Przemieniecki, R. M. Bader, W. F. Bozich, J. R. Johnson, and W. J. Mykytow, editors, *Matrix Methods in Structural Mechanics*, AFFDL-TR-66-80, pages 479–502, Wright-Patterson Air Force Base, Ohio, November

1966. Air Force Flight Dynamics Laboratory, Research and Technology Division, Air Force Systems Command and Air Force Institute of Technology, Air University.

[22] C. Mei. Nonlinear vibration of beams by matrix displacement method. *AIAA Journal*, 10(3):355–357, March 1972.

[23] C. Mei. Finite element displacement method for large amplitude free flexural vibrations of beams and plates. *Computers and Structures*, 3:163–174, March 1973.

[24] K. Bathe, E. Ramm, and E. L. Wilson. Finite element formulations for large deformation dynamic analysis. *International Journal for Numerical Methods in Engineering*, 9:353–386, 1975.

[25] K. Bathe. *Finite Element Procedures in Engineering Analysis.* Prentice Hall, New Jersey, 1982.

[26] G. V. Rao, K. K. Raju, and I. S. Raju. Finite element formulation for the large amplitude free vibrations of beams and orthotropic circular plates. *Computers and Structures*, 6, 169–172 1976.

[27] E. B. Becker, G. F. Carey, and T. J. Oden. *Finite Elements an introduction.* volume 1. Prentice-Hall, Inc., Englewood Cliffs, New Jersey, 1981.

[28] A. I. Beltzer. *Variational and Finite Element Methods.* Springer-Verlag, 1990.

[29] A. Cardona and M. Geradin. A beam finite element nonlinear theory with

finite rotations. *International Journal for Numerical Methods in Engineering*, 26:2403–2438, 1988.

[30] D. J. Dawe. *Matrix and Finite Element Displacement Analysis of Structures.* Oxford Engineering Science. Oxford University Press, Oxford, 1984.

[31] G. A. Dupuis. Incremental finite element analysis of large elastic deformation problems. Technical Report N00014-0007/6, Department of Navy, Office of Naval Research, May 1971.

[32] G. Dhatt and G. Touzot. *The Finite Element Method Displayed.* Wiley Interscience Publication. John-Wiley & Sons, Toronto, 1984.

[33] Singiresu S. Rao. *The Finite Element Method in Engineering.* Butterworth-Heinemann, third edition, 1998.

[34] P.R. Sethna. Vibrations of dynamical systems with quadratic nonlinearities. *Journal of Applied Mechanics*, 32:576–582, 1965.

[35] W. Stupnicka. On the phenomenon of the combination type resonance in nonlinear two-degree of freedom systems. *International Journal of Non-Linear Mechanics*, 4:335–359, 1969.

[36] R. Van Dooren. Combination tones of summed type in a nonlinear damped vibratory system with two-degrees of freedom. *International Journal of Non-Linear Mechanics*, 4:237–254, 1969.

[37] A.G. Haddow, A.D. Barr, and D.T. Mook. Theoretical and experimental study

of modal interaction in a two-degree of freedom structure. *Journal of Sound and Vibration*, 97:451–473, 1984.

[38] D.T. Mook, R.H. Plaut, and N. HaQuang. The influence of internal resonance on nonlinear structural vibrations under subharmonic resonance conditions. *Journal of Sound and Vibration*, 102, 1985.

[39] M. F. Golnaraghi. Vibration suppression of flexible structures using internal resonance. *Mechanics Research Communications Journal*, 18, 1991.

[40] M. F. Golnaraghi. Regulation of flexible structures via nonlinear coupling. *Journal of Dynamics and Control*, 1:405–428, 1991.

[41] W.Keats Wilkie, Paul H. Mirick, and Chester W. Langston. Rotating shake test and modal analysis of a model helicopter rotor blade. Technical report, 1997.

[42] A. H. Nayfeh and D. T. Mook. *Nonlinear Oscillations*. Wiley, New York, 1979.

[43] SS. Oueini, Ali H. Nayfeh, and Pratt. A nonlinear vibration absorber for flexible structures. *Nonlinear Dynamics*, 15:259–282, 1998.

[44] Sayam Saguranrum, Donald L. Kunz, and Hanafy M. Omar. Numerical simulations of cantilever beam response with saturation control and full modal coupling. *Computers and Structures*, 81:1499–1510, 2003.

[45] S. S. Oueini and M. F. Golnaraghi. Experimental implementation of the internal resonance control strategy. *Journal of Sound and Vibration*, pages 377–396, 1996.

[46] P. F. Pai, B. Wen, A. S. Naser, and M. J. Schulz. Structural vibration control using pzt patches and nonlinear phenomena. *Journal of Sound and Vibration*, pages 273–296, 1998.

[47] C. W. Gear. Ordinary differential equation techniques for partial differential equations. In K. Bathe, J. T. Oden, and W. Wunderlich, editors, *Formulations and Computational Algorithms in Finite Element Analysis*, chapter 24, pages 691–717. The Massachusetts Institute of Technology, 1977.

[48] W.H. Press, S.A. Teukolsky, W.T. Vetterling, and B.P. Flannery. *Numerical Recipes in C.* Cambridge University Press, Cambridge, United Kingdom, 1992.

[49] Yue Huang. Development of a moving mass vibration controller for nonlinear multi-body continuous systems. Master's thesis, Lakehead University, Ontario, Canada, 2003.